DISSERTATION

HYDROPHOBIC VANADIUM COMPLEXES FOR USE IN ANTICANCER ACTIVITY

Submitted by

Heide Murakami

Department of Chemistry

In partial fulfillment of the requirements

For the Degree of Doctor of Philosophy

Colorado State University

Fort Collins, Colorado

Spring 2023

Doctoral Committee:

Advisor: Debbie C. Crans

Melissa M. Reynolds
Joseph M. Zadrozny
Dean C. Crick

ABSTRACT

HYDROPHOBIC VANADIUM COMPLEXES FOR USE IN ANTICANCER ACTIVITY

This dissertation contains the development, synthesis, and characterization of vanadium metal complexes in both biological environment and organic solutions for the purpose of novel medical treatments. As cancer is a disease that causes uncontrollable growth of mutated cells over time, treatments need to also improve to account for an ever-increasing cancer types. Although platinum-based drugs have found successful in treating multiple forms of cancer, inorganic metal based drugs are relatively uncommon in the medical field. It was found in 2020, that a vanadium compound was more potent than cisplatin and efforts were made to investigate and improve that compound. The compound is a ternary V(V) complex that consists of VOL^1L^2 where L^1 is N-(salicylideneaminato)-N'-(2-hydroxyethyl)ethane-1,2-diamine and L^2 is 3,5-di-*tert*-butylcatechol. It is believed that that hydrophobicity of the catechol ligand was significant in keeping the compound intact long enough to cause cytotoxicity in bone cancer cells.

In Chapter 1, the biological effects of vanadium and the reasoning that vanadium may be used as a potent medical treatment for various illnesses such as bone cancers, brain cancers and/or tuberculosis are investigated. Chapter 2 describes the synthesis and characterization of halogenated version of the original vanadium Schiff base complexes to test how electronegativity affects the activity as well as testing how modification of the salicyaldehyde portion affects the metal complex. Chapter 3 reports the development of adamantanol catechol ligands to improve hydrophobicity in the vanadium Schiff base complex. Chapter 4 explains the speciation of working with a metal complex in a biological system by comparing two different vanadium systems and

how they hydrolyze and form multiple different species in various environments. Chapter 5 summarizes the conclusions and proposes future works based on the research done that can move new projects forward.

ACKNOWLEDGEMENTS

This work would not have been possible without the mentorship and guidance from several people: Dr. Debbie Crans (my advisor, who is the most dedicated scientist I'll ever know), Dr. Aviva Levina and Dr. Peter Lay for the biological components of our research. I'd also like to thank my family and friends. Without them, I would have never gotten this far.

Chapter 2: This work was funded by Colorado State University, the Arthur Cope Foundation, the Australian Research Council (ARC) (DP160104172), University of Sydney, and Scientific and Technological Research Council of Turkey (TUBITAK). This dissertation chapter contains the manuscript of an article that is published in 2022 in Inorganic Chemistry. [Murakami, H. A.; Uslan, C.; Haase, A. A.; Koehn, J. T.; Vieira, A. P.; Gaebler, D. J.; Hagan, J.; Beuning, C. N.; Proschogo, N.; Levina, A.; Lay, P. A.; Crans, D. C. Vanadium chloro substituted Schiff base catecholate complexes are reducible, lipophilic, water stable, and have anticancer activities. 2022. Inorg. Chem. 61 20757- 20773. doi: 10.1021/acs.inorgchem.2c02557

Chapter 3: This work was funded by Colorado State University, the Arthur Cope Foundation, the Australian Research Council (ARC) (DP160104172), University of Sydney, and Scientific and Technological Research Council of Turkey (TUBITAK). This dissertation chapter contains the manuscript of an article that is under preparation during the writing of this dissertation. [Bates, A.; Murakami, H. A.; Levina, A.; Lay, P. A.; Crans, D. C. The vanadium Schiff base di-adamantyl catecholate complex with potent anticancer activities. (Manuscript under preparation)]

Chapter 4: This dissertation contains parts of two articles [Samart, N.; Arhouma, Z.; Kumar, S.; Murakami, H. A.; Crick, D. C.; and Crans, D. C. Decavanadate Inhibits Mycobacterial Growth More Potently Than Other Oxovanadates. 2018. Front. Chem. 6. 1-16. doi:

10.3389/fchem.2018.00519] and [Bergeron, A.; Kostenkova, K.; Selman, M.; Murakami, H. A.; Owens, E.; Haribabu, N.; Arulanandam, R.; Diallo, J. S.; Crans, D. C. Enhancement of oncolytic virotherapy by vanadium(V) dipicolinates. 2019. Biometals. 32. 545-561. doi: 10.1007/s10534-019-00200-9.

TABLE OF CONTENTS

Chapter 1- Introduction

Vanadium is a first-row transition metal that has various properties that makes the metal a topic of research, especially in biological systems. Being an early first row transition metal, it has three open electrons in its d-subshell and can have multiple cations and oxidation states if the shell fills or empties through its ligands.[1] The oxidation states can vary from -2 to +5 but in biological systems the focus is more on the V^{IV} and V^{V} oxidation states.[2-4] The transition metal is the 20th most abundant element in the Earth's crust but the elemental metal itself is extremely rare compared to vanadium oxides. Vanadate, the simplest anionic vanadium(V) oxide has similar structural and electronical properties to phosphate.[2, 5] From a biological standpoint, the pKa's are also very similar to each other.[6] This similarity of coordination geometry has made it a topic of research as this has relevance in areas related to regulatory phosphatase dependent processes in diseases such as diabetes or cancer.

Cancer is still one of the leading causes of death even after decades of research. To this day, the most common forms of treatments for cancer involve destruction of every cell in the cancerous area through radiation or chemotherapy and preventing the cancer from spreading to a different location through metathesis. As such the research continues for a better treatment that can be applied to multiple forms of cancer, even cancers with little to no treatments such as glioblastoma, a brain cancer.[7] The most common forms of cancer are treated with chemo, surgery or radiation, Figure 1.1. One form of treatment involves immunotherapy where the immune system is stimulated to fight off the cancer cells.[8] Usually, this treatment is used in tandem with another treatment as immunotherapy is not viable by itself.[8] But in the case of immunotherapy, the combination of two treatments have shown to have a far greater effect than the two separately.[8]

Another treatment option is a direct injection into the tumor itself. If the tumor is in a readily accessible location, a larger variety of compounds can be used.[7, 9] Readily accessibility of the tumor is important for compounds that may be more toxic to the body as well as the tumor. Compounds that would be toxic in the body in large amounts can be decreased if the administration is intratumeral as the compounds would not have to travel through the body as far and risk degradation over time.[10] Comparing these two treatments, immunotherapy strives to boost the immune system and kill off the cancer cells with another treatment in tandem while a direct injection is a straight injection of a cytotoxic drug to the tumor site. One treatment, immunotherapy is usually weaker than the direct injection, but it is less harmful to the body and overall improves the immune system towards that specific form of cancer from a resurgence. Direct injections at the site of the tumor can be more difficult if the tumor is not in a readily accessible area, but the treatment can use more reactive compounds as the compounds will be injected into a specific tumor location.

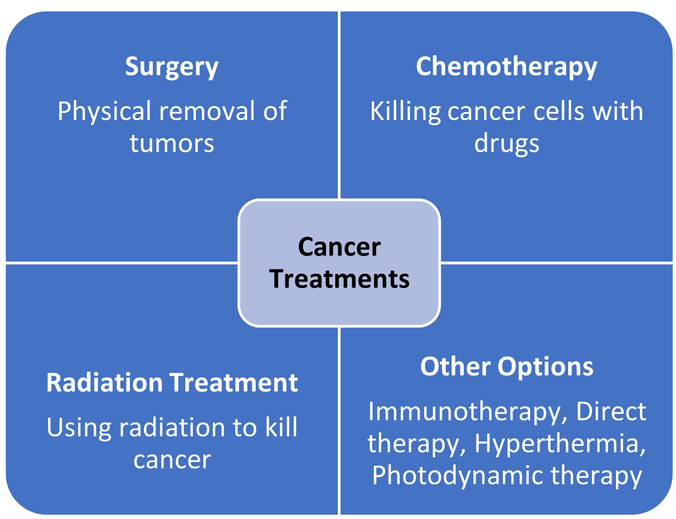

Figure 1.1. Overview of cancers and their methods of treatment.

For cancer compounds, cisplatin is the most notable inorganic cancer treatment as of the present day from its discovery 40 years ago, Figure 1.2.[7, 11] Before the discovery of cisplatin's anti-cancer properties, most success chemotherapeutics were organic compounds. Cisplatin's mode of action is by killing cancerous cells by interfering with DNA replication through cross-linking to the DNA and blocking cell repair enzymes.[12-13] Currently oxaliplatin, carboplatin, and cisplatin are still used in cancer treatment. Transplatin was initially found to be biologically inactive, but since then has been found to work by a different mode of action and is being investigated for its potential use.[14] Our synthesized compounds in this thesis build off the previous reported compounds that were known to be more potent than cisplatin.

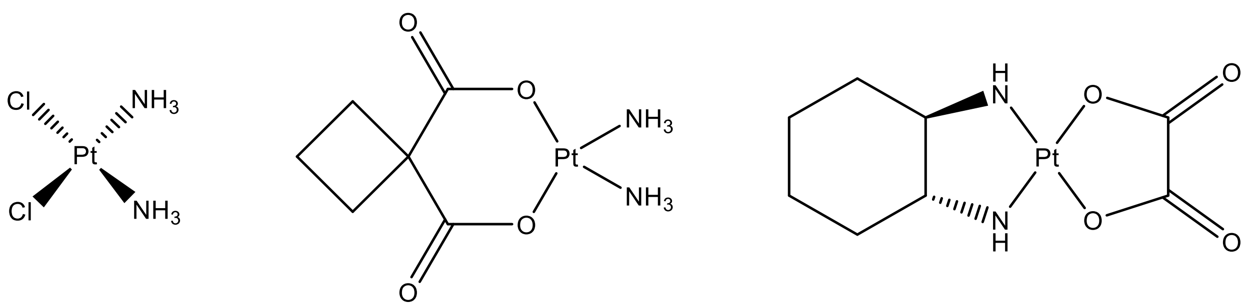

Figure 1.2. The structure of cisplatin and two other platinum based anticancer agents carboplatin and oxaliplatin

A discovery was made in our collaboration with a group from the University of Sydney where one of our vanadium complexes was reported to have anticancer effects better than cisplatin even when the compounds were allowed to degrade in solution over time, Figure 1.3.[7] Our focus was to improve on this activity and to understand why this compound was better than cisplatin. The compounds were vanadium Schiff bases that consisted of a catechol ligand and a Schiff base precursor.[7] The most potent of the vanadium Schiff base complexes was a vanadium complex with a di-tert butyl catechol ligand.[7, 9] We soon realized that the anti-cancer activity increased with hydrophobicity and sterics.[9] The hydrophobicity is critical to the activity as the compound remains intact as a metal complex before degrading into the various vanadium compounds that arise from being in a biological system. We could improve on the hydrophobicity in three different locations, but there were two areas of focus for the compounds presented in this thesis: increasing the size of the catechol ligand and increasing the electronegativity of the compound by adding halogens to the system. From our studies in the synthesis, characterization, and redox chemistry, we found that as of currently, the size of the catechol ligand was the biggest contributor to the hydrophobicity of the complex. Along with this, we expected that the electron withdrawing groups (EWGs) on the Schiff base would increase hydrophobicity and stability, but the change to biological activity was insignificant. As a result, we focused on designing and synthesizing new catechol ligands for our complexes.

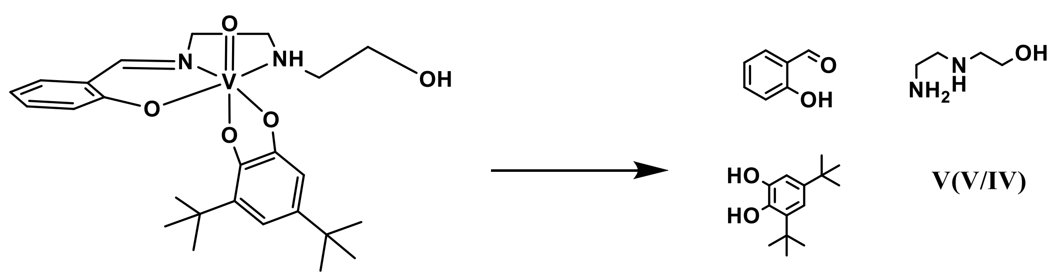

Figure 1.3. VO(HSHED)(DTB) and its decomposition products

To test for cancer treatment efficacy, another avenue we investigated was the speciation of the compounds in a biological system including hydrolysis and redox processes. Many vanadium species will undergo hydrolysis and form different species based on the pH of the system.[15-17] For example, coordination complexes can exchange their ligands with water or undergo various protonation events. Similarly, the vanadium atom can oxidize or reduce depending on the environment or the ligands coordinated to the vanadium atom. We can model speciation profiles through a program known as HySS.[18] HySS is a modelling program where variables such as concentrations, stoichiometry ratios, and ionic strengths can be added to known pKa values to form a profile for that compound as a function of pH.[18] This type of speciation analysis is important to interpret what vanadium compound is interacting with a biological system as vanadium can change significantly at biological pH values.

Although cancer is the main target, vanadium complexes could also have different activities that may affect other illnesses. The medicinal properties of vanadium have been investigated as far back as 1899, Figure 1.4.[1] Although vanadium can be toxic at extremely high concentrations, the beneficial effects of vanadium can be reached before those amounts. Vanadium sulfate is sold as a supplement for body builders and vanadium salts and compounds were tested for anti-diabetic properties. As far back as the 1990s, it was known that BMOV and BEOV had the potential to be used for diabetes treatment and even went to Phase 2 clinical trials.[19-20] While those compounds failed in Phase 2 clinical trials due to toxicity and financial issues, the clinical trial opened new doors for vanadium to be used in different medicinal treatments such as cancer as previously mentioned and tuberculosis.[5, 20]

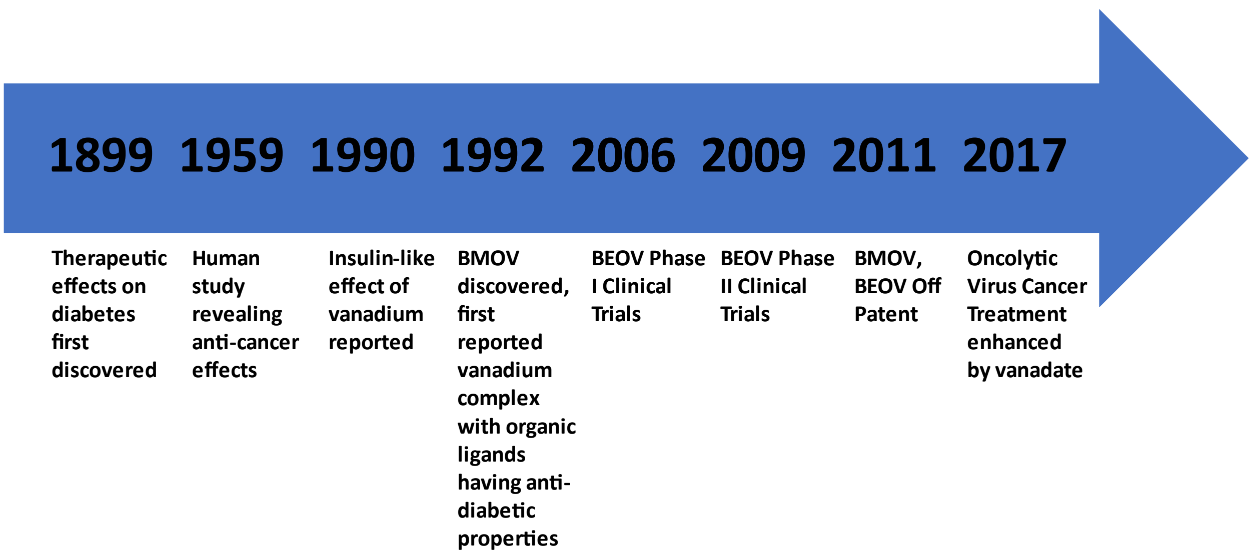

Figure 1.4. Historical biological and biomedical activities of vanadium.

It was reported that vanadium compounds can also affect the growth rate of mycobacteria which is directly related to tuberculosis.[15] The larger vanadium complexes such as decavanadate greatly inhibits two Mycobacterial strains.[15] Though the pathways are still relatively unknown, it is believed that decavanadate undergo hydrolysis into multiple smaller vanadates, which may interact with the bacterial cells, or the material excreted by the bacterial cells.[15, 21] Notably however is the fact that decavanadate and the monomeric vanadate have different activities in the cells which may show that they act via different pathways. These compounds were investigated by both speciation and by modification of the compound itself.

In the following thesis, based on our best compounds synthesized in the Crans group, a structure activity relationship (SAR) was investigated by synthesizing several derivatives of vanadium compounds and characterizing them synthetically for biological activity. The second chapter covers the synthesis of Schiff bases that were modified on the salicylic acid moiety with a halogen, the characterization of the novel compounds, and the structure activity relationships of the halogen on the molecule under biological conditions. The third chapter describes the design and synthesis of hydrophobic catechol ligands to form new Schiff bases for characterization and biological studies based on our SAR studies. Finally, the last chapter covers the speciation of vanadium metals under biological conditions which is important to study the function of vanadium and vanadium complexes in solution.

Chapter 2- Vanadium chloro substituted Schiff base catecholate complexes are reducible, lipophilic, water stable, and have anticancer activities

Introduction-

It has been reported that vanadium Schiff bases complexes have anti-cancer effects on bone cancer variants.[7] The combination of the non-innocent Schiff base component and the catechol ligand provide a hydrophobic redox active compound with medicinal properties. The more hydrophobic the catechol ligand was, the more cytotoxic towards cancer the compound was. This is believed to be due to the stability of the complex. The longer the compound could maintain structural integrity, the more effective the complex was in the tumor site. While the catechol ligand was explored previously with various substituents, the Schiff base portion of the complex was left aside in comparison. The precursor Schiff base was composed of a salicylaldehyde and at the start, ethylene diamine. This was later expanded to imidazole and ENSAL components, but in this report, ethylene diamine will be the focus.[22] For these new compounds, the salicylaldehyde component was modified with a halogen to test how impactful modifying the precursor would have been. These compounds were synthesized, characterized, and tested for biological activity against the known parent derivatives.

Aggressive cancers that include some brain and pancreatic cancers are notably difficult to treat and continue to present a challenge for life scientists to develop new anticancer strategies and therapies including intratumoral injections.[23-26] In the following study we report a series of new hydrophobic vanadium complexes, and characterize their chemical and anticancer properties but with different redox properties than the lead complex shown in Figure 2.1a.

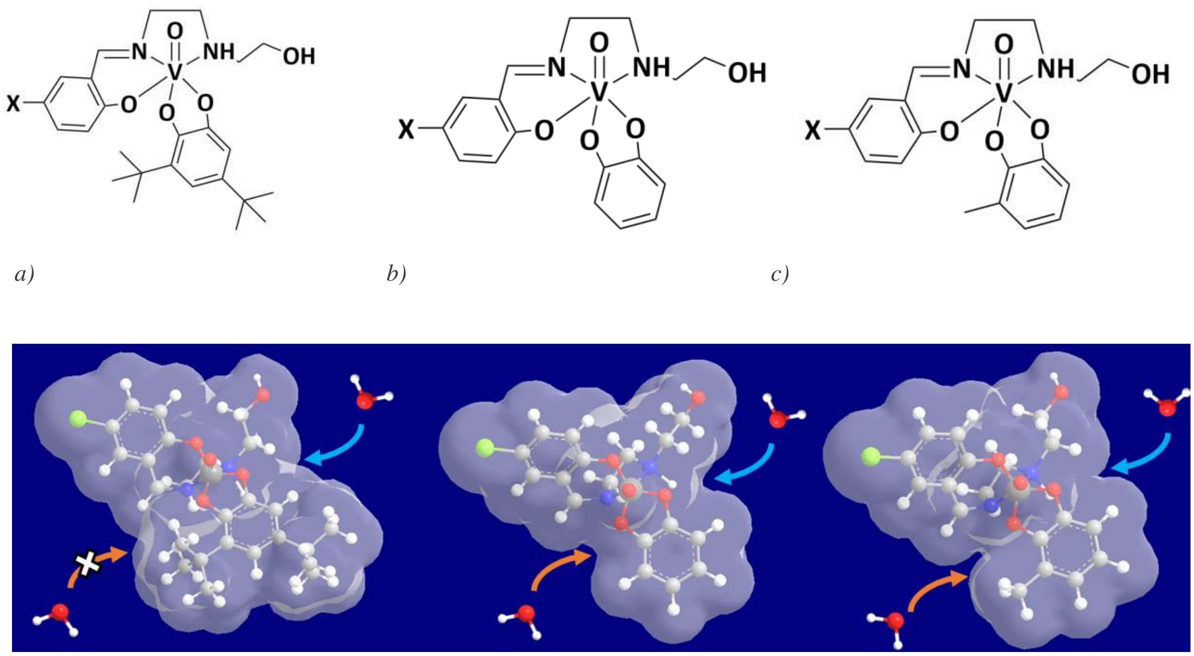

a) b) c)

d) e) f)

Figure 2.1. Structures of two known vanadium Schiff bases complexes (when X=H) a) [VO(X-HSHED)(DTB)] b) [VO(X-HSHED)(Cat)], and a third new complex c) [VO(X-HSHED)(3-MeCat)]. The three new chloro-substituted Schiff base complexes were designed with X=Cl and ([VO(HSHED)(R_2Cat)] (R_2 = H,H; H,Me; or ^{t}Bu,^{t}Bu) (HSHED = *N*-(salicylideneaminato)-*N*′-(2-hydroxyethyl)-1,2-ethanediamine, Cl-HSHED = 4-chloro-*N*-(salicylideneaminato)-*N*′-(2-hydroxyethyl)-1,2-ethanediamine, Cat = pyrocatecholato, 3-MeCat = 3-methylcatecholato, DTB = 3,5-di-*t*-butylcatecholato). The hydrophobicity of the three new chloro-substituted Schiff base complexes is illustrated using space filling models in d), e) and f) and the different hydrolytic stability are illustrated by the blue and orange arrows showing access of H_2O molecules.

Vanadium complexes act through many mechanisms in biology, which in broad strokes can be described by impacting signal transduction, interacting with regulatory protein phosphatases and kinases, transporting proteins as well as affecting the redox states of cells presumably through reactive oxygen species (ROS).[9, 27-29] Since cancer cells are known to support a more reducing environment, the design of a new class of Schiff base V-catecholates described in this work is to explore a series of complexes with different redox potential. These non-innocent Schiff base V-catecholates complexes are oxidation state V vanadium complexes stabilized by a ternary ligand and coordinated to a redox active catecholato ligand. Non-innocent complexes are redox active complexes that contain a ligand, which can undergo a redox reaction in addition to the metal, and thus making it difficult to determine if the redox reaction took place on the metal, or on the ligand or was substantially delocalized over both. The extent of such delocalization can be probed by a combination of XAS studies on XANES to determined metal oxidation state, and bond lengths combined with DFT calculations.[30-31] The complex design originated from one vanadium Schiff base complex with the di-*t*-butylcatecholato ligand (Figure 2.1a, X=H) that was more cytotoxic compared to cisplatin by one order of magnitude in T98g cells (glioma multiforme, an aggressive brain cancer). It is also more active than cisplatin against models for other hard-to-treat cancers, A549 (lung), PANC-1 (pancreatic) and SW1353 (bone chondrosarcoma) cells.[7, 32-33] In contrast this compound was not toxic in normal cells, such as normal human foreskin fibroblasts (HTT-1),[7, 32-33] or in animal studies in mice.[34]

Members of the class of non-innocent Schiff base V-catecholates were designed to have sufficient stability and hydrophobicity to enter cells rapidly before decomposition in biological media.[7, 32, 35-36] The essential design feature requires the compound to remain intact for uptake to occur but not too long to induce more systemic toxicity. After injection directly into a tumor, the complexes will enter the tumor cells rapidly and exert their action at which point the decomposition products can diffuse away from the tumor and into healthy cells where they exhibit low cytotoxicity and potentially beneficial neuroprotective and other beneficial effects .[7, 9, 32, 35] Hundreds of clinical trials are ongoing using these intratumoral drug-delivery methods with one drug, T-Vec already in the clinics for treatment of late stage cancers.[35, 37] Seven of these ongoing clinical trials involve platinum-based drugs,[35, 37] so the fact the best of the non-innocent V-complexes are an order of magnitude more potent than cisplatin fuel the focus of this manuscript on the development on a new class of non-innocent chloro-substituted Schiff base V-catecholates.[7] Complexes with superior antiproliferative effects compared to cisplatin have the potential to be suitable for intratumoral injection (Figure 2.1) and related administration methods[35] and are important targets for future therapeutic agent development.

Schiff bases are formed as condensation products between an aldehyde and an amine to generate versatile ligands with large structural diversity. Complexation with metal ions can lead to a wide range of metal complexes used in catalysis, as novel materials, and as bioactive complexes.[22, 38-43] These ligands offer several approaches to tailor a complex by changing the coordinating moieties of the Schiff base, substitution on the aromatic rings and changes in the hydrophobicity of the ligands.[44-45] The non-innocent vanadium-Schiff base complexes represent a much smaller class of V-Schiff base complexes containing a redox active ligand. Early work by Pecoraro and others explored some of the chemistry of this class of complexes mapping out structures and spectroscopic features of the parent and substituted systems.[22, 46-49] However, as described previously, the Schiff base scaffold can form a vanadium(IV) complex but with catecholate co-ligands, the Schiff base ligand serves to stabilize the vanadium(V) oxidation state.[22]

Vanadium tris-catecholates are generally known to contain vanadium in oxidation state III or IV except for the vanadium tris-catecholato complex formed from 3,5-di-*t*-butyl catechol where the vanadium is in oxidation state V.[7, 9-10, 30, 50-51] X-ray absorption spectroscopy, in particular, demonstrated that the redox chemistry was mainly at the metal center rather than on the catecholato ligand.[30] The non-innocent vanadium(V) Schiff base complexes of interest are shown in Figure 2.1 and have the vanadium stabilized by a ternary Schiff base-ligand. When a hydrophobic sterically hindered catecholato ligand is used, the complexes hydrolytic stabilities have been significantly increased.[9, 32] We and others have previously investigated the electrochemical properties and electronic structure of these VO(HSHED) and related catecholate systems, however, little is known about how their solution redox chemistry impact their antiproliferative activities.[33, 36, 46, 52] Since biological properties of other vanadium(V)-complexes are known to involve reactive oxygen species (ROS),[20, 30, 33, 38, 44, 53-55] we designed the series of new chloro-substituted Schiff base V-complexes to explore if complexes that more readily undergo redox chemistry have improved anticancer effects. Hence the new chloro substituted non-innocent vanadium(V) Schiff base complexes were developed and their chemistry and anticancer properties are described.

In this work, we present three new complexes ([VO(HSHED)(R_2Cat)] (R_2 = H,H; H,Me; or ^{t}Bu,^{t}Bu) (HSHED = *N*-(salicylideneaminato)-*N′*-(2-hydroxyethyl)-1,2-ethanediamine, Cl-HSHED = 4-chloro-*N*-(salicylideneaminato)-*N′*-(2-hydroxyethyl)-1,2-ethanediamine, Cat = pyrocatecholato, 3-MeCat = 3-methylcatecholato, DTB = 3,5-di-*t*-butylcatecholato, Figure 2.1a-2.1c; X=Cl) designed to have different redox potential, hydrophobicity (Figure 2.1d-2.1f) and water stability compared to the compound shown in Figure 2.1a when X=H. Specifically, the complexes were designed to test the following two hypotheses that: 1) both hydrophobicity and stability are important to the anticancer properties of the complexes, as well as: 2) redox chemistry is important because the mode of action may involving reactive oxygen species (ROS). Furthermore, this work will provide additional examples of non-innocent Schiff base V-catecholate complexes with different redox potentials and document their anticancer properties.

Experimental

General materials. 5-Chlorosalicylaldehyde, *N*-(2-hydroxyethyl)-1,2-ethanediamine, vanadyl sulfate hydrate, catechol, 3,5-di-*t*-butylcatechol, and 3-methylcatechol were purchased from Sigma Aldrich. Chemicals were used as-is. Silver nitrate, ferrocene, and tetra-*n*-butylammonium perchlorate (TBAP) were purchased from Merk Millipore for the electrochemistry experiments. Ultrapure Ar (AR UHP300) from Airgas was used for degassing solutions. Deuterated PBS was prepared following a known protocol, replacing the water with deuterated water.[56] The pH values of buffered solutions were adjusted with DCl and NaOD. The pre-sterilized media and sterile plasticware used in cell culture studies were purchased from Thermo Fisher Scientific Australia.

General Methods and Instrumentation. The complexes were also characterized by UV-Vis spectroscopy (AvaLight UV-Vis/NIR Light Source and AvaSpex-UL S2048 Fiber-Optic Spectrometer), MS (Bruker amaZon SL spectrometer), and elemental analysis (ALS Environmental, Tucson, AZ). The hydrophobicity was calculated using Chemicalize software developed by ChemAxon and downloaded in May 2020.[57]

General Syntheses. $[V(O)_2(HSHED)]$ and the non-halogenated analogues [VO(HSHED)(Cat)] and [VO(HSHED)(DTB)] were prepared as reported previously.[7, 46] The new vanadium(V) complexes were prepared in situ after condensation of the chloro-substituted Schiff base from 5-chlorosalicylaldehyde and N-(2-hydroxyethyl)-1,2-ethanediamine with vanadyl sulfate because the Schiff base ligand was not stable and found to decompose upon storage.

[VO(HSHED)(3-MeCat)]: To a 250-mL round bottom Schlenk flask was added acetone (100 mL, which was then degassed with Ar. $[V(O)_2(HSHED)]$ (0.29 g, 1.0 mmol) was added to the degassed acetone, followed by 3-methylcatechol (0.12 g, 1.0 mmol). A deep purple solution resulted after 3 h. The reaction was vacuum filtered and then concentrated to dryness under reduced pressure at room temperature. The purple residue was dissolved in a minimal amount of acetone and then *n*-hexane (100 mL) was added. The solution was allowed to stand in a -20 °C freezer overnight. The dark microcrystalline precipitate was vacuum filtered, washed with cold n-hexane (< 0 °C, 2 x 25 mL), and dried under vacuum for 3 d to yield 0.33 g (79%) purple solid. X-ray quality crystals were obtained by slow evaporation of a methanol solution. $\delta^{51}V$ NMR (101 MHz,

CD_3CN): 287 ppm (major), 324 ppm (minor). ^{1}H NMR (400 MHz, CD_3CN): δ 8.61 (s, 1H), 7.49 (m, 2H), 6.84 (t, 1H), 6.76 (m, 1H), 6.32 (d, 1H), 6.07 (d, 1H), 5.97 (d, 1H), 4.17 (m, 2H), 4.05 (m, 2H), 3.90 (s, 2H), 3.79 (m, 2H), 3.65 (m, 2H), 3.36 (m, 2H), 2.82, (t, 1H). λ_{max} (DMSO) 546 nm. Elemental *Anal. Calc.* for ($VC_{18}H_{21}N_2O_5$): C, 54.55; H, 5.34; N, 7.07. Found C, 54.55; H, 5.41; N, 6.60.

[V(O)$_2$(Cl-HSHED)]: 5-Chlorosalicylaldehyde (2.94 g, 18.8 mmol) and *N*-(2-hydroxyethyl)-1,2-ethanediamine (1.96 g, 18.8 mmol) were added to degassed methanol (75 mL) and the mixture was allowed to react for 1 h under Ar. Vanadyl sulfate hydrate (3.74 g, 18.8 mmol), dissolved in 50 mL of degassed water, was added to this solution, and after 3 h stirring under Ar, the solution was dark red/brown in appearance. Then, solid NaOH (1.12 g, 37.6 mmol) was added to the mixture, the solution was opened to the air, and the reaction mixture was stirred overnight. The light-yellow reaction mixture was cooled in a dry ice/acetone bath for ~1 min, vacuum filtered, washed with cold EtOH (60 mL, < 0 °C), washed with cold diethyl ether (60 mL, < 0 °C), and then dried under vacuum for 3 d to yield 5.25 g (86% yield) as a light-yellow powder. δ^{51}V NMR (101 MHz, CD_3CN): -531 ppm. ^{1}H NMR (400 MHz, CD_3CN): δ 8.63 (s, 1H), 7.45 (s, 1H), 7.40 (d, 1H), 6.81 (d, 1H), 4.44 (m, 1H), 4.16 (m, 1H), 4.01 (m, 1H), 3.84 (m, 1H), 3.34 (m, 2H), 3.28 (d, 1H), 3.01 (m, 1H), 2.74 (m, 1H). λ_{max} (DMSO) 335 nm. HRMS (ESI) calc. for $C_{11}H_{14}ClN_2O_4V$ $[MNa]^+$ 346.9979, found 346.99739.

[VO(Cl-HSHED)(Cat)]: To a 250-mL round bottom Schlenk flask was added acetone (100 mL), which was then degassed with Ar. [V(O)$_2$(Cl-HSHED)] (0.33 g, 1.0 mmol) was added to the degassed acetone, followed by catechol (0.11 g, 1.0 mmol). A deep purple solution resulted in approximately 5 s. The solution was stirred overnight under Ar. The reaction mixture was vacuum filtered and then concentrated to dryness under reduced pressure at room temperature. The purple

residue was dissolved in a minimal amount of acetone, and then *n*-hexane (100 mL) was added. The solution stood in a -20 °C freezer overnight. The dark microcrystalline precipitate was vacuum filtered, washed with cold *n*-hexane (< 0 °C, 2 x 25 mL), and dried under vacuum for 3 d to yield 0.34 g (80%) as a purple solid. δ ^{51}V NMR (101 MHz, CD_3CN) 282 ppm (major), 322 ppm (minor). ^{1}H NMR (400 MHz, CD_3CN): δ 8.55 (s, 1H), 7.50 (d, 1H), 7.40 (dd, 1H), 6.75 (s, 1H), 6.73 (s, 1H), 6.52 (d, 1H), 6.33 (d, 2H), 4.25 (m, 1H), 4.08 (m, 3H), 3.77 (m, 1H), 3.61 (m, 1H), 3.44 (m, 1H), 3.32 (m, 1H), 2.94 (qd, 1H), 2.79 (t, 1H). λ_{max} (DMSO) 531 nm. Elemental *Anal. Calc.* for ($VC_{17}H_{18}N_2O_5Cl$): C, 49.00; H, 4.35; N, 6.72. Found C, 48.78; H, 4.10; N, 6.47. HRMS (ESI) calc. for $C_{17}H_{19}ClN_2O_5V$ [MH]$^+$ 417.04167, found 417.04116.

[VO(Cl-HSHED)(3-MeCat)] was synthesized following the [VO(Cl-HSHED)(Cat)] procedure to yield 0.34 g (79%) as a purple solid. δ^{51}V NMR (101 MHz, CD_3CN) 331 ppm (major), 362 ppm (minor), 369 ppm (minor), 409 ppm (minor). ^{1}H NMR (400 MHz, CD_3CN): δ 8.56 (s, 1H), 7.51 (d, 1H), 7.41 (dd, 1H), 6.75 (d, 1H), 6.63 (m, 1H) 6.21 (d, 1H), 4.05 (m, 2H), 3.77 (m, 1H), 3.59 (m, 2H), 3.41 (m, 1H), 3.30 (m, 1H), 2.91 (m, 1H), 2.20 (s, 3H). λ_{max} (DMSO) 549 nm. HRMS (ESI) calc. for $C_{18}H_{21}ClN_2O_5V$ [MH]$^+$ 431.05732, found 431.05702.

[VO(Cl-HSHED)(DTB)] was synthesized following the [VO(Cl-HSHED)(Cat)] procedure to yield 0.37 g (70%) as a purple solid. δ ^{51}V NMR (101 MHz, CD_3CN) 427 ppm (major), 467 ppm (minor). ^{1}H NMR (400 MHz, CD_3CN): δ 8.51 (s, 1H), 7.45 (d, 1H), 7.35 (dd, 2H), 6.67 (d, 1H), 6.35 (s, 1H), 6.29 (s, 1H), 4.03 (m, 2H), 3.80 (m, 1H), 3.51 (m, 2H), 3.41 (m, 1H) 3.33 (m, 1H), 2.95 (dd, 1H), 2.48 (m, 1H), 1.40 (s, 9H). λ_{max} (DMSO) 552 nm. HRMS (ESI) calc. for $C_{25}H_{34}ClN_2O_5V$ [MH]$^+$ 528.15904, found 528.15892.

NMR spectroscopy. Complexes were characterized using ^{51}V NMR spectroscopy recorded on a Bruker model AVANCE Neo400 spectrometer equipped with a BBFO smart probe and an automated tuning module operating at 101 MHz as reported previously. [5,38-39] The ^{51}V NMR spectra were acquired with a spectral window of 86200 Hz, 2048 scans, a 90° pulse, an acquisition time of 0.08 s, and a 0.01 s relaxation delay, as reported previously.[32, 52, 58-59] 1D ^{51}V NMR studies were referenced against $[V(O)_2(HSHED)]$ at -529 ppm as a standard and reported in reference to $VOCl_3$ (0 ppm).[19] 1D and 2D ^1H NMR studies were carried out in organic solvents using a Bruker NEO400 spectrometer operating at 400 MHz at an ambient temperature. Chemical shift values (δ) are reported in ppm and referenced against TMS using the internal solvent peaks in ^1H NMR spectra (d_6-DMSO, δ at 2.50 ppm; $CDCl_3$, δ at 7.26 ppm; d_3-acetonitrile, δ at 1.94 ppm; C_6D_6, δ at 7.16 ppm) as internal standards. 1D ^{51}V NMR studies were recorded on the Bruker NEO400 spectrometer at 105.2 MHz at an ambient temperature. All complexes were dissolved in either CD_3CN or d_6-DMSO at 10 mM concentrations for spectral comparison. Spectroscopic studies were carried out using solutions of isolated complexes, and both ^1H and ^{51}V NMR spectra were recorded on the same samples. 1D samples were run within 5 h of preparation; no significant differences were observed in spectra recorded within 24 h.

$^1H-^1H$ 2D COSY and NOESY NMR spectra in organic solutions were run overnight and recorded within 12 h of sample preparation. 2D NMR spectroscopic studies in organic solutions were carried out on a Bruker NEO400 spectrometer at 400 MHz at 26 °C. A routine COSY pulse sequence provided by the Bruker software was used. A standard NOESY pulse sequence was used consisting of either 200 or 256 transients with 16 scans in the f1 domain using a 500 ms mixing time, 45° pulse angle, and a 1.5 s relaxation delay. The NMR was locked onto either d_6-DMSO or d_3-CH_3CN and referenced to the internal solvent peak. The resulting spectrum was processed using MestReNova NMR software (version 12.0.1).

Mass Spectrometry. Low-resolution electrospray ionization mass spectrometry (ESI-MS) data were collected on a Bruker amaZon SL spectrometer, using the following parameters: nebulizer pressure, 27.3 psi; spray voltage, 4.5 kV; capillary temperature, 453 K; N_2 flow rate, 4 L per min; *m/z* range, 100-1000 (alternating positive- and negative-ion modes). The compound stability parameter was set at 15% for all V(V) complexes, which provided mild ionization conditions at the expense of lower sensitivity. Smart parameter settings were fixed to the exact mass for each compound. Analyzed solutions (~10 μM V in acetonitrile) were injected using a syringe pump (flow rate, 8 μL per min). Acquired spectra were the averages of 100-200 scans (scan time, 100 ms). Simulations of the mass spectra were performed using IsoPro 3.0 software (M. Senko, IsoPro 3.0, Sunnyvale, CA, USA, 1998). High-resolution positive ion ESI-MS was performed on a Thermo Velos Pro Orbitrap mass spectrometer via a syringe infusion (flow rate, 8 μL per min). Resolving power was set to 200,000 at 200 m/z. The instrument was externally calibrated before analysis and internally calibrated using dioctyl phthalate as a lock mass.

Electrochemistry. Electrochemistry was conducted using a WaveDriver 40 DC Bipotentiostat/Galvanostat and a Low Volume Three Electrode Cell Basic Kit (AF01CKT1006) purchased from Pine Research Instrumentation. The software used during data acquisition was AfterMath v 1.5.9807 with the *iR* compensation option turned off, while eL-Chem Viewer and Microsoft Excel were used for post-acquisition processing.[60-64]

Cyclic voltammograms (CVs) were measured in acetonitrile (2.0 mM V(V)) with an internal standard (ferrocene) in the presence of 0.1 M TBAP. Catecholates are well known to exhibit complex redox chemistry, which includes more than one redox step.[65-66] The cyclic voltammograms were recorded from 1 V to -1.5 V to 1 V vs. a non-aqueous Ag^+/Ag reference electrode in triplicate at 100 mV s^{-1}.

Stock solutions of electrolyte and analyte were prepared on the day of the experiment by first creating a 100 mM stock solution of TBAP dissolved in the solvent. The reference electrode was prepared by being filled with ~2 mL of 10 mM silver nitrate and 100 mM TBAP in the solvent used for the electrochemical experiment. Analysis solutions consisted of one vial of 100 mM TBAP in the solvent, three 5.0 mL samples of 2.0 mM analyte, 2.0 mM ferrocene, and 100 mM TBAP. Some samples were run without ferrocene in order to obtain voltammograms that were clear from potential interference of the $Fc^{+/0}$ redox chemistry on the redox chemistry of the vanadium complex.

All electrochemistry experiments were undertaken using the classic three-electrode setup. All electrodes were purchased from BASi Research products. The working electrode was a glassy carbon electrode (GC) with a 3.0 mm diameter (2.997 mm-2.972 mm) and an area of approximately 7 mm^2 (Catalog # MF-2012). The counter electrode was a platinum wire with a gold-plated connector mounted in a CTFE cylinder (Catalog # MW-1032). A non-aqueous silver(I)/silver/ (Ag^+/Ag) reference electrode consisted of a silver wire of 99.9% purity with a 0.5 mm diameter, is 30 cm long, and is contained within a double-junction reference electrode chamber with porous CoralPor™ tips, that are 1/8 inch long (Catalog # MF-2062). All solvents used for electrochemistry were dried on a Solv-Tek alumina drying column under argon to minimize water content.

Cell Culture and Growth Conditions. The well-established human glioblastoma multiforme cell line (T98g) and human foreskin fibroblast (HFF-1) cell lines were purchased from American Type Culture Collection (ATCC, Cat. No. CRL-1690 and SCRC-1041). Due to their limited life span in culture, HFF-1 cells were used at passages four to six. The cells were cultured in Advanced DMEM (Thermo Fisher Scientific Cat. No. 12491-015), supplemented with L-glutamine (2.0 mM), antibiotic-antimycotic mixture (100 U mL^{-1} penicillin, 100 mg mL^{-1} streptomycin and 0.25 mg mL^{-1} amphotericin B) and foetal calf serum (FCS; heat-inactivated; 2% vol). For proliferation and cytotoxicity experiments, cells were seeded in 96-well plates at an initial density of 1.5×10^3 viable cells per well in 100 µL medium and left to attach overnight.

Freshly prepared stock solutions of V(V) complexes (10 mM in DMSO) were used for cell assays. These solutions were further diluted so that all the cell treatments, including controls, contained 1.0% (vol.) of DMSO, which did not significantly affect the cell growth during the assays. Stock solutions of the treatment complexes were diluted with fully supplemented cell culture media to the required final concentrations, and the resultant media were either added to the cells within 1 min (fresh solutions), or left in cell culture incubator (310 K, 5% CO_2) for 24 h prior to the cell treatments (aged solutions).

Each treatment included six replicate wells with cells and two background wells without cells that contained the same components. After the addition of treatment complexes, the plates were incubated for 72 h at 310 K and 5% CO_2, then MTT reagent (1-(4,5-dimethylthiazol-2-yl)-3,5-diphenylformazan, Sigma M5655) was added (50 µL per well of freshly prepared 2.0 mg/mL solution in complete medium), and incubation was continued for 4-6 h. After that, the medium was removed, the blue formazan crystals were dissolved in 0.10 mL per well of DMSO, and the absorbance at 600 nm was measured using Victor V3 plate reader. Typically, the treatment complexes were applied in a series of nine two-fold dilutions, starting from (100 ± 20) µM V, plus the vehicle control. Exact V concentrations in the assays were verified by ICP-MS measurements using samples of cell culture media and used in the calculations of the IC_{50} values. Fitting of the experimental data and calculations of the IC_{50} values were performed using Origin 6.1 software (Microcal Origin, 1999). For all the cell assays, consistent results were obtained in at least two independent experiments using different passages of cells and varying stock solutions of the treatment complexes.

Results and Discussion

Design of new vanadium Schiff base complexes. Pecoraro and other groups have reported several Schiff base vanadium(V) catecholate complexes, and carried out limited characterization exploring the scaffold and a number of derivatives.[22, 46-47, 49] We have previously showed that increased hydrophobicity and steric bulk of the catecholato ligand improved cytotoxic properties of vanadium complexes with the di *t*-butyl catechol complex being the most potent.[7, 32] Here we report solution characterization and anticancer properties of three new derivatives in a new class of Schiff base V-catecholate complexes with the addition of a single electron withdrawing group (EWG) group on the Schiff base scaffold. These complexes were developed to modify parent complex stability, hydrophobicity, and redox properties. However, as we discovered with multinuclear NMR spectroscopic studies in several organic solvents, these complexes form rapidly interconverting isomers in solution. Our structural studies of solution species complement the previous solid-state structures reported by the Pecoraro group and others.[32, 46, 49, 52, 58-59]

Syntheses of Chloro Schiff Base V(V) Catecholato Complexes. The Schiff base V(V) precursor complex, $[V(O)_2(Cl\text{-}HSHED)]$, was synthesized using a similar procedure as for the $[V(O)_2(HSHED)]$ precursor.[7, 46] The Schiff base was first formed from a condensation reaction between chlorosalicyaldehyde and ethylenediamine which was then reacted in situ with vanadyl sulfate to form the vanadium scaffold, which was isolated as a solid after the addition of two equivalents of NaOH. Isolation of the Schiff base ligand was found to be less optimal because the ligand did not store well and subsequently led to less pure and lower yielding V-complexes. In contrast the solid vanadium Schiff base scaffold complex stored well, and it was reacted with a catechol ligand to form the desired vanadium catecholato complex in higher yields. In the catecholato complex synthesis, there was an immediate color change upon addition of the catechol for the chloro-substituted system, but for the parent catechol system it took a few minutes. Prior protocols reduced the volume of organic solvent before the solution was let stand overnight at -20 °C. Here, we reduced the solution to dryness by rotary evaporation, re-dissolved the solid in minimal acetone, and then added 100 mL of hexane to the solution before allowing the mixture to stand overnight at -20 °C with yields increasing from 40% vs. 80%.[22, 46] The higher yields were attributed to the increased reaction times and changes in the crystallization conditions. The [$V(O)_2$(Cl-HSHED)] complex was a paler yellow than [$V(O)_2$(HSHED)] and the halogenated-Schiff base/catecholato complexes were deep purple like the complexes with the unsubstituted Schiff base. These Cl-HSHED complexes were characterized using UV-Vis spectrophotometry, multinuclear NMR spectroscopy, electrochemistry, and MS-ESI spectrometry, as described in detail below.

Lipophilicity and P-value. The lipophilicity of the V-compounds can be measured as a partition between an lipophilic organic phase, generally octanol, and a polar aqueous phase as reported previously.[67-68] The partitioning P-value is an important measure of cell uptake and useful information in addition to the antiproliferative activity of these compounds. The problem with such measurements is that they are based on compounds that are hydrolytically stable, and hence this experiment is difficult to conduct on compounds that hydrolyze within a few minutes and such experiments would be meaningless.[7, 32, 36] We therefore carried out the shake-flask method studies monitoring the partitioning using UV-visible spectroscopy only on the V-complexes with sterically hindered catecholates, [VO(HSHED)(DTB)] and [VO(Cl-HSHED)(DTB)].[67-68] The results were at ~200µM, the parent complex separates into 0.6 % in the water phase and 99.4% in the octanol phase, giving P = 160 and log*P* 2.2 and the chloro-substituted complex separated into 1.3% in the water phase and 98.7% in the *n*-octanol phase, giving P = 75 and log*P* = 1.9.[67-69] We observed that the parent complex was more hydrophobic than the chloro-substituted complex by 0.6%. However, it should be noted that it is difficult to measure the low concentration of complex in aqueous solutions, and that the observed ratios are a lower limit of the data.

To get a better understanding of the effects of the lipophilicity of the compounds that are readily hydrolyzed we turned to computational methods which have been found to be successful in the analysis of a wide range of organic compounds.[69] We used the website Chemicalize to estimate the log*P* values (Figure 2[69-71]) for the V(V) structures shown in Figure 2.2.[7, 46,57] Since this program was developed for organic molecules, its use requires the assumption that a covalent bond can approximate a coordinate bond description in these metal complexes. Since all the complexes contain the same coordinate bonds, this method should be able to estimate the relative differences in these metal complexes. As anticipated, the larger the alkyl group (CH_3 and ^{t}Bu) were on the catecholato ligand, the more hydrophobic were the complexes. The addition of the 4-chloro-substituted Schiff base ligand increased the hydrophobicity of the [VO(Cl-HSHED)(Cat)] to be comparable to that of [VO(HSHED)(3-MeCat)] as the chloro and the methyl groups are similar in size and effects in an aromatic system. Accordingly, the chloronated Schiff base V-catecholato complexes were estimated to be slightly more hydrophobic than their unsubstituted analogs. As shown in Figure 2.2, the hydrophobicity estimated range from 1-4.5 (the yellow area) is based on Lipinski's rule of five.[70-71] Furthermore, comparing these estimations with the experimental values obtained for [VO(HSHED)(DTB)] and [VO(Cl-HSHED)(DTB)] we find that the patterns observed with Chemicalize is as observed experimentally using the shake-flask method. However, the calculated values are larger than the experimental values but within the range for most common drugs.

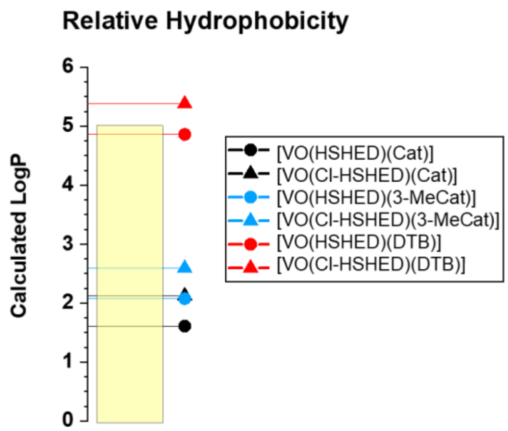

Figure 2.2. Relative Hydrophobicity was estimated using log*P* values from Chemicalize calculations, by ChemAxom.[57] These calculations required the assumption that a covalent bond description can approximate a coordinate bond in these metal complexes. The yellow box shows hydrophobicity regions where most complexes are found to penetrate living cells based on Lipinski's rule of five.[70-71]

Characterization of Vanadium Schiff Base Catecholate Complexes in DMSO. The UV-Vis spectra of the halogenated complexes and the parent complexes (0.10 mM, DMSO) exhibited maxima at approximately 390, 550, and 850 nm (Figure 2.3) with $\boldsymbol{\lambda}_{max}$ and $\boldsymbol{\varepsilon}_{\mathbf{max}}$ listed in Table 2.1. The [VO(Cl-HSHED)(DTB)] and [VO(Cl-HSHED)(3-MeCat)] complexes had higher extinction coefficients than the parent complexes. For the Cl-HSHED and the HSHED complex with the unsubstituted catechol, no difference in the λ_{max} was observed. This data reflects the stabilizing effects the halogen substituent imparts on the alkyl substituted catecholate complexes and the corresponding observed differences in the HOMO and LUMO orbital of these complexes responsible for the observed absorption properties of the molecules.[22, 52]

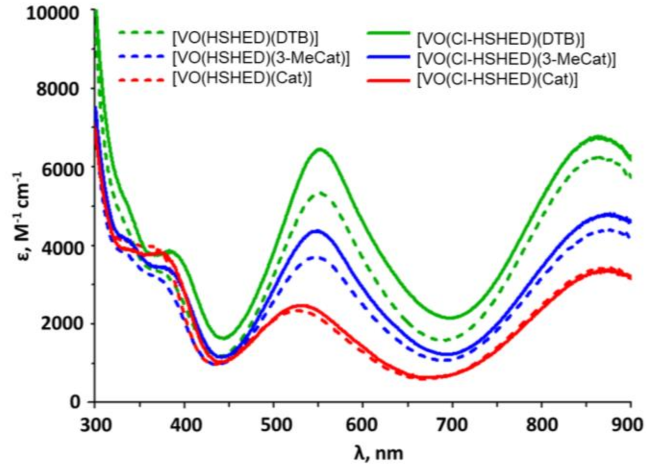

Figure 2.3. UV-Vis spectra of the halogenated V(V) complexes [VO(Cl-HSHED)(R)] and the parent complexes [VO(HSHED)(R)] recorded at 0.10 mM V in DMSO.

Table 2.1. Band Positions and Corresponding Extinction Coefficients of the [VO(HSHED)] and [VO(Cl-HSHED)] compound series

Compound	**λ_{max}**	**ε (M^{-1} cm^{-1})**	**λ_{max}**	**ε (M^{-1} cm^{-1})**
[VO(Cl-HSHED)(DTB)]	552 nm	6.5×10^3	863	6.8×10^3
[VO(Cl-HSHED)(3-MeCat)]	549 nm	4.4×10^3	873	4.8×10^3
[VO(Cl-HSHED)(Cat)]	531 nm	2.5×10^3	873	3.4×10^3
[VO(HSHED)(DTB)]	551 nm	5.3×10^3	861	6.2×10^3
[VO(HSHED)(3-MeCat)]	546 nm	3.7×10^3	875	4.4×10^3
[VO(HSHED)(Cat)]	528 nm	2.3×10^3	873	3.4×10^3

Characterization of [VO(X-HSHED)(DTB)], [VO(X-HSHED)(Cat)], and [VO(X-HSHED)(3-MeCat)] by ESI-MS. Mass-spectrometric characterization of the new V(V) complexes was particularly important because the elemental analysis proved problematic presumably due to the highly hygroscopic nature and air-sensitivity of the isolated solids. Low-resolution ESI-MS data (positive-ion mode) for the newly synthesized Cl-HSHED complexes and their parent HSHED complexes are shown in Figure 2.4, and assignments of the main signals are given in Table 2.2.[15, 46] Prominent signals of all the intact complexes were observed in the form of their

Na^+ or K^+ adducts (Table 2.2), and the identities of these signals were confirmed by high resolution mass spectrometry, where the same complexes were observed as H^+ adducts (see Figures S2.9-12). These results confirm the composition of intact [VO(Cl-HSHED)(DTB)], [VO(Cl-HSHED)(Cat)], and [VO(Cl-HSHED)(3-MeCat)] and the formation of the new halogenated Schiff-base (Cl-HSHED) V(V) complexes.

Extensive decomposition of all the complexes was observed under ESI-MS conditions (Figure 2.4 and Table 2.2). Relative intensities of signals due to decomposition products decreased when milder ionization conditions were employed (Figure 2.4b vs 2.4a), which showed that decomposition of the original V(V) complexes occurred in the gas phase in

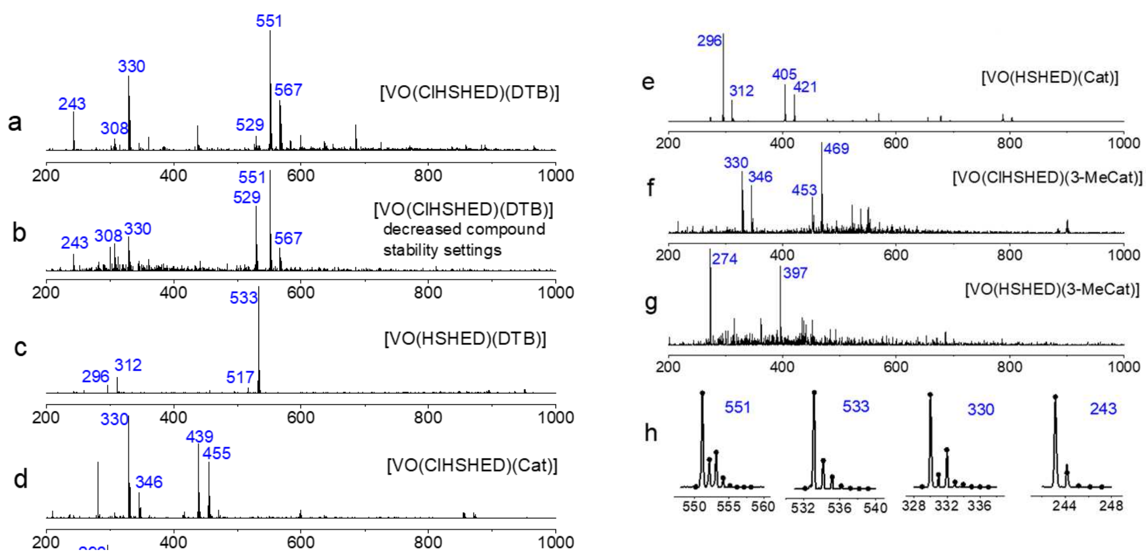

Figure 2.4. Typical positive-ion low-resolution ESI-MS data for V(V)-Schiff base-catecholato complexes (a-g; ~10 µM solutions in acetonitrile, m/z values in positive ion mode) and (h) experimental (lines) and fitted (points) isotopic distributions for selected signals. The assignment of the marked signals is shown in Table 2.2.

addition to decomposition in solutions. Analysis of the decomposition products (Table 2.2) showed that redox chemistry of V(V)-Schiff base-catecholato complexes is taking place. Oxidation of catechols is known to occur in solution and is also observed in the gas phase now.[7, 9, 30, 32, 72]

Oxidation of catechols may be observed under some biological conditions in the presence of oxygen and metal complexes.

Table 2.2. Assignment of ESI-MS signals for the complexes and their decomposition products

Schiff base V-Complex / Catechol (C)/[a] / Fragment	[VO(Cl-HSHED)(DTB)][b]	[VO(HSHED)(DTB)][b]	[VO(Cl-HSHED)(Cat)][b]	[VO(HSHED)(Cat)][b]	[VO(Cl-HSHED)(3-MeCat)][b]	[VO(HSHED)(3-MeCat)][b]
[VO(Cl-HSHED)(C[c])]·K^+	567	533	455	421	469	-
[VO(Cl-HSHED)(C[c])]·Na^+	551	517	439	405	453	-
[VO(Cl-HSHED)(C[c])]·H^+	529	-	-	-	-	397
[V(OH)(Cl-SHED)]·K^+	-	312	346	312	346	-
[V(OH)(Cl-SHED)]·Na^+	330	296	330	296	330	-
[V(OH)(Cl-SHED)]·H^+	308	--				274
C[c]·Na^{+d}	243					

[a] Designations of the ligands correspond to those listed in Figure 1. [b] The *m/z* values (positive-ion mode) correspond to the most abundant peaks in the isotope distribution (blue numbers in Figure 1a-g). [c] The catechol derivative abbreviations [c] represent DTB, Cat, or 3-MeCat depending on the compound investigated. [d] Signal is due to quinone, the oxidation product of catechol.

Characterization by ^{51}V and ^{1}H NMR spectroscopy. ^{51}V NMR spectroscopy was used to demonstrate that interconverting isomers formed in solution at ambient temperature. Specifically,

^{51}V NMR spectra of 1.0 mM solutions of the Cl-HSHED/catecholato complexes in CD_3CN and in d_6-DMSO showed more than one signal. We verified that these multiple signals were not due to impurities or hydrolysis product by concentration and time dependent studies in different solvents. In addition, no ^{51}V NMR signal assigned to the vanadium precursor complexes, [V(O)$_2$(HSHED)] and [V(O)$_2$(Cl-HSHED)] were present in CD_3CN at -530 ppm and −531 ppm, respectively. Similarly, the ^1H NMR signals of these precursors were also absent in the corresponding spectra of the catecholato complexes though similarly to the ^{51}V NMR, we note that the signals are broad possibly also showing a reduction of V(V) to V(IV).

The multiple signals for each compound shown in Figure 2.5 varied in ratio as solvent is changed as described below and consistent with the various peaks representing different isomers.

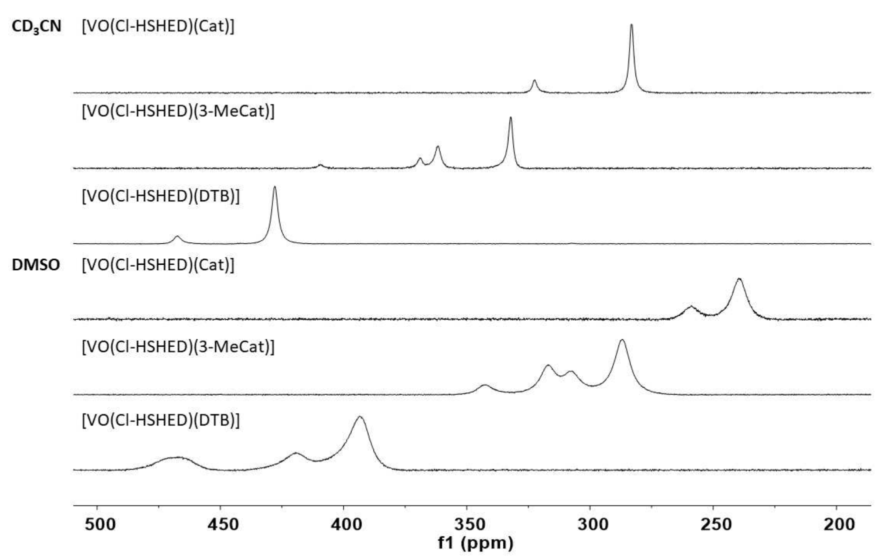

Figure 2.5. ^{51}V NMR (400 MHz) of [VO(Cl-HSHED)(Cat)], [VO(Cl-HSHED)(3-MeCat)], [VO(Cl-HSHED)(DTB)] in CD_3CN and d_6-DMSO.

The combination of the Schiff base and the catechol have the potential to form multiple racemic and diastereomeric complexes and in Figure 2.6 we show four of eight possible geometric isomers. Spectra for [VO(Cl-HSHED)(Cat)] in CD_3CN (Figure 2.5) showed a sharp prominent peak at 283 ppm, and a minor peak at 323 ppm. When dissolved in d_6-DMSO, the peaks were shifted to 238 ppm and 259 ppm, respectively, a shift of about 50 ppm and the linewidths increased consistent with a more rapid exchange in d_6-DMSO. For the catecholate complex, in CD_3CN, the ratio of major to minor peaks was 5:1, and in d_6-DMSO, the ratio was 3:1. The change in isomer ratio is indicative that the signals are due to exchanging isomers. In the case of [VO(Cl-HSHED)(DTB)] in CD_3CN, a difference of about 200 ppm with a significant peak at 428 ppm and a minor peak at 468 ppm was observed. In d_6-DMSO [VO(Cl-HSHED)(DTB)] three signals are observed, a major peak at 394 ppm, and two other minor overlapping peaks of comparable intensity at 420 and 469 ppm.

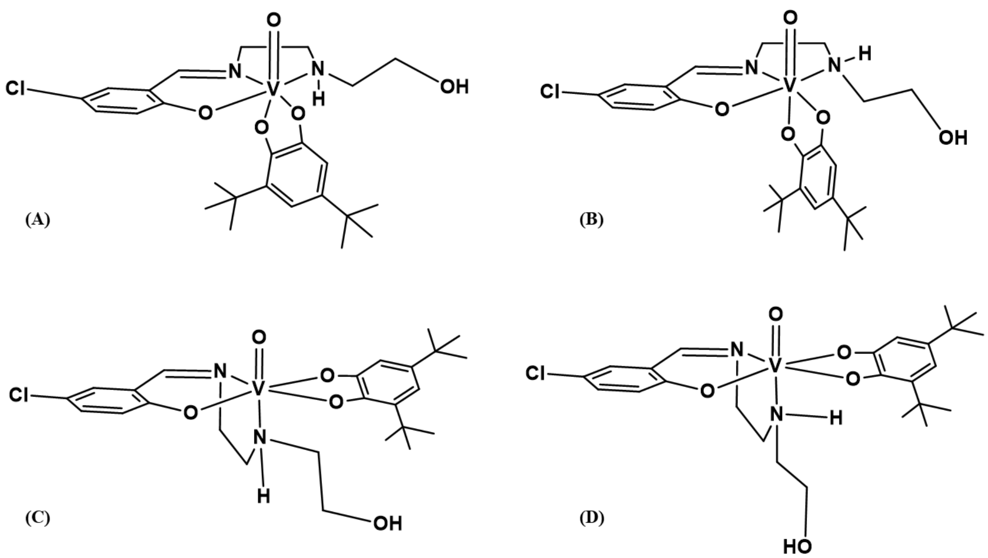

Figure 2.6. Four of the possible isomers of [VO(Cl-HSHED)(DTB)] are shown with the major isomer illustrated as structure A. The structures vary with how the Schiff base is coordinated to the vanadium and the stereocenter of the alkyl amine. Note that each of the isomers shown in Figure 6 are chiral and racemic mixtures form in solution, even though only one isomer is shown.

The changes in chemical shifts and the different number of isomers formed for [VO(Cl-HSHED)(DTB)] suggest that the complexes are labile in solution. Furthermore, the differences in linewidths in the two solvents are consistent with the kinetics of the isomer exchange in two different solvents, which confirmed that these signals are due to isomers and not impurities or hydrolysis products. Finally, similarly for the complex with the asymmetric DTB ligand, [VO(Cl-HSHED)(DTB)], that with the asymmetric 3-MeCat ligand, [VO(Cl-HSHED)(3-MeCat)] showed four signals in the ^{51}V NMR spectra in both solvents which are attributed to four isomers. The ^{1}H NMR spectra confirmed the interpretation that isomers are observed for the catecholate complex, the DTB complex, and the 3-MeCat complexes in solution.

The 2D NMR spectra were recorded in CD_3CN and d_6-DMSO, and selected spectra in CD_3CN are shown in Figures 2.7-2.9, and in S2.2c in SI. To assign the protons in the conformation of [VO(Cl-HSHED)(Cat)], ^{1}H-^{1}H 2D COSY and the ^{1}H-^{1}H 2D NOESY were run in d_3-CD_3CN and $d_6$$^{-}$DMSO. The NMR spectra contained groups of larger signals and groups of smaller signals, as anticipated for a compound with both major and minor isomers in solution but we focused on the assignment of the major isomer by identifying the three spin systems (X, Y and Z) in the compound. Figure 2.7 shows the labeled [VO(Cl-HSHED)(Cat)]. Based on integrations in the ^{1}H, the cross peaks in the COSY, and the fact that H_c and H_d had coupling constants NMR spectra and correlations in the COSY (Figure 2.7B), we assigned H_a as the proton on the imide and H_b, H_c and H_d are defined as splitting system X (the Schiff base). These assignments had a coupling constant of 8.9Hz. This left the assignments of the signals for H_f and H_e on splitting system Y, which showed that both protons had a coupling constant of 8.1Hz. The slightly larger integration of the H_f signal is due to overlapping signals from the minor isomer.

The ^{1}H-^{1}H COSY NMR spectra of the aliphatic region of [VO(Cl-HSHED)(Cat)] (Figure 2.7C) displayed cross-peaks between H_q and $H_{v/w/x}$, which corresponded to the proton on the imine and one of the protons on the 1,2-ethanediamine chelate ring adjacent to the imide (H_y) and the H_w and H_x on the ethanol arm in spin system Z. Furthermore, the coupling between the triplet at 2.8

ppm (H_r) and $H_{y/z}$ were assigned to the proton on the oxygen (H_r) and the adjacent downfield protons H_y and H_z that corresponded to the CH_2 adjacent to the OH group. Since H_y sees H_z, H_w and H_x the ethanol arm spin system is defined. The fact that both H_w and H_x interact with the NH (H_q) confirms these protons are adjacent to the amine nitrogen in the same splitting system.

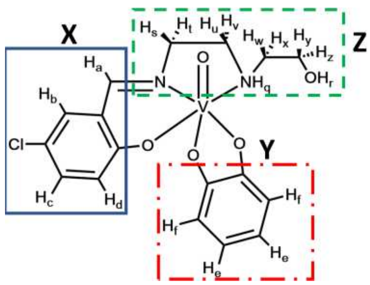

[VO(Cl-HSHED)(Cat)]

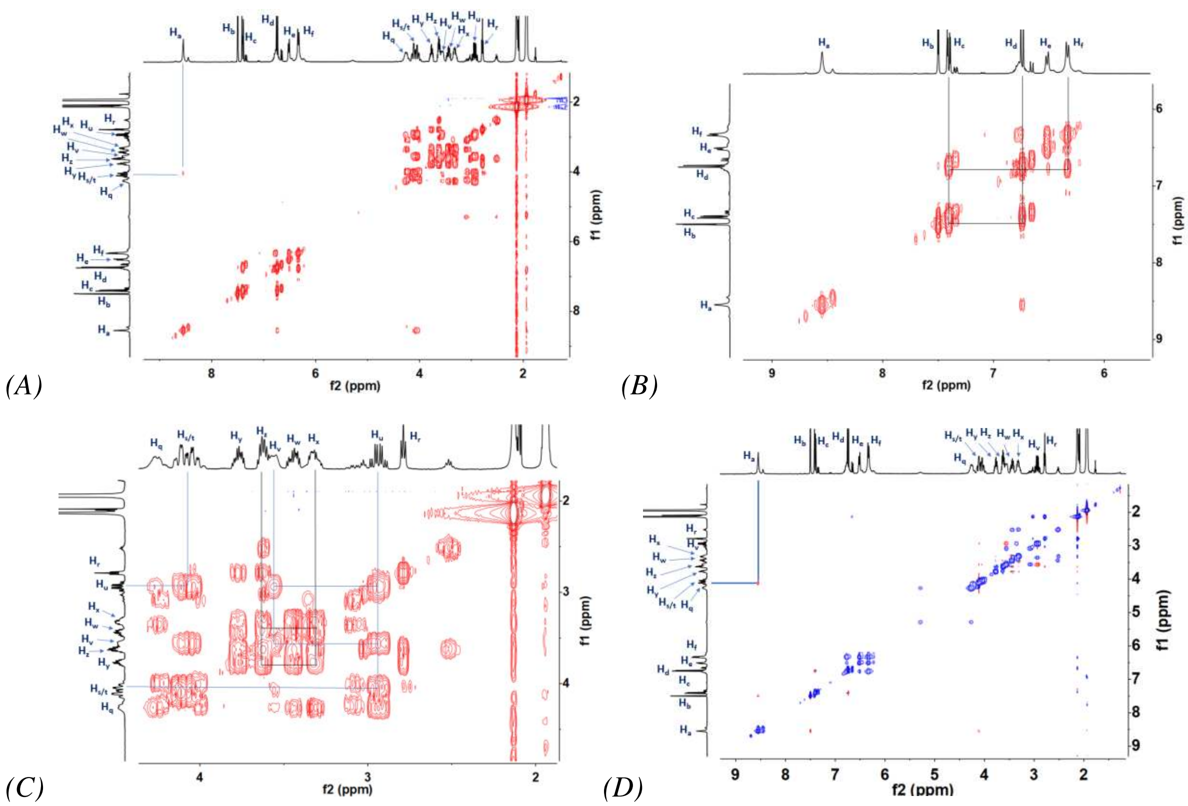

Figure 2.7. The structure of [VO(Cl-HSHED)(Cat)] with the three spin systems X, Y and Z is shown. ^1H-^1H COSY and ^1H-^1H NOESY NMR (400MHz) spectra of 10 mM [VO(Cl-HSHED)(Cat)] in CD_3CN at 26 °C. (A) Full ^1H-^1H COSY NMR spectrum of [VO(Cl-HSHED)(Cat)] in CD_3CN. (B) Zoom in of aromatic region ^1H-^1H COSY NMR spectrum of [VO(Cl-HSHED)(Cat)]. (C) Zoom in of aliphatic region ^1H-^1H COSY NMR spectrum of [VO(Cl-HSHED)(Cat)]. (D) Full ^1H-^1H NOESY NMR spectrum of [VO(Cl-HSHED)(Cat)] in CD_3CN. Blue intensity contours represent negative NOEs and red intensity contours represent positive NOEs. A standard NOESY sequence was used consisting of 200-256 transients with 16 scans in the f1 domain using a 500 ms mixing time and a 1.5 s relaxation delay. The structure of [VO(Cl-HSHED)(Cat)] is shown with a proton labelling scheme.

NOESY NMR spectra were collected to gather information on through-space interactions through spin-lattice relaxation within the 3D structure. Observation of off-diagonal cross-peaks between signals in Figure 2.9b enabled reports on which protons are within the 5 Å.[73] The NOESY of [VO(Cl-HSHED)(Cat)] Figure 2.7d, H_a saw $H_{s/t}$ which showed that the 1-2-ethanediamine chelate ring saw the imine nitrogen. In the case of [VO(Cl-HSHED)(DTB)], the spectra showed less clear coupling patterns (Figures 2.8 and 2.9). Since coupling was observed with both the OH proton and the NH proton, ^1H NMR spectra were recorded with these groups deuterated with the

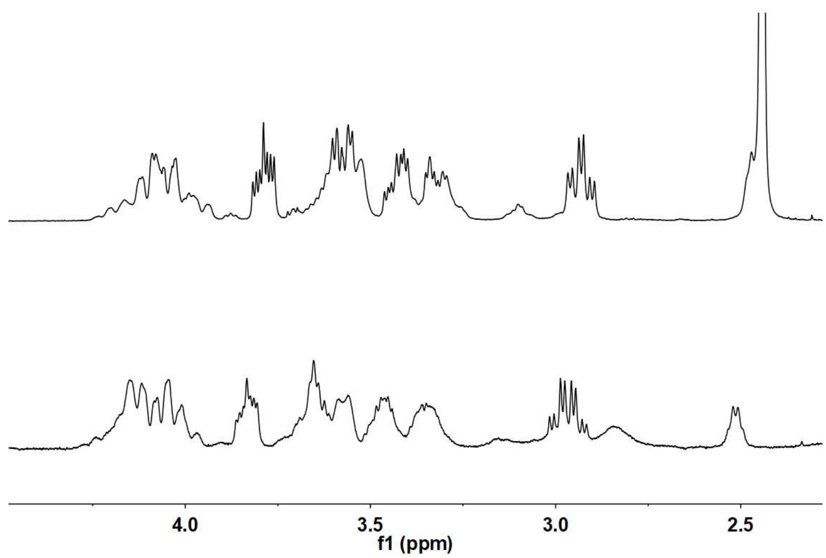

Figure 2.8. ^1H NMR (400 MHz) spectrum of 1 mM [VO(Cl-HSHED)(DTB)] from the 2.0-4.5 ppm in CD_3CN (bottom) and in CD_3CN with one drop of D_2O (top).

intent to clarify the observed coupling patterns (Figure 2.8). Deuteration simplified the coupling pattern and spin system was divided into two spin systems; in the partial spectrum shown in Figure 2.8 from 2.0-4.5 ppm of [VO(Cl-HSHED)(DTB)] with and without the D_2O spike show simplification of the doublet quartet (near 3.0 ppm) and the multiplet from 4.0 to 4.2 ppm. The full spectra under these conditions are added in the supplemental material (Figure S2.5), as well as the detailed interpretation of the two spin systems formed from spin system Z both in the 1D and 2D spectra. Not only did the D_2O remove the exchangeable OH and NH protons, but the integrations and the resolution of the remaining coupling patterns were simplified which enabled a more reliable interpretation of the spectra.

For [VO(Cl-HSHED)(DTB)], based on integrations in the ^{1}H NMR spectra and correlations in the COSY (Figure 2.9a, 2.9b and 2.9c), H_a was assigned as the proton

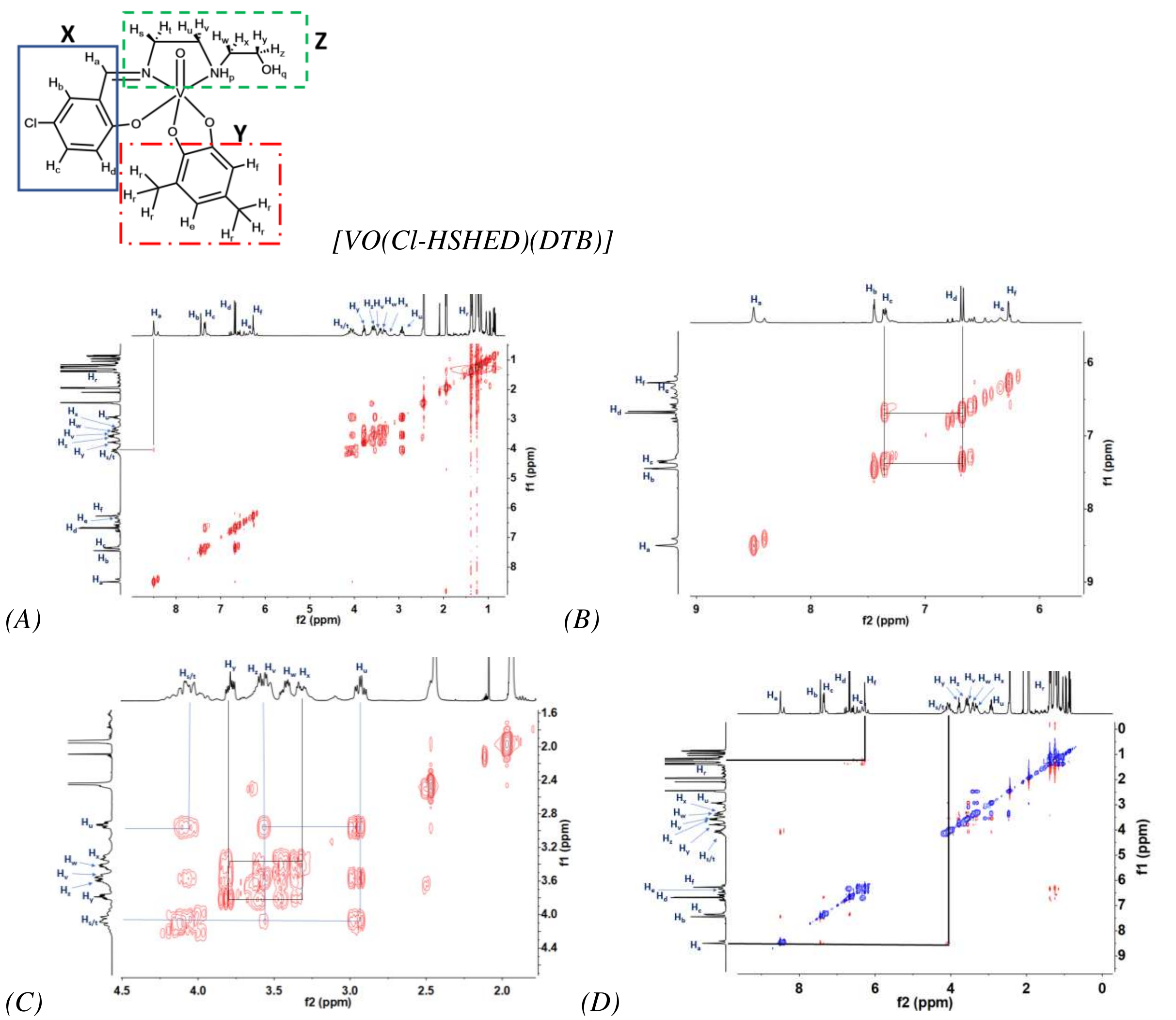

Figure 2.9. The structure of [VO(Cl-HSHED)(DTB)] with the three spin systems X, Y and Z is shown. ^{1}H-^{1}H COSY and ^{1}H-^{1}H NOESY NMR (400 MHz) spectra of 10 mM [VO(Cl-HSHED)(DTB)] in CD_3CN and a D_2O spike at 26°C. (A) Full ^{1}H-^{1}H COSY NMR spectrum of [VO(Cl-HSHED)(DTB)] in CD_3CN. (B) Zoom of aromatic region ^{1}H-^{1}H COSY NMR spectrum of [VO(Cl-HSHED)(DTB)]. (C) Zoom of aliphatic region ^{1}H-^{1}H COSY NMR spectrum of [VO(Cl-HSHED)(DTB)]. Zoom of aromatic region ^{1}H-^{1}H COSY NMR spectrum of [VO(Cl-HSHED)(DTB)]. (D) Full ^{1}H-^{1}H NOESY NMR spectrum of [VO(Cl-HSHED)(DTB)]. Blue intensity contours represent negative NOEs and red intensity contours represent positive NOEs. A standard NOESY sequence was used consisting of 200-256 transients with 16 scans in the f1 domain using a 500 ms mixing time and a 1.5 s relaxation delay. The structures of [VO(Cl-HSHED)(DTB)] are shown with a proton labelling key.

on the imine (8.48 ppm) on spin system X. H_b was assigned as the doublet at 7.45 ppm, and H_c as the doublet of doublets at 7.36 ppm. The extra smaller peaks in the NMR such as the peak at 8.39 ppm arose from another isomer in solution. H_d was assigned as the doublet at 6.68 ppm and completed the spin system X (the Schiff base aromatic ring). The H_e and H_f protons were assigned to the peaks at 6.34 ppm, and 6.26 ppm on spin system Y (the catechol). Cross-peaks observed between H_a and $H_{s/t}$ were similar to those of [VO(Cl-HSHED)(Cat)] at 4.10 ppm and 4.02 ppm in the ^{1}H-^{1}H 2D COSY and NOESY, which enabled the aromatic part of the spectrum to be linked to the solution assignments for the aliphatic region on spin system Z. Specifically, the NOESY NMR spectrum collected from [VO(Cl-HSHED)(DTB)] enabled the determination of the proximity between protons in the two aromatic regions and between aromatic and aliphatic regions, and between five-membered aliphatic ring and ethanol group. For instance, a NOE cross peak between H_d and H_r, showed a close vicinity between the Schiff base aromatic group and the *t*-Bu protons. Cross-peaks between H_r and $H_{y/z}$ showed a close proximity between these two aliphatic protons and showed that one *t*-Bu group was near the CH_2OH group.

In summary, as shown in Figure 2.6, the most likely isomers are structures A and B for [VO(Cl-HSHED)(DTB)] observed in a CD_3CN solution. The isomer interchange is consistent with the catechol dissociating in a stepwise manner; first, the axial Cat-O-bond will break. Next the cat ligand will rotate, followed by a bond reformation to form an equatorial Cat-O-bond. This process would correspond to conversion of isomer A into an isomer not shown. The NOESY and COSY spectra of [VO(Cl-HSHED)(DTB)] are consistent with the 1D ^{51}V NMR and the ^{1}H NMR spectra, in that the DTB catechol is labile. This gives rise to multiple isomers in solution as shown by the NMR spectra in Figure 2.5. The focus on the spectrum illustrated in Figure 2.6A is structure elucidation of the [VO(Cl-HSHED)(Cat)] complex where the *t*-Bu groups are replaced by H-atoms. Finally, for the [VO(Cl-HSHED)(3-MeCat)] complex, both ^1H-^1H 2D COSY and a NOESY were collected and shown in the Supplemental Materials (Section S2.2c). As in the cases of [VO(Cl-HSHED)(Cat)] and [VO(Cl-HSHED)(DTB)], major and minor isomers were visible in the ^{51}V NMR spectra. Four isomers were observed in the ^{51}V NMR spectra for the [VO(Cl-HSHED)(3-MeCat)] complex, three of which were also observed in the ^1H NMR spectra, making this system more difficult to interpret. The NMR spectrum was simplified by spiking the sample with a drop of D_2O to remove coupling across the heteroatoms. In summary, these spectra are consistent with the interpretations that multiple isomers are being formed in solution, and that for this complex, the minor isomers were more stable and had higher relative concentrations with respect to the major isomer than for the [VO(Cl-HSHED)(Cat)] and [VO(Cl-HSHED)(DTB)] complexes.

Electrochemistry of non-innocent ligand [VO(Cl-HSHED)] complexes in CH_3CN. The redox chemistry for these non-innocent vanadium complexes was particularly interesting because the reduction could happen at either the ligand or the vanadium center. The values are reported vs. Fc^+/Fc and also reported against the decamethylferrocenium/decamethylferrocene redox couple ($Me_{10}Fc^+$/$Me_{10}Fc$, SI). While Fc^+/Fc is the IUPAC redox standard and more prevalent in the literature, the $Me_{10}Fc^+$/$Me_{10}F$ standard is less solvent dependent and, hence, more useful to translate the results in organic solution to aqueous solution where the vanadium complexes were too unstable to conduct the redox chemistry of relevance to the biological studies.[74-75] CVs are measured in acetonitrile, which provides a large solvent window with excellent solubility of the vanadium complexes with 0.1 M tetrabutylammonium perchlorate (TBAP) as the supporting electrolyte and ferrocene as the internal standard.[51] Solutions of 2.0 mM vanadium complexes, 2.0 mM ferrocene, and 100 mM TBAP CVs were recorded at 100 mV s^{-1} (Figure 2.10).

Spectroelectrochemical data were also obtained to further characterize these complexes, see SI Section 2.4.e.

Two quasi-reversible waves were observed, one involving the catechol between 0.0 V and 1.0 V and the other showing the V(V/IV) couple at ~–0.7 to –0.8 V vs Fc^+/Fc.[74-76]

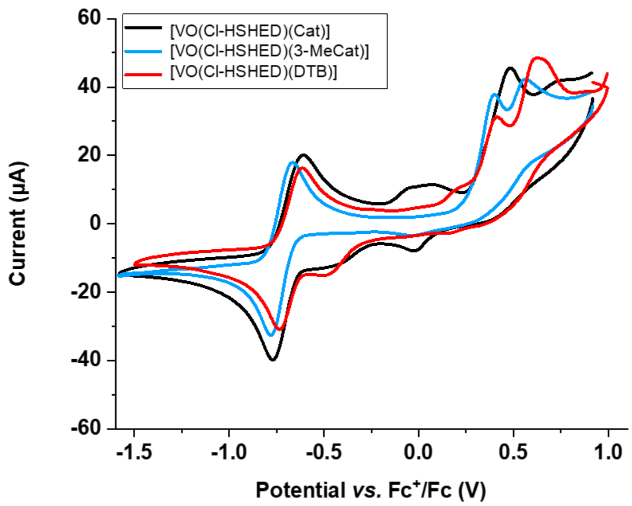

Figure 2.10. Superimposed cyclic voltammograms of 2.0 mM of [VO(Cl-HSHED)(Cat)], [VO(Cl-HSHED)(3-MeCat)], [VO(Cl-HSHED)(DTB)], 100 mM of TBAP in CH_3CN, run at 100 mV s^{-1}.

The voltammograms of the free catechol ligand (see SI) shows ligand oxidations in a similar region as for the complexes. The $E_{1/2}$ values are listed in Table 2.3 and in the SI. For these complexes, the observed chemically reversible redox couple in the –0.7 to –0.8 V region was consistent with reduction at the vanadium center and not the catechol. These values correspond to –0.17 to –0.30 vs $Me_{10}Fc^{+/0}$ acetonitrile, or close to 0 V in water vs the NHE, ignoring the solvent dependence of the V(V/IV) couple, which is less affected in comparing values in different solvents using measurements referenced vs $Me_{10}Fc^{+/0}$ than $Fc^{+/0}$.[74] Thus, the reduction potentials of the V(V) complexes are such that they are easily reduced by intracellular biological reductants.

As the substituent varied, so did the $E_{1/2}$ potential of the [VO(Cl-HSHED)] series and the [VO(HSHED)] series of complexes (Table 2.3). The most negative $E_{1/2}$ values reported for the complexes (most difficult to reduce) had the more electron donating catechol (Figure 2.10, Table 2.3). This showed that [VO(Cl-HSHED)(Cat)] was more readily reduced compared to the other Cl-HSHED and HSHED complexes. The vanadium center accepted electrons more readily for the complex with the catechol that was is less electron-donating (Cat) than 3-Me (3-MeCat) and 3,5-di-*t*-Bu (DTB) substituted catechols.[22] A similar pattern was observed for the parent complexes.

Table 2.3. $E_{½}$ potentials and other electrochemical data for the V(V/IV) couples of the Cl-HSHED and HSHED catecholate complexes averaged with standard deviations from three samples.[a]

Complex	$E_{½}$ vs. Fc^+/Fc (V)	ΔE_p (V)	D_{co} * 10^{-6} (cm^2 s^{-1})	I_{pa} (µA)	I_{pc} (µA)	I_{pa}/I_{pc} (µA)
[VO(Cl-HSHED)(Cat)]	-0.679 ± 0.002	0.17 ± 0.01	6 ± 2	31± 4	-31± 5	1.06 ± 0.09
[VO(Cl-HSHED)(3-MeCat)]	-0.709 ± 0.005	0.145 ± 0.003	5 ± 2	29 ± 4	-28 ± 5	1.02 ± 0.03
[VO(Cl-HSHED)(DTB)]	-0.782 ± 0.004	0.14 ± 0.03	5 ± 2	26 ± 2	-27 ± 4	0.98 ± 0.08
[VO(HSHED)(Cat)]	-0.698 ± 0.001	0.092 ± 0.003	21 ± 4	62 ± 12	-63 ± 12	1.00 ± 0.01
[VO(HSHED)(3-MeCat)]	-0.727 ± 0.001	0.089 ± 0.003	10 ± 3	38 ± 5	-38 ± 6	0.99 ± 0.05
[VO(HSHED)(DTB)]	-0.802 ± 0.002	0.159 ± 0.001	7 ± 1	34 ± 2	-36.55 ± 0.04	0.93 ± 0.04

[a.] Cyclic voltammograms ran at 100 mV s^{-1} in CH_3CN

The electronic structure of the vanadium is altered based on the electron-donating nature of the catecholate substituents, which was in turn directly observed in the V(V/IV) redox process in the CV, as was previously reported in the ligand-to-metal charge transfer bands in the absorption spectroscopy of similar mono-oxido vanadium complexes.[22, 52] When the catechol is deprotonated and coordinated to the vanadium, it is more readily oxidized than the free catechol. In addition, the electrochemical measurements showed differences between the complexes with the halogenated Schiff base ligand and those of the corresponding complex with the parent Schiff base, with the latter being somewhat more difficult to reduce.

This smaller Schiff base substituent effect compared to those on the catecholato ligands arose because of the change in the electronic structure, with the addition of an EWG Cl-atom on the vanadium scaffold. The substitution of the EWG Cl-atom involved effects in the σ framework of the vanadium complexes, as well as the backbonding in the π-framework, which depended on the nature of the catechol as there are two oxidation processes, one for the complex as well as for the ligand. The V(V/IV) couples were chemically reversible (I_{pa}/I_{pc} values between 0.90-1.05, Figure S2.16 and Table 2.3) but electrochemically quasi-reversible in CH_3CN as the peak-to-peak separations were large. These effects were not due to the lack of *iR* compensation in these measurements because the ΔE_p values were much larger than those for the $Fc^{+/0}$ couple under the same conditions.[22, 46-49] The diffusion coefficients were measured from the peak currents in the cyclic voltammograms at three different scan rates (See Section S4 for the equation). A pattern emerges that more substituted catechol complexes diffuse slower for both series of complexes. As expected, Similar diffusion values were observed for [VO(Cl-HSHED)(DTB)] and [VO(HSHED)(DTB)]. The diffusion rates are one of the factors that affect how rapidly, and the extent by which the complexes enter the cells by passive diffusion. Other factors include hydrophobicity and stability under biologically relevant conditions. For a similar hydrophobicity, the lower the diffusion rate, the slower the complex enters into the cell. This is an important factor to consider for these labile complexes. Similarities between diffusion constants between the two DTB complexes means that any differences in uptake are due to changes in hydrophobicity and stability in the media.

The observed large values of ΔE_p for the V(V/IV) couples compared to the $Fc^{+/0}$ couple under the same conditions were consistent with the presence of the geometric isomers that would have somewhat different redox potentials,[77] as the isomers in the ^{51}V NMR spectra have quite different chemical shifts and, hence, different electron densities at the V(V) centers. The equilibrium of different isomers for the V(V) and V(IV) oxidation states on the electrochemical timescales would shift between the two oxidation states because of changes in electronic and steric interactions (bond length changes). Therefore, the redox process was a weighted average of the reduction potentials of the V(V) isomers, whereas the oxidation process was the weighted average of the oxidation potentials of the V(IV) isomers, which complicated further interpretation of the electrochemical data with respect to one isomer. A study designed to sort out these details[77] is beyond the scope of the current work.

Anti-proliferative Activities of Vanadium Complexes. As described previously, we conducted experiments from freshly prepared solutions in which the Schiff base vanadium(V)-catechol complexes were intact at least initially. Activities were also examined with solutions that have complexes that had been decomposed for 24 h, at which time the complex had reacted completely with the components of the media.[7] At that time, the decomposed complex was added to the assay medium resulting in the measurement of the activity of completely decomposed complex. These experiments enabled a comparison of the activity of the intact complex and the products that formed on its decomposition.

The IC_{50} values were measured for T98g (human glioblastoma) cells in a 72 h assay of both fresh solutions of vanadium complexes and 24 h aged solutions in culture media. No intact complexes were detected after the incubation with cell culture medium after 24 h at 310 K (shown in Figure S2.24 in Supporting Information).[7] The most favorable activity ratio of fresh and aged was observed for [VO(HSHED)(DTB)] solutions and [VO(Cl-HSHED)(DTB)] solutions. Consistent with the earlier results,[7] fresh solutions of [VO(HSHED)(DTB)] showed higher activity (IC_{50} = 1.9 ± 0.2 μM in a 72 h assay, Table 2.4 and Figure S2.25 in Supporting Information) in T98g cells, while aged solutions of this compound were ~10-fold less active under the same conditions (Table 2.4).[7] All the complexes decomposed within minutes after having been added to cell culture buffer, as was observed using UV-Vis spectroscopy (see the $t_{1/2}$ values in Table 2.4). The activities of fresh solutions of [VO(HSHED)(DTB)] and [VO(Cl-HSHED)(DTB)] in T98g were about an order of magnitude higher than those of fresh solutions of Na_3VO_4 or a standard anti-cancer drug, cisplatin, in the same cell line (Table 2.4).

Table 2.4. Antiproliferative activities in T98g cells and stabilities under cell culture conditions for [VO(HSHED)] and [VO(Cl-HSHED)] complexes

Compound	**IC_{50}, μM**			
	T98g (fresh)[b]	**T98g (aged)**[c]	**HFF-1 (fresh)**[b]	**$t_{1/2}$ (295 K)**[a]
[VO(Cl-HSHED)(DTB)]	4.1 ± 0.5	9 ± 1	1.1 ± 0.1	~15 min
[VO(Cl-HSHED)(3-MeCat)]	34 ± 7	18 ± 3	22 ± 2	~15 s
[VO(Cl-HSHED)(Cat)]	19 ± 2	8.1 ± 0.6	8.7 ± 2	~15 s
[V(O)$_2$(Cl-HSHED)]	37 ± 4	67 ± 7	ND[d]	ND[d]
[VO(HSHED)(DTB)]	1.9 ± 0.2	21 ± 1	1.9 ± 0.4	~ 5 min
[VO(HSHED)(3-MeCat)]	46 ± 9	20 ± 5	26 ± 7	<15 s
[VO(HSHED)(Cat)]	19 ± 7	22 ± 4	6.7 ± 0.9	<15 s
[V(O)$_2$(HSHED)]	44 ± 4	70 ± 8	ND[d]	ND[d]
Na_3VO_4	26 ± 4	24 ± 4	23 ± 3	ND[d]
Cisplatin[7]	31 ± 1	>50	45 ± 4	

[a] Half-life times of the complexes in fully supplemented cell culture medium (measured by UV-Vis spectroscopy at 295 K, [V] = 100 μM, Figure S2.24 in Supporting Information). [b] IC_{50} values in T98g cells or HFF-1 (72 h treatments) when the complexes were mixed with cell culture medium at ~1 min (295 K) before the cell treatment. [c] IC_{50} values in T98g cells (72 h treatments) when the compounds were pre-incubated with cell culture medium for 24 h at 310 K, 5% CO_2 before addition to the cells. [d] Not determined due to the absence of prominent absorbance bands in the visible range (Figure S2.24). [e] Human foreskin fibroblasts.[78]

Generally, the complexes with Cl-HSHED ligand were slightly more stable in cell culture medium compared with those with HSHED ligand, and the complexes with DTB ligand were more stable than those with Cat and 3-MeCat ligands (Table 2.4). Despite a longer lifetime of [VO(Cl-HSHED)(DTB)] in cell culture medium compared with [VO(HSHED)(DTB)] (Table 2.4 and Figure S2.25a), the Cl-substituted compound was slightly less active (IC_{50} = 4.1 ± 0.5 μM for the fresh complex in a 72 h assay), and there was only ~2-fold difference in the activities of fresh and decomposed [VO(Cl-HSHED)(DTB)] (Table 2.4 and Figure S2.25a). These results showed that the Cl atom in the Schiff base ligand increased hydrolytic stability and ease of reduction but slightly decreased the biological activity of V(V) complexes (see Table 2.3, Figure 2.10 and Figure S2.25a). This demonstrates that stability alone is not the only factor that affects the biological activity. Further work is needed to understand the effects of the redox activity by investigating complexes that are less easily reduced compared to the control.

Since cancer cells exist in the presence of normal cells, it is important that the compounds being developed for treatment of cancer cells in the presence of normal cells, the compounds and the components (ligands and metal) show lower toxicity against the normal cells. Studies with cells in which the proliferative cell effects are investigated, are often accompanied with cells in a normal cell line. The cytotoxicities of V(V) complexes in a human brain cancer cell line, T98g, were compared with those in a human non-cancer (foreskin fibroblasts, HFF-1) cell line. Cytotoxicities of fresh compounds in 72 h assays were similar or higher in HFF-1 cells compared with T98g cells, judging from the IC_{50} values listed in Table 2.4. These results are consistent with the toxicity of anticancer drugs to rapidly growing non-cancer cells, including fibroblasts, which is the main source of side effects of cancer chemotherapy.[79] On the other hand, analysis of concentration-viability profiles (Supplemental Figure S2.25b) has shown that treatments of non-cancer HFF-1 cells with low concentrations (0.4-5 μM V) of fresh V(V) complexes for 72 h has led to increased cell viability (120-140%) compared with no-V controls. This effect was most pronounced for the two V(V) complexes with di-*tert*-butylcatecholato ligands ([VO(HSHED)(DTB)] and ([VO(Cl-HSHED)(DTB)]), to a lesser extent, in [VO(HSHED)(3-MeCat)] (Figure S2.25b).

Previously we demonstrated that the free ligands showed negligible cytotoxicity in the absence of V (IC_{50} > 50 μM).[7] We found that the greatest antiproliferative activities of the ligands were due to the catechols compared to the Schiff base scaffold. In the case of the normal human foreskin fibroblasts cell line HFF-1, and furthermore, we reported that they show medium cytotoxicity at 14.7 ± 0.5 μM for the [VO(HSHED)(DTB)] (Table 2.4).[7] The 10-fold higher cytotoxicity in the current study towards HFF-1 cells, 1.9 ± 0.4 μM, presumably reflect the fact that cytotoxicities of HFF-1 cells are more sensitive to the details of the experiment, such as number of cells, the doubling rates, the number of passages and other factors. The increase in cell viability at low V concentrations was not observed for the cancer T98g cell line (Figure S2.25a) but was reported previously for bone fibroblasts (osteoblasts) and can contribute to the known tissue-regenerating properties of V compounds.[80-83] Data within Figure S2.25b emphasize that the activities of anti-cancer drugs in various cell lines cannot be compared based on the IC_{50} values alone. Indeed, studies in other cells such as M.smeg. documented that the Schiff base scaffold and the catechols are at least 10-fold less toxic than the complex in *M. smeg.*.[55] These studies showed a 100-fold lower toxicity in M. smeg. than observed in the T98g cells.[55] Importantly, the most toxic catechol was the parent catechol and the sterically hindered catechols were much less toxic. This conclusion was confirmed in animal studies, in mice, that showed the complex was less toxic than vanadate and the DTB ligand.[34]

Typical IC_{50} values for the parent and Cl-substituted complexes that rapidly decomposed (~20-40 μM in 72 h assays, Table 4, those not containing the DTB ligand) were close to those of their decomposition products (~20 μM), and for Na_3VO_4 (~40 μM) in T98g cells. This was consistent with the interpretation that the complexes had decomposed in the medium before they had the opportunity to enter the cells by passive diffusion to any significant extent, and that V(V/IV) decomposition products were responsible for their antiproliferative activities.[7] In the case of [VO(Cl-HSHED)(Cat)], the decomposed complex was ~2-fold more active than the fresh solution (Table 2.4 and Figure S2.25b). This may be due to the redox reactions of the catechol ligand and V(V) in cell culture medium under ambient atmosphere generating a range of cytotoxic species, including V(V) peroxido complexes and semiquinone radicals.[84-87]

Relatively low antiproliferative activities (IC_{50} ~ 40 μM in a 72 h assay) were observed for fresh solutions of the Schiff base scaffold complexes (both $[V(O)_2(HSHED)]$ and $[V(O)_2(Cl\text{-}HSHED)]$ in Table 2.4). These complexes were both less potent after pre-incubation with cell culture medium for 24 h at 310 K (IC_{50} ~ 70 μM in a 72 h assay, Table 2.4). In contrast, anti-proliferative activity of a pre-incubated solution of Na_3VO_4 has similar potency as that of a fresh solution.[7] These results, together with the data of UV-Vis spectroscopy (Figure S2.24b) support the interpretation that the HSHED or Cl-HSHED ligands remain at least partially bound to V(V) for a sufficient time to enable some intact complex to enter cells for the DTB complexes during the cell assays but the complexes with the other catecholato ligands decompose too rapidly to enter cells intact (Figure S2.24a). These results are consistent with the interpretation that the observed greater toxicity of aged solutions of the [VO(Cl-HSHED)(Cat)], [VO(Cl-HSHED)(3-MeCat)] and [VO(HSHED)(3-MeCat)] complexes are due to the free catechol (or substituted methyl substituted catechol) reactions in the culture medium suggested above.

In summary, the three new complexes designed were more hydrophobic, more hydrolytically stable and more redox active than their HSHED analogs. The patterns observed for the [VO(Cl-HSHED)] series of complexes were similar to those for the [VO(HSHED)] complexes. Most importantly, the [VO(Cl-HSHED)(DTB)] and the [VO(HSHED)(DTB)] complexes were by far the anti-proliferative complexes in their respective series and an order of magnitude more potent than cisplatin under the same conditions. This observation confirms the fact that the most sterically hindered and hydrophobic complex in both series were most effective. However, the electronic effects are more difficult to evaluate because the electronic changes were accompanied by changes in hydrophobicity and sterics/stability. For the DTB complexes, the Cl-substitution made the complex more stable, hydrophobic and more easily reduced. The higher stability and greater lipophilicity of the complex with the Cl-substituted Schiff base scaffold should change its intracellular distribution in a way that influences antiproliferative activities beneficially. This suggested that future complex designs should focus on complexes less easily reduced than the parent complexes, since the ease of intracellular reduction may have been responsible for the reduced antiproliferative efficacy.

Conclusion

Developing new complexes and comparing their potency as anticancer agents will be important for structure-activity relationships for future complex development. Access to additional complexes will allow future studies on the anticancer mode of action of non-innocent Schiff base V-catecholate complexes. The newly synthesized [VO(Cl-HSHED)(Cat-X)] complexes where the catecholate is either Cat, 3-MeCat or DTB were characterized by UV-Vis, multinuclear and multidimensional NMR, MS-ESI and electrochemistry. The three new complexes designed and tested demonstrated that the sterically hindered, more hydrophobic and less easily reduced non-innocent Schiff base V-catecholato complex is the most potent antiproliferative complex, with the lowest IC_{50} for the fresh solutions, and a higher IC_{50} value for aged solutions. In summary, the studies of the three new complexes with Cl-substituted Schiff base scaffold and substituted catecholates have provided an additional example of an anticancer agent that superior to cisplatin in the T98g cell line. The observed activity ratio of fresh and decomposed solutions of the best of the new complexes, [VO(Cl-HSHED)(DTB)], showed similar improved activity compared to cisplatin as the parent [VO(HSHED)(DTB)] complex in the T98g cell line that is an in vitro model for difficult to treat gliomas. This antiproliferative activity is sensitive to the stability and hydrophobicity of the complex in biological media in both the parent and Cl-substituted Schiff base V-complexes. Our research has enhanced our knowledge and shown that the increased redox properties of the Cl-substituted complexes has not been favorable with regard to the complexes antiproliferative effects, but steric effects that increased hydrolytic stability of the complexes are important in optimizing the activity in both the HSHED and Cl-HSHED series.

Where does this leave us with regard to structure-reactivity relationships? In this work three new non-innocent vanadium Schiff base complexes were introduced, and the addition of the Cl-group improved stability, increased hydrophobicity and increased the ease of reduction of the complexes. Importantly our studies have introduced a second complex, [VO(Cl-HSHED)(DTB)], with potential for intratumoral injection. Such complexes should enter cancer cells by passive diffusion leading to rapid cancer cell death, while the non-toxic V(V/IV) decomposition products that diffuse away from the tumor cause no toxic effects to the healthy cells.[7, 35] One important aspect of the current work is that it has provided detailed characterization of the three new complexes introduced and combined with previous complexes allowed us to carry out a structure-activity analysis. We conclude that the limited stability and hydrophobicity of V(V)-Schiff base-catecholato complexes under cell culture conditions remains a crucial factor for the observed antiproliferative activity *in vitro*.[7, 10, 35] The ~10-fold decrease in the observed IC_{50} values and antiproliferative activities of [VO(HSHED)(DTB)] and [VO(Cl-HSHED)(DTB)] in cancer cell lines after its decomposition in cell culture medium (24 h at 310 K) remains an advantage for the potential use in intratumoral injections.[7] We hypothesize that rapid cellular uptake and rapid reactions within cancer cells in tumor tissue are likely to have beneficial effects in vivo.[7, 10, 35] However, since the introduction of the Cl-group did not lead to significant increase in antiproliferative effects compared to parent complex, the combined introduced changes in properties in the new series of complexes have not all been beneficial. Since increased stability and hydrophobicity have been reported to increase antiproliferative activity, the ease of reduction of these complexes may have counteracted the increased stability and hydrophobicity of the new complexes, and/or the increased stability and changes in hydrophobicity may have affected intracellular biodistributions, yielding complexes with somewhat less activity. Combined our analysis led us to continue to identify stability and hydrophobicity as key factors to be targeted in the future design of these complexes and that decreased ease of reduction may improve anticancer effects of complexes.

Chapter 3 - The vanadium Schiff base di-adamantyl catecholate complex with potent anticancer activities

Introduction-

Non-innocent V-Schiff base complexes were recent investigated for their anticancer properties with specific application for intratumoral applications.[7, 35] Members of the class of compounds were designed to remain intact long enough to enter the cancer cells but react quickly when injected directly into a tumor and then rapidly decompose to non-toxic components within 24 hours. The most hydrophobic and stable complex of the series of compounds that was found to be most potent and significantly more potent than cisplatin against T98g (glioma multiforme) brain cancer cells was the vanadium Schiff base complex with the di-*tert*-butylcatecholato ligand abbreviated [VO(HSHED)(DTB)], Figure 3.1A.[7, 32, 35-36] Considering that there is always a need for new and potent anticancer agents, in this work, a new potential anticancer agent is introduced belonging to the class of non-innocent V-complexes, vanadium Schiff base complex with the di-adamantyl catecholato ligand abbreviated VO(HSHED)(Ad), Figure 3.1B. We believe that the increased steric bulk over the di-*tert*-butylcatecholato would increase the potency against T98g cells.

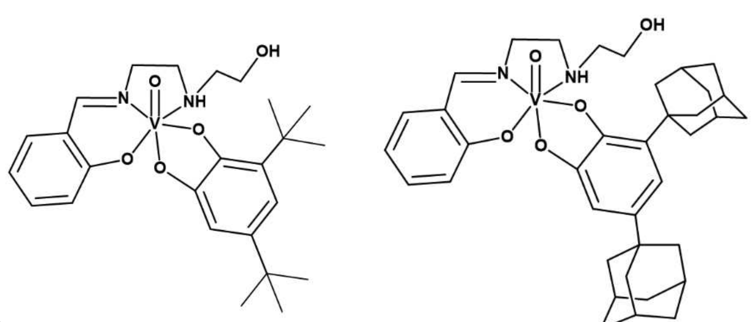

A) B)

Figure 3.1. Non-innocent V-Schiff base complexes. A. The most potent anticancer complex against T98g cells, VO(HSHED)(DTB). B. The synthesized complex VO(HSHED)(Ad).

Many catechol derivatives are known, some are natural derivatives such as dopamine, an important neurotransmitter.[88 55] Vanadium catechol complexes in particular have been previously prepared and their chemistry reported.[22, 46] A number of synthetic catechol derivatives include substituents such as tetrabromo, cyano, nitro, methoxy and a coumarin derivative were reported for forming non-innocent V-complexes with HSHED, a complexation compound between salicylaldehyde and *N*-(2-hydroxyethyl)-1,2-ethanediamine. Recently, they were all found to be weak to moderate inhibitors for *M. smegmatus*, which was recently reclassified as *Mycolicibacterium smegmatis*.[55] These compounds were found to have varying stability under the assay conditions. Some of these complexes were found to be more potent growth inhibitors as complexes, and other compounds as the ligands by themselves.[55] However, the most potent growth inhibiting complex is that formed from the most hydrophobic and sterically hindered catechol, di-*tert*-butylcatechol. The di-*tert*-butylcatechol was found to differ from the monosubstituted catechols derivatives and tri-catechol substituted derivatives could be observed for this catechol.[9] In comparison, the base catechol and monosubstituted catechols formed vanadium compounds at lower oxidation state.[9] The sterically hindered catechol, di-*tert*-butylcatechol, was found to show significantly different biological properties and significantly less toxic.[34] Since there are no more sterically hindered catechols that are commercially available, di-adamantyl substituted catechols have been synthesized.[89-90] In the following work we have prepared the non-innocent Schiff base V-complex of the di-adamantyl substituted catechol and tested its anticancer properties.

Experimental

General materials. Salicylaldehyde, *N*-(2-hydroxyethyl)-1,2-ethanediamine, 1,2-Dihydroxybenzene, 1-adamantanol, vanadyl sulfate hydrate were purchased from Sigma Aldrich. Chemicals were used as-is. Ultrapure argon (AR UHP300) from Airgas was used for degassing solutions. Deuterated PBS was prepared replacing the water with deuterated water.[56] The pH values of buffered solutions were adjusted with DCl and NaOD. The pre-sterilized media and sterile plasticware used in cell culture studies were purchased from Thermo Fisher Scientific Australia.

General Methods and Instrumentation. The compounds were also characterized by UV-Vis spectroscopy (AvaLight UV/Vis/NIR Light Source and AvaSpex-UL S2048 Fiber-Optic Spectrometer), MS (Bruker amaZon SL spectrometer), and elemental analysis (ALS Environmental, Tucson, AZ). The hydrophobicity was calculated using Chemicalize software developed by ChemAxon and downloaded in May 2020.[57]

NMR spectroscopy. Compounds were characterized using ^{51}V NMR spectroscopy recorded on a Bruker model AVANCE Neo400 spectrometer equipped with a BBFO smart probe and an automated tuning module operating at 101 MHz as reported previously.[5,38-39] The ^{51}V NMR spectra were acquired with a spectral window of 86200 Hz, 2048 scans, a 90° pulse, an acquisition time of 0.08 s, and a 0.01 s relaxation delay as reported previously.[32, 52, 58-59] 1D ^{51}V NMR studies were referenced against $[V(O)_2(HSHED)]$ at -529 ppm as a standard and reported in reference to $VOCl_3$ (0 ppm).[19] 1D and 2D ^{1}H NMR studies were carried out in organic solvents using a Bruker NEO400 spectrometer operating at 400 MHz at an ambient temperature. Chemical shift values (δ) are reported in ppm and referenced against TMS using the internal solvent peaks in ^{1}H NMR spectra (d_6-DMSO, δ at 2.50 ppm; $CDCl_3$, δ at 7.26 ppm~~;~~ d_3-acetonitrile, δ at 1.94 ppm; C_6D_6, δ at 7.16 ppm) as internal standards. 1D ^{51}V NMR studies were recorded on the Bruker NEO400 spectrometer at 105.2 MHz at an ambient temperature. All complexes were dissolved in d_6-DMSO at 10 mM concentrations for spectral comparison. Spectroscopic studies were carried out using solutions of isolated complexes, and both ^{1}H and ^{51}V NMR spectra were recorded on the same samples. 1D samples were run within 5 h of preparation; no significant differences were observed in spectra recorded within 24 h.

$^1H-^1H$ 2D COSY and NOESY NMR spectra in organic solutions were run overnight and recorded within 12 h of sample preparation. 2D NMR spectroscopic studies in organic solutions were carried out on a Bruker NEO400 spectrometer at 400 MHz at 26 °C. A routine COSY pulse sequence provided by the Bruker software was used. A standard NOESY pulse sequence was used consisting of either 200 or 256 transients with 16 scans in the f1 domain using a 500 ms mixing time, 45° pulse angle, and a 1.5 s relaxation delay. The NMR was locked onto either d_6-DMSO and referenced to the internal solvent peak. The resulting spectrum was processed using MestReNova NMR software (version 12.0.1).

Mass Spectrometry. Low-resolution electrospray ionization mass spectrometry (ESI-MS) data were collected on a Bruker amaZon SL spectrometer, using the following parameters: nebulizer pressure, 27.3 psi; spray voltage, 4.5 kV; capillary temperature, 453 K; N_2 flow rate, 4 L per min; *m/z* range, 100-1000 (alternating positive- and negative-ion modes). The compound stability parameter was set at 15%, which provided mild ionization conditions at the expense of lower sensitivity. Smart parameter settings were fixed to the exact mass for each compound. Analyzed solutions (~10 µM V in acetonitrile) were injected using a syringe pump (flow rate, 8 µL per min). Acquired spectra were the averages of 100-200 scans (scan time, 100 ms). Simulations of the mass spectra were performed using IsoPro 3.0 software (M. Senko, IsoPro 3.0, Sunnyvale, CA, USA, 1998). High-resolution positive ion ESI-MS was performed on a Thermo Velos Pro Orbitrap mass spectrometer via a syringe infusion (flow rate, 8 µL per min). Resolving power was set to 200,000 at 200 m/z. The instrument was externally calibrated before analysis and internally calibrated using dioctyl phthalate as a lock mass.

General Synthesis. [$V(O)_2$(HSHED)] was prepared as reported previously.[46]

Adamantyl catechol: A 50 mL round bottom flask charged with a stir bar was flame dried and purged with Argon. Catechol (0.661 g, 6.0 mmol) was added along with 1-adamantanol (1.851 g, 12 mmol) and Trifluoroacetic acid (12 mL). The system was fitted with an Argon balloon and the mixture was left to react at room temperature for two days. A milky-white precipitate was observed after 15 minutes. After two days the precipitate was filtered and washed with DI H_2O until the filtrate was neutral. The crude solid was purified by flash column chromatography (1000 mL of 230-400 mesh SiO_2, 70 mm column 20:1 hexane/ethyl acetate). The clear oil obtained was dried under reduced pressure to yield 1.84 g (83%) as a while solid. ^{1}H NMR (400 MHz, $CDCl_3$): δ 6.81 (s, 1H), 6.74 (s, 1H), 5.45 (s, 1H), 4.69 (s, 1H), 2.14 (m, 6H), 2.08 (m, 6H), 1.87 (m, 6H), 1.75 (m, 6H).

[VO(HSHED)(Ad)]: To a 250-mL round bottom Schlenk flask was added acetone (100 mL, which was then degassed with Ar. [VO_2(HSHED)] (0.29 g, 1.0 mmol) was added to the degassed acetone, followed by adamantanol catechol (0.38 g, 1.0 mmol) A deep purple solution resulted after 30 min but stirred for 12 h. The reaction was vacuum filtered and washed with hexanes and dried under vacuum for 3d to yield 0.46 g (71%) purple solid δ^{51}V NMR (101 MHz, d_6-DMSO): 352 ppm (major), 386 ppm (minor), 409 ppm (minor). ^{1}H NMR (400 MHz, d_6-DMSO): δ 8.73 (s, 1H), 7.51 (d, 1H), 7.41 (t, 1H), 6.76 (t, 1H), 6.70 (d, 1H), 6.19 (s, 1H), 6.15 (d, 1H), 4.82 (m, 1H), 4.73 (t, 1H), 4.15 (d, 2H), 3.93 (m, 2H), 3.74 (m, 2H), 3.47 (m, 2H), 3.32 (d, 4H), 2.10 (m, 8H), 1.74 (m, 18H).

Cell Culture and Growth Conditions. The well-established human glioblastoma multiforme cell line (T98g) was purchased from American Type Culture Collection (ATCC, Cat. No. CRL-1690). The cells were cultured in Advanced DMEM (Thermo Fisher Scientific Cat. No.

12491-015), supplemented with L-glutamine (2.0 mM), antibiotic-antimycotic mixture (100 U mL^{-1} penicillin, 100 mg mL^{-1} streptomycin and 0.25 mg mL^{-1} amphotericin B) and foetal calf serum (FCS; heat-inactivated; 2% vol). For proliferation and cytotoxicity experiments, cells were seeded in 96-well plates at an initial density of 1.5×10^3 viable cells per well in 100 μL medium and left to attach overnight.

Freshly prepared stock solutions of V(V) complexes (10 mM in DMSO) were used for cell assays. These solutions were further diluted so that all the cell treatments, including controls, contained 1.0% (vol.) of DMSO, which did not significantly affect the cell growth during the assays. Stock solutions of the treatment compounds were diluted with fully supplemented cell culture media to the required final concentrations, and the resultant media were either added to the cells within 1 min (fresh solutions), or left in cell culture incubator (310 K, 5% CO_2) for 24 h prior to the cell treatments (aged solutions).

Each treatment included six replicate wells with cells and two background wells without cells that contained the same components. After the addition of treatment compounds, the plates were incubated for 72 h at 310 K and 5% CO_2, then MTT reagent (1-(4,5-dimethylthiazol-2-yl)-3,5-diphenylformazan, Sigma M5655) was added (50 μL per well of freshly prepared 2.0 mg/mL solution in complete medium), and incubation was continued for 4-6 h. After that, the medium was removed, the blue formazan crystals were dissolved in 0.10 mL per well of DMSO, and the absorbance at 600 nm was measured using Victor V3 plate reader. Typically, the treatment compounds were applied in a series of nine two-fold dilutions, starting from (100 ± 20) μM V, plus the vehicle control. Exact V concentrations in the assays were verified by ICP-MS measurements using samples of cell culture media and used in the calculations of the IC_{50} values. Fitting of the experimental data and calculations of the IC_{50} values were performed using Origin

6.1 software (Microcal Origin, 1999). For all the cell assays, consistent results were obtained in at least two independent experiments using different passages of cells and varying stock solutions of the treatment compounds.

Results and Discussion

Design and strategy for synthesis of newly sterically hindered catecholates. The known 3,5-di-t-butyl substituted catechol is an example of a sterically hindered catechol which when combined with a Schiff base V-complex result in the formation of a non-innocent V-Schiff base HSHED complex. Since the sterically hindered catechol has significantly lower toxicity than the unsubstituted catechol, we explored the synthesis of new sterically hindered catechols. In Figure 3.2 we show the preparation of the 3,5-di-Adamantyl substituted catechol prepared using a slightly

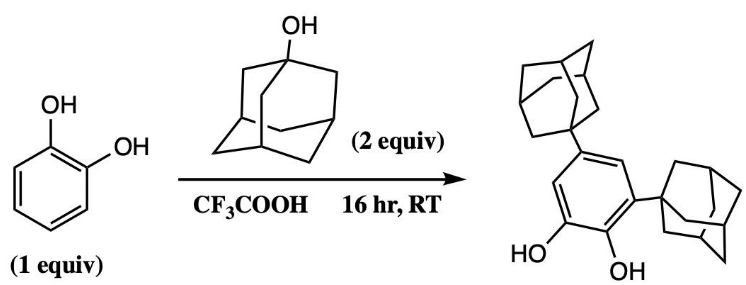

Figure 3.2. Preparation of 3,5-di-Adamatyl catechol

modified literature procedure.[89-90]

Synthesis of catechol and non-innocent V-Schiff base. Formation of this ligand was found to be sensitive to the presence of air, under which condition the ligand oxidized to the corresponding 1,2-cis-quinone. The oxidation reaction was also sensitive to the scale of the reaction. To avoid the oxidation, the reaction was run in the absence of oxygen and air and then resulted in formation of pure 3,5-di-Adamatyl catechol, Figure 3.3. The spectrum shows the two protons in the aromatic region as well as the two hydroxyl protons in the 5-6 ppm region. The aliphatic protons of the adamantyl can be found in the 1-2 ppm region.

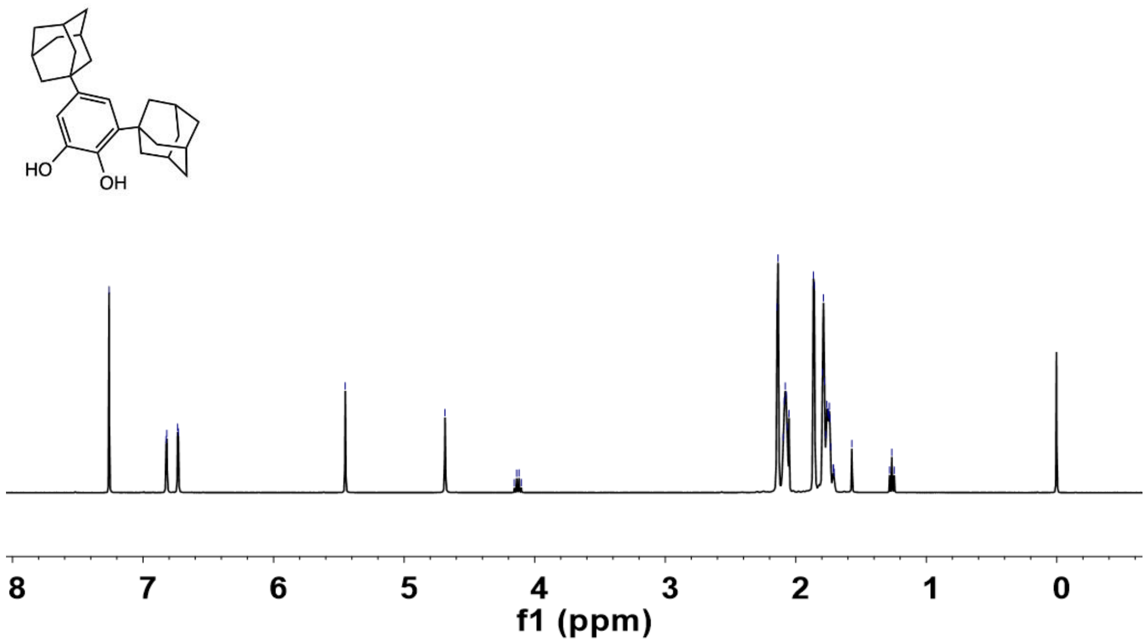

Figure 3.3 ^{1}H NMR (400MHz) of ad catechol ligand in $CDCl_3$ with structure for reference

The newly synthesized ligand was used for preparation of the non-innocent V-Schiff base using the synthetic approach reported for the other non-innocent Schiff base complexes shown in Figure 3.4.

Characterization of the [VO(HSHED)(Ad)]. The compound was confirmed using MS

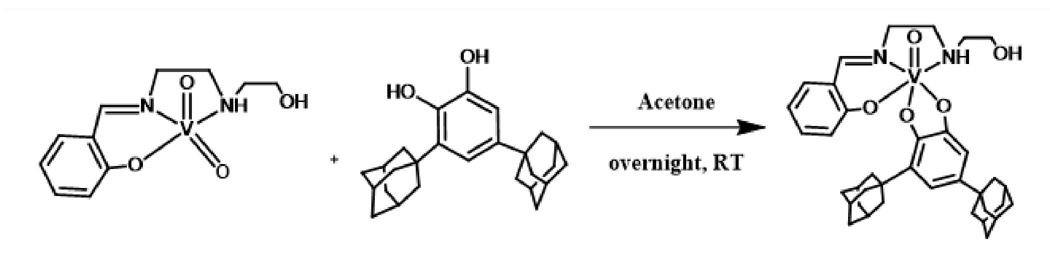

Figure 3.4. Synthesis of [VO(HSHED)(ad)] complex based on the general approach reported by Pecoraro and coworkers and optimized to accommodate the properties of the 3,5-di-Ad ligand.

spectroscopy and mass-spectrometric characterization of the new V(V)

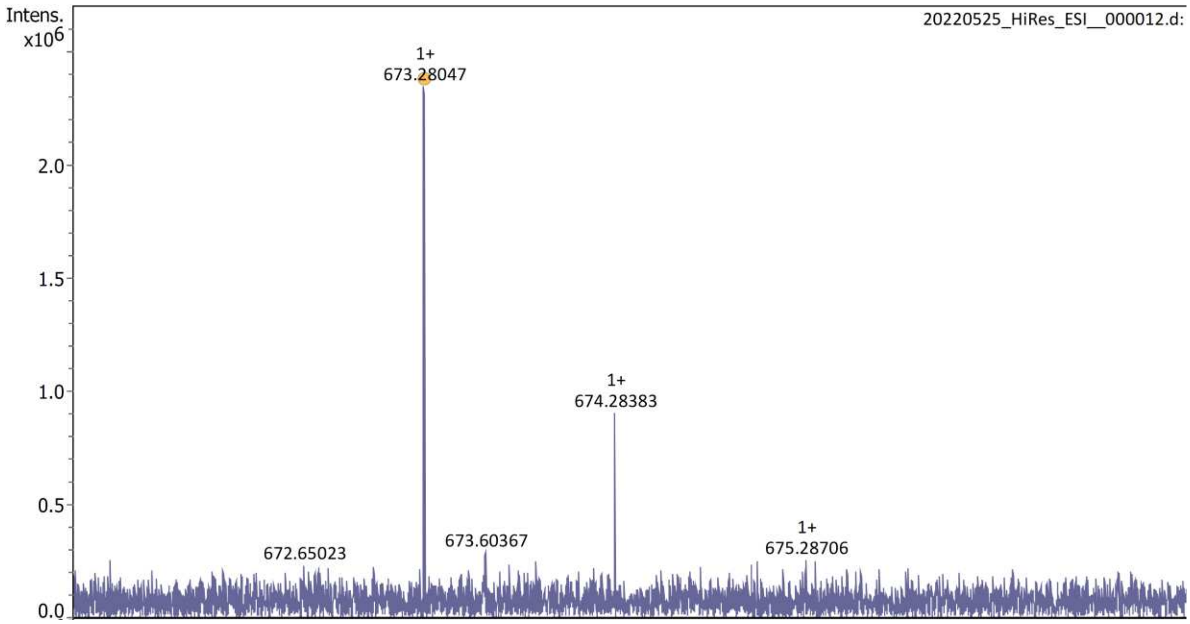

Figure 3.5. Typical low-resolution ESI-MS data for the V(V)-Schiff base-catecholato complex (a-g; ~10 µM solution in acetonitrile, m/z values in positive ion mode).

complex is shown in Figure 3.5. The prominent signal of the intact complex was observed in the form of their Na^+ adduct at a m/z of 673.

The new compound was also characterized using UV-Vis spectroscopy and ^{51}V NMR spectroscopy (Figure 3.6). ^{51}V NMR spectra of [VO(HSHED)(Ad)] were obtained in three different solvents, $CDCl_3$, CD_3CN and DMSO. Only one broad signal was observed in $CDCl_3$ at 470 ppm, whereas two signals were observed in CD_3CN (at 395 and 465 ppm). In d_6-DMSO two signals overlap to a total of 4 different signals. These signals are broader than the signals observed in other solvents. The differences in signals in these 3 solvents is consistent with formation of different isomers as was observed for [VO(Cl-HSHED)(DTB)].[91]

Since the ^{51}V NMR suggest the presence of isomers, the structure of compounds in solution was investigated in greater detail using 1D and 2D ^1H NMR spectroscopy (Figure 3.6 and 3.7). Similarly, to the [VO(Cl-HSHED)(DTB)] system, we assigned H_a as the proton on the imide and

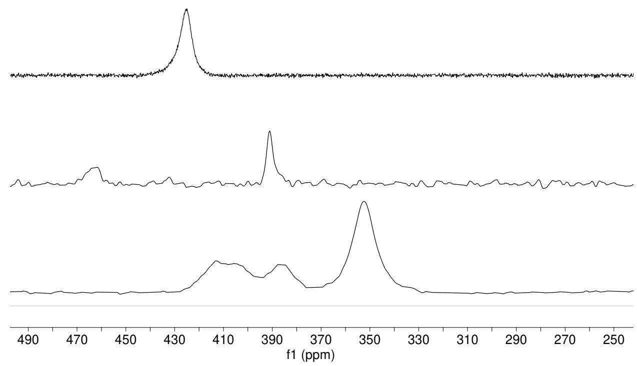

Figure 3.6. ^{51}V NMR spectra of [VO(HSHED)(Ad)] in different solvents, $CDCl_3$ (top), CDCN (center) and *d6*-DMSO

H_b, H_c, H_d, and H_e were defined in splitting system X (the Schiff base).[91] These assignments were based on the cross-peaks found in the COSY and that H_c and H_d had coupling constants of 7.3Hz. This left the assignments of H_f and H_g on splitting system Y. The larger signal for H_g was due to overlapping signals from the minor isomers.

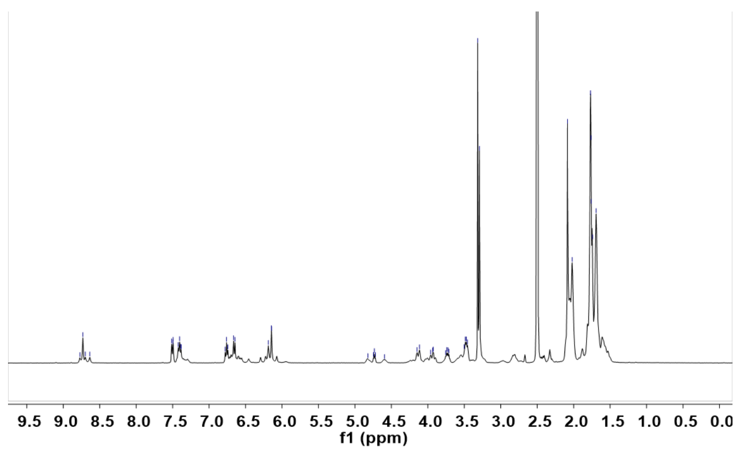

Figure 3.7. ^{1}H NMR (400MHz) of [VO(HSHED)(Ad)] in d_6-DMSO.

The 2D NMR spectra was recorded in d_6-DMSO and selected spectra are shown in Figure 3.8. To assign the protons in the [VO(HSHED)(Ad), ^{1}H-^{1}H 2D COSY and the ^{1}H-^{1}H 2D NOESY were performed. The NMR spectra contained groups of larger signals and groups of smaller signals as both major and minor isomers existed in solution, but the focus was on the assignment of the major isomer. The d_6-DMSO as the solvent was chosen as the complex was the most soluble in DMSO.

While in the aromatic region, H_b and H_c show clear cross-peaks between H_d and H_e, in the alphatic region, it is more complex and may require a D_2O spike to clear that region similar to the [VO(Cl-HSHED)(DTB)] determination.[91]

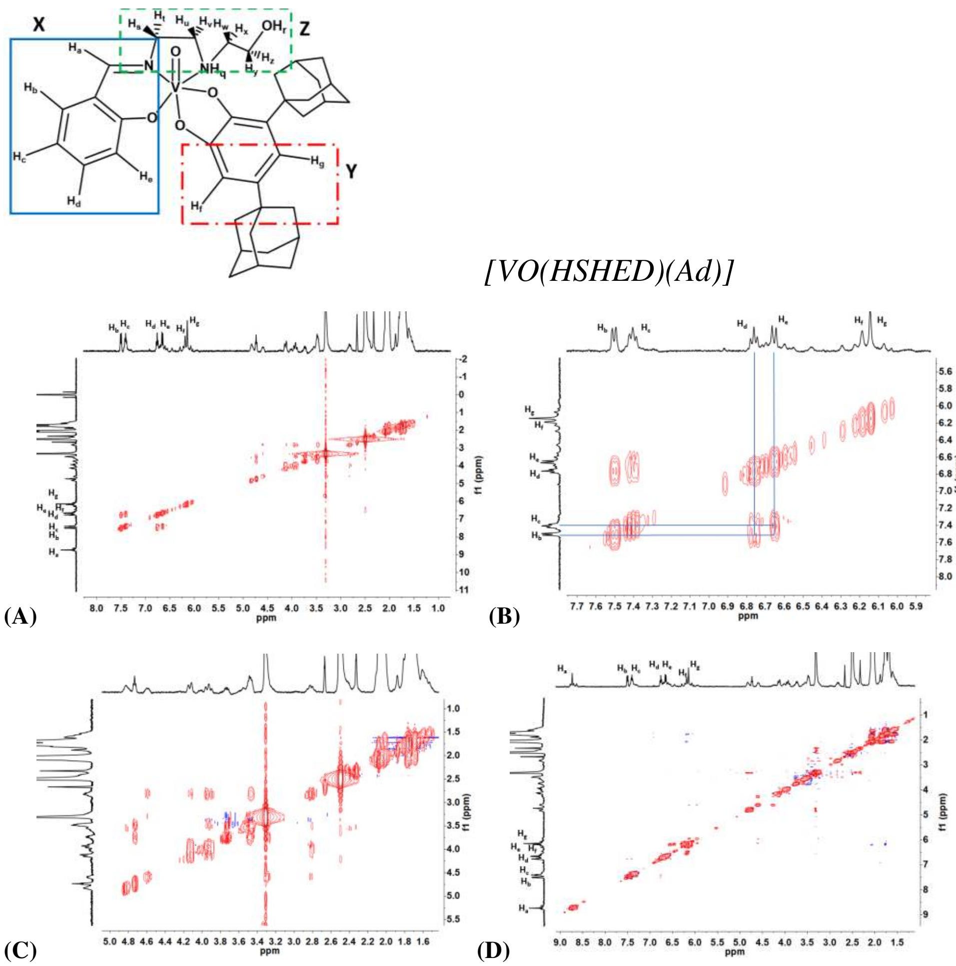

Figure 3.8. The structure of [VO(HSHED)(Ad)]. ^{1}H-^{1}H COSY and ^{1}H-^{1}H NOESY NMR (400MHz) spectra of 10 mM [VO(HSHED)(Ad)] in DMSO at 26°C. (A) Full ^{1}H-^{1}H COSY NMR spectrum of [VO(HSHED)(Ad)] in DMSO. (B) Zoom of aromatic region ^{1}H-^{1}H COSY NMR spectrum of [VO(HSHED)(Ad)]. (C) Zoom of aliphatic region ^{1}H-^{1}H COSY NMR spectrum of [VO(HSHED)(Ad)]. Zoom of aromatic region ^{1}H-^{1}H COSY NMR spectrum of [VO(HSHED)(Ad)]. (D) Full ^{1}H-^{1}H NOESY NMR spectrum of [VO(HSHED)(Ad)]. Blue intensity contours represent negative NOEs and red intensity contours represent positive NOEs. A standard NOESY sequence was used consisting of 200-256 transients with 16 scans in the f1 domain using a 500 ms mixing time and a 1.5 s relaxation delay. The structures of [VO(HSHED)(Ad)] are shown with a proton labelling key

Hydrolytic stability of the [VO(HSHED)(Ad)]. As with the [VO(HSHED)(DTB)] and its hydrophobic di-*tert*-butyl ligand, this new complex, [VO(HSHED)(Ad)], is also hydrophobic and has the potential of its stability be superior to any other non-innocent complexes reported to date. Hence the stability [VO(HSHED)Ad] was investigated. The absorbance maximum of the complex was at 550 nm. The stability of the complex was observed in DMSO as a function of time and in the presence of some amounts of water, Figure 3.9.

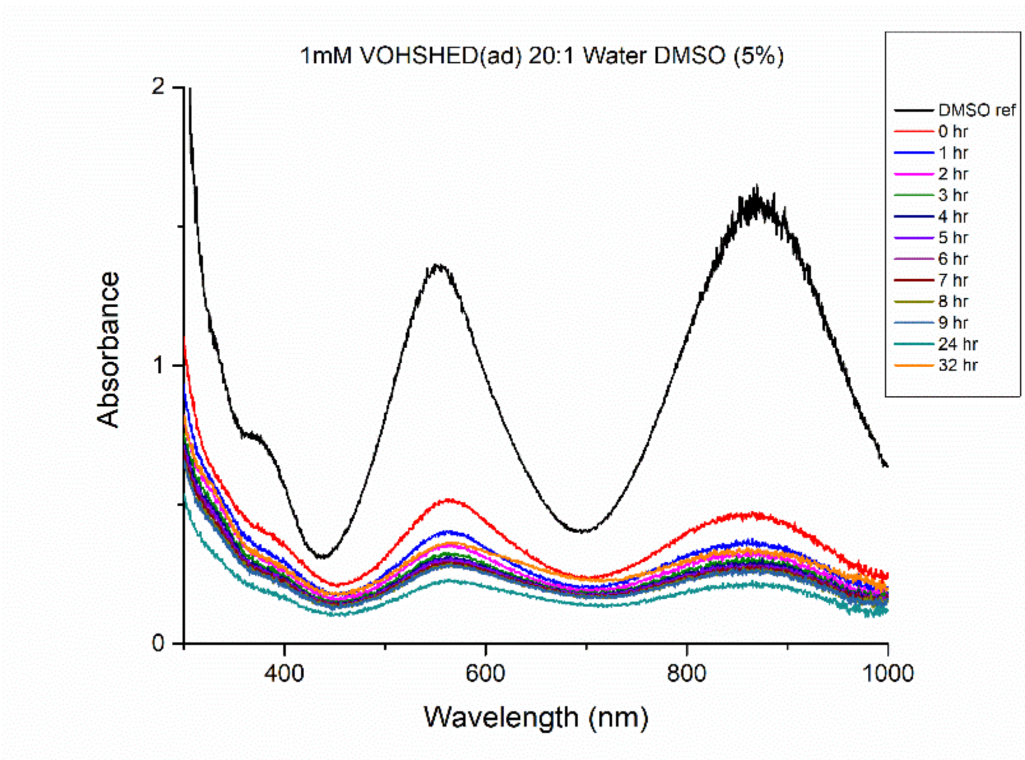

Figure 3.9. UV-Vis Stability Studies in 1mM VOHSHED(Ad) in 20:1 water to DMSO.

Similarly, the absorbances were measured when the VO(HSHED)Ad complex was dissolved in PBS assay solution at 310 K under the conditions that the T98g cells were assayed. As shown in Figure 3.10a, significant amounts of the VO(HSHED)Ad compound remained intact in aqueous buffer under the conditions of the biological assay. However, intact VO(HSHED) complex began to decrease rapidly after the first hour, and, as time progressed the absorption maximum for the solution shifted. The absorbance of a V-hindered complex, $V(DTB)_3$ was assigned to a V-complex with three catecholates. At 48 h the absorbance had shifted to near 620 nm and is assigned to the V(Ad)$_3$ complex. After 3 h the λ_{max} in the solution shifted approaching the λ_{max} for the VO(HSHED)-complex with three catecholates, V(Ad)$_3$. The concentration of this complex increased when the solution was monitored after 48 h. Similar complexes with three AdOH derivatives have not yet been prepared and characterized previously, however corresponding complexes have been reported for V(DTB)$_3$.[9] The corresponding stability study of [VO(HSHED)(DTB)] is shown in Figure 3.10b. The [VO(HSHED)(DTB)] complex only survive for a few min, and by 30 min the absorbance at 620 nm indicate that the V(DTB)$_3$ complex was formed. At 24 h the concentration of the [VO(HSHED)(DTB)] complex had decreased significantly documenting the limited stability of these complexes.

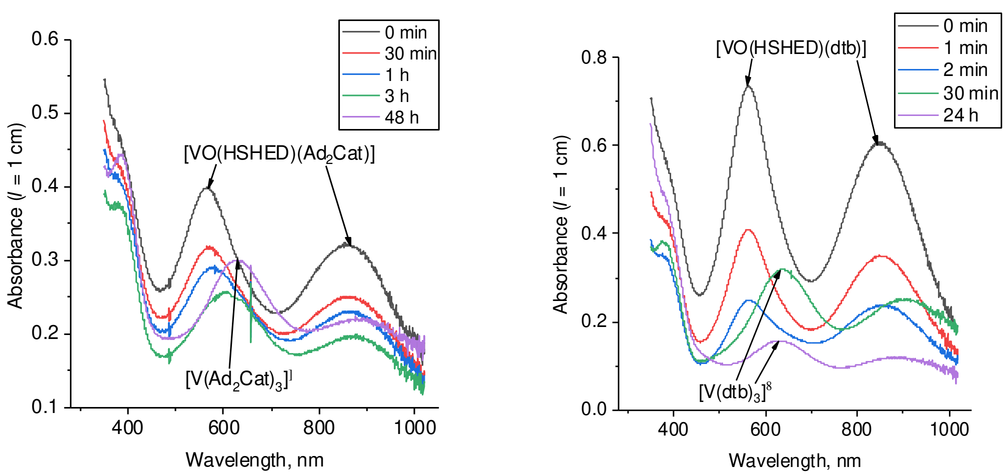

a) **b)**

Figure 3.10. The absorbance of 1 mM [VO(HSHED)(Ad)] and b) [VO(HSHED)(DTB)] in PBS assay buffer measured as a function of time at 310 K. a) [VO(HSHED)(Ad)] and b) [VO(HSHED)(DTB)].

The stability studies carried out DMSO:H$_2$O and PBS buffer show a remarkable difference with regard to the stability of the VO(HSHED)-catecholate complex and the formation of the V(Ad)$_3$ and the V(DTB)$_3$ complexes. For both systems the Ad-derivative was significantly more stable than the corresponding DTB compounds. The logP value for [VO(HSHED)(Ad)] was calculated through Chemicalize and found to be 3.53 compared to [VO(HSHED)(DTB)] with a logP value of 2.191.[57, 91]

Biological Activity of Vanadium Complexes. The IC_{50} values were measured for T98g (human glioblastoma) cells in a 72 h assay of both fresh solutions of vanadium compound and 24 h aged solutions in culture media. The most favorable activity ratio of fresh and aged was observed for fresh solutions of [VO(HSHED)(Ad)]. Consistent with the earlier results, fresh solutions of [VO(HSHED)(Ad)] showed higher activity (IC_{50} = 11 ± 2 μM or 14 ± 2 μM in a 72 h assay, Table 3.1 and Figure 3.11) in T98g cells, while aged solutions of this compound were ~2/3-fold less active under the same conditions (Table 3.1).[7] As shown in Figure S3.1 the results are reproducible using the same assays to within 25% with experiments done at different times.

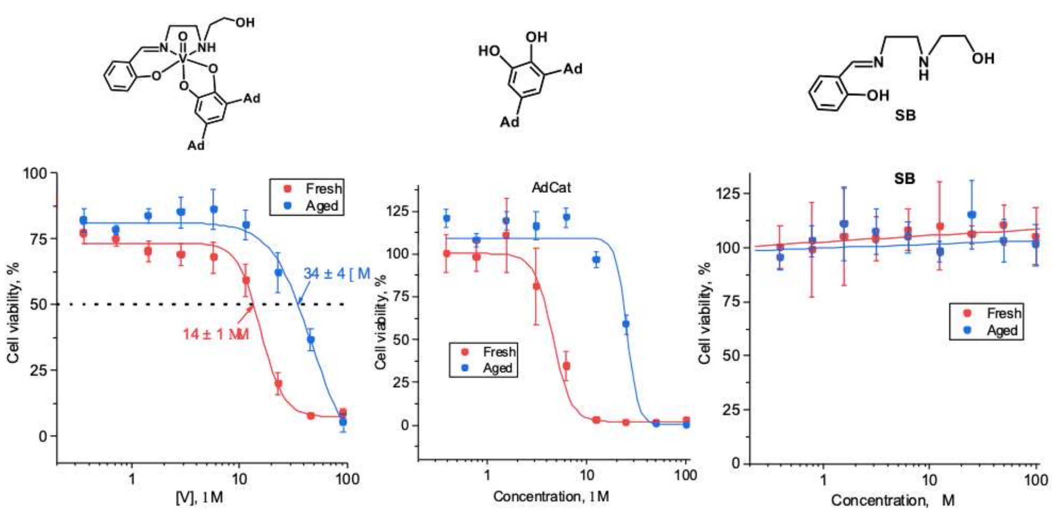

Figure 3.11. The growth curves are shown for treatment of [VO(HSHED)(Ad)], AdOH and the Schiff base of T98g cells at 310 K.

The effects of [VO(HSHED)(Ad)] both in fresh and 24 h aged solutions reflect the effects of the compound and its decomposition products in the T98g assay. In addition, we were interested in examining the effects of each of the components of these molecules since the effects of compounds in assay media is complex. Hence subjecting the 3,5-diadamantyl catechol ligand and the Schiff base ligand to similar studies allows the determination of the components as well. Data for the complexes and components are shown in Figure 3.12. These growth curves show that the 3,5-diadamantyl catechol has a lower IC_{50} value than V-complex by a factor of about 3 for both fresh solutions and solutions of compounds aged for 24 h. In contrast, when the compounds are aged for 72 h [VO(HSHED)(Ad)] is more efficient than the AdOH. A study of 3,5-diadamantyl catechol in the presence of 1:1 ligand to vanadate shows similar affinity as the solutions of fresh [VO(HSHED)(Ad)] solution complex.

Table 3.1. Antiproliferative activities in T98g cells and stabilities under cell culture conditions for [VO(HSHED)(Ad)] and AdOH.

Compound	***IC_{50}*, μM (fresh)**[b]	***IC_{50}*, μM (aged)**[c]	***$t_{1/2}$* (295 K)**[a]	***Publication***
[VO(HSHED)(Ad)]	11 ± 2	36 ± 4	~200 min	This work
AdOH	4.6 ± 1.3	25 ± 1		This work
[VO(Cl-HSHED)(DTB)]	4.1 ± 0.5	9 ± 1	~15 min	Ref. [91]
[VO(Cl-HSHED)(3-Me)]	34 ± 7	18 ± 3	~15 s	Ref. [91]
[VO(Cl-HSHED)(Cat)]	19 ± 2	8.1 ± 0.6	~15 s	Ref. [91]
$[V(O)_2$(Cl-HSHED)]	37 ± 4	67 ± 7	ND[d]	Ref. [91]
[VO(HSHED)(DTB)]	1.9 ± 0.2	21 ± 1	~ 5 min	Ref. [32, 91]
[VO(HSHED)(3-Me)]	46 ± 9	20 ± 5	<15 s	Ref. [91]
[VO(HSHED)(Cat)]	19 ± 7	22 ± 4	<15 s	Ref. [32]
$[V(O)_2$(HSHED)]	44 ± 4	70 ± 8	ND[d]	Ref. [32]
cisplatin[a]	5 ± 1	33 ± 12		Ref. [7]

Since the [VO(HSHED)(Ad)] complex is more stable and potentially more hydrophobic than the [VO(HSHED)(DTB)] complex, we examined the cellular V uptake to determine if the hypothesis that the V-compound resulting in greater V-uptake would be most active. This was determined by measuring the millions of V-atoms per cell and the amount are shown in Figure 3.10. These measurements show that the order of V-uptake are as follows: [VO(HSHED)Ad], [VO(HSHED)(DTB)], vanadate, and lastly the $[V(O)_2$(HSHED)] scaffold. Thus, despite the greater stability and higher uptake of V-atoms, the antiproliferative effects of the

[VO(HSHED)Ad] complex is less than the [VO(HSHED)(dtb)] complex suggesting that properties other than hydrophobicity and stability such as redox properties may be responsible for the biological activities of this complex.

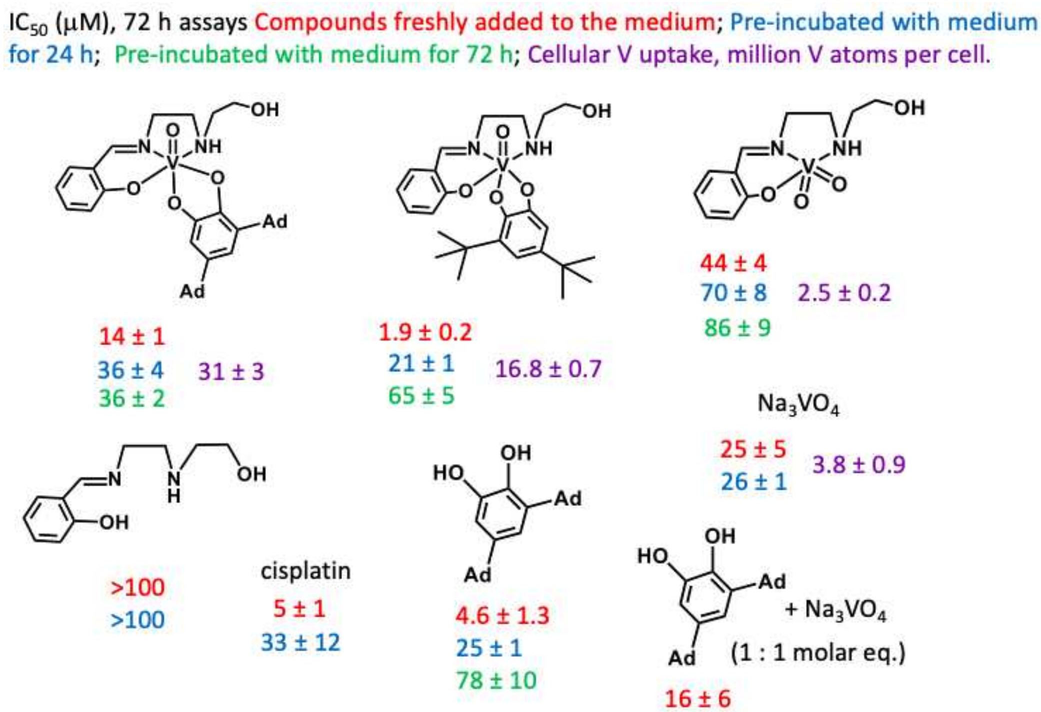

Figure 3.12. 72 hours assays of various ligand and vanadium complexes to test IC_{50} values.

The synthesis of the 3,5-diadamantyl catecholate was done following the reported procedures. We found that repeating these conditions at Colorado State University at 1 mile elevation and at elevated pressure, the reaction is very sensitive to the presence of oxygen and a significant amount of ligand oxidized. Hence, we conducted the reaction under inert atmosphere to yield pure product of the 3,5-diadamantyl-1,2-quinone. This product could then be used to synthesize the [VO(HSHED)(Ad)] complex. Multinuclear NMR spectroscopy was used to characterize the compound in solution. ^{51}V NMR spectroscopy show that one signal is observed in $CDCl_3$, two signals is observed in CD_3CN and four signals are observed in d_6-DMSO. The broad signal observed in $CDCl_3$ could be a result of two species that are in rapid exchange since the signal is very broad. This is confirmed by the ^1H NMR where we find multiple isomers in solution. The 2D NMR was done in DMSO and the aromatic region were able to be identified clearly, but the aliphatic region is more complex. The [VO(HSHED)(Ad)] complex was found to be significantly more stable than the other sterically hindered non-innocent V-complexes which makes it more difficult to solubilize and maintain in common solvents at a concentration and time needed for taking 2D NMRs.

In Table 3.1 we list the IC_{50} values for the new complex as well as the reported non-innocent V-Schiff base catecholate systems reported previously and a new series of compounds with Chloro-substituted Schiff base. The biological studies show that the [VO(HSHED)(Ad)] complex have an IC_{50} value of 14μM which is slightly higher than cisplatin (Figure 3.11). Table 3.1 shows the activity of the [VO(HSHED)(Ad)] compared to previous analogs demonstrating that this new analog belongs to the top compounds with activities of the non-innocent V-Schiff base complexes that have been investigated to date. The reason why [VO(HSHED)(Ad)] was slightly less active than [VO(HSHED)(DTB)] might be due to differences in redox potential from the change of catecholato ligand or the conversion to the $VO(Ad)_3$ over time affecting biological activity.

Conclusion-

When developing new complexes, structure activity relationships are important to investigate and consider. The new compound [VO(HSHED)(Ad)] was synthesized and characterized by UV-Vis, multinuclear and multidimensional NMR, and MS-ESI. The biological stability and activity studies showed that the [VO(HSHED)(Ad)] was one of the most stable complexes that we have synthesized, but still showed less activity from the [VO(HSHED)(DTB)] complex. While the newly synthesized [VO(HSHED)(Ad)] complex was slightly less active that the [VO(HSHED)(DTB)] series, this compound shows that while hydrophobicity is key to future development of increasing anticancer activity, there are more factors such as redox potential or formation of the tris-catecholate product that affect the biological activity overall.

Chapter 4- Speciation of vanadium polyoxometalates and complexes in biological environments

Introduction-

There are a variety of vanadium compounds that can dissociate in different systems as the compounds can be unstable in varying biological systems. Decavanadate a polyoxometalate, prefers a system at a pH of 4-6 while vanadium dipicolinate systems are stable in at more acidic conditions (Figure 4.1).[16, 21, 92-93] While these conditions can be significantly lower than pH 7, we can take advantage of the dissociation rates by making compounds where the medicinal effects are in the degradation products. It is important to note that while the benefits of a polyoxometalate like decavanadate can come from the multiple vanadates that comprise the complex, the decavanadate complex itself has a different activity than 10 individual vanadates.[15] The activity difference of decavanadate compared to vanadate was notable enough to have also been investigated by modifying the cage to swap out a vanadium for a molybdate or a platinum.

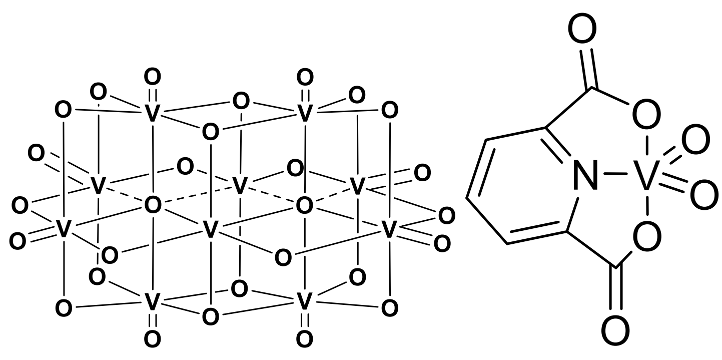

Figure 4.1 Structures of decavanadate and vanadium dipicolinate

The dipicolinate systems were also investigated by modifying the substituents on the dipicolinate. As such we have provided two different vanadium complexes and their speciation profiles from two different publications to illustrate how the metal complexes can change in various environments. In one, we show the results of decavanadate in a bacterial environment, and in the other we show the results of a vanadium dipicolinate complex in a system suitable for viral growth. For both conditions, they fall apart in these systems showing that in a system that would resemble a human or animal biological system, we would have to consider the vanadium species that would form under these conditions. To characterize metal complexes in biological systems, we can model the species that the complex may disassociate into when placed into a variety of pHs.

Polyoxometalates

Polyoxometalates (POMs) are a class of compounds that have been investigated in a range of biological and biomedical systems, as their effects in cell culture studies and in vivo suggest that these compounds have potential for use as therapeutic agents.[13, 94-106] Decavanadate is a homopolyoxometalate anion, and one of the POMs that has been reported to have known biological effects, as documented by studies reported with cells as well as with isolated enzyme systems.[97-100, 107-112]. Protein crystal structures have been reported for some protein-POM complexes such as those reported between the ribosome and a Dawson oxometallate.[113-116] Other protein-POM complexes include protein complexes with smaller oxometalates such as decavanadate.[117] The limited stability of decavanadate at neutral pH would suggest that hydrolysis intermediates may form and generate stable complexes with proteins or cellular components. Speciation studies are important in this regard, and different species and possibilities must be considered when investigating the mode of action of systems that are not thermodynamically stable.[10, 97] Even if the speciation is characterized, the active species and mode of action of these complex systems can be non-trivial to interpret.[118-124] However, a wide range of activities have been reported depending on the protein, biological system or specific vanadium species.[123, 125-127] Recently, it has become clear that compound uptake is critical to the mode of action because many vanadium compounds are modified during the uptake process.[10, 128-130] In the case of a large anion such as decavanadate, the question is simply whether the species is too large to enter through protein channels and thus must be taken up through endocytosis or passive transport mechanisms. The alternative possibility is that the uptake is of the smaller vanadium oxovanadates, such as monomeric vanadate, which then oligomerizes to form decavanadate inside the cell. The formation of decavanadate has been demonstrated in yeast (S. cerevisiae) and thus makes this anion a desirable system to understand in greater detail.[118-119]

Vanadium is a first-row transition metal ion and is in the group of transition metals that can form POMs.[72, 131-136] Vanadium is particularly prone to forming homopolyoxometalate ions as well.[97, 131] Indeed, pure crystalline metavanadate and orthovanadate upon dissolution will form several oxovanadate species containing vanadate monomer, V_1, vanadate dimer, V_2, vanadate tetramer, V_4, vanadate pentamer, V_5 and decavanadate, V_{10}, Figure 4.2.[137-139]

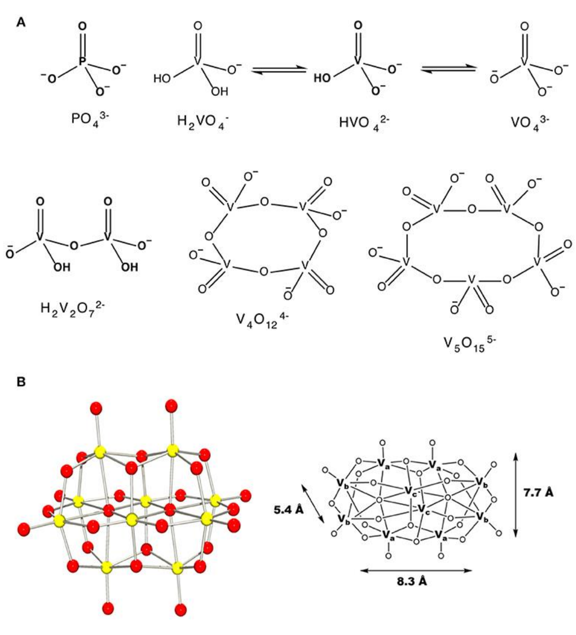

Figure 4.2. The schematic structures of (A) monomeric vanadate, monomeric and polymeric vanadate series (B) X-ray structure of V_{10} and the three different types of vanadium atoms in this complex ion with indicated dimensions.[140] This figure was adapted with permission from Aureliano and Ohlin (2014), Crans et al. (2017).[100, 136]

Some of these species have been characterized using X-ray crystallography and have been found to interconvert in aqueous solution.[139-140] However, the specifics of the reactions and their conditions vary. For example, vanadate and oligomeric species containing 2, 4, and 5 vanadium atoms are colorless and rapidly convert at neutral pH, Figure 4.2A.[139] In contrast, decavanadate will form rapidly at acidic pH, but is only kinetically stable at neutral pH, Figure 4.2B.[97, 131, 134, 136] Indeed, the kinetic studies have shown that decamer formation is a rapid process and much faster than the V10 decomposition in both neutral and basic solution.[136] The decomposition pathways investigated follow several different mechanisms and are dependent on the concentrations of H^+ and OH^- and the other counter ions present in solution.[141-145] Information is needed describing how decavanadate interacts with membrane interfaces and cellular systems, including how decavanadates biological activities compare to monomeric vanadate. Specifically, an attractive alternative mode of action to simple decavanadate binding would be the direct delivery of a vanadium atom from decavanadate to a biomolecule resulting in the dissolution of the decavanadate cluster. The X-ray characterization of decavanadate shows that its dimensions are 5.4 Å × 7.7 Å × 8.3 Å, Figure 4.2, a large size that cannot be accommodated by many biological transport channels.[140] Therefore, any uptake of decavanadate is likely to be through endocytosis or a passive mechanism. An attractive alternative mode of uptake would involve dissolution of the cluster by direct delivery of vanadium atoms, for example, into a system such as a protein. However, such a mechanism is more difficult to investigate and will require more information regarding the potential interactions of the anion with ligands and interfaces. We have been addressing related questions for some time and exploring the interactions of V10 with interfaces.[136, 146-148] Indeed, more information is needed to be able to characterize the process of how the decavanadate converts to the vanadate monomer and smaller clusters, but such processes undoubtedly involve the molecular association of structures that form in solution. Combined these studies demonstrate that vanadium compounds may be inhibitory or protective, depending on the environment and ligands that may be complexed to it, and thus it is of interest to investigate the effects of simple vanadium complexes prior to formation of a coordination complex. These studies directly compare the effects of the two vanadium salt species and in doing so, will allow researchers to address the issue of whether such oxometalate species exert different effects, possibly due to uptake or conversion of the salt under physiological conditions.

Speciation of vanadium was calculated using the integration of the vanadium peak(s) within the ^{51}V NMR spectra. The concentration of each species was determined using the known added concentration [assuming all vanadium is in the form of V(V)], the integration of the vanadium peak(s) in the spectrum and by using the mole fractions for each signal, the concentration of each species could be calculated as shown in Table 4.1.[139]

The interpretation of the ^{51}V NMR spectral data was supplemented by speciation calculations based on constants measured previously.[137, 149-150] The species distribution diagrams were calculated by using HySS 2009 software and known speciation constants of the system at hand.[18, 137, 149-151] The citrate and the phosphate concentrations found in the Middlebrook 7H9 broth medium supplemented with 5% BSA, 2% dextrose, 5% catalase (ADC) enrichment, glycerol (0.2%, v/v), and Tween 80 (0.05%, v/v) were 0.48 and 24 mM, respectively.[152] The vanadium concentrations that were investigated were concentrations of 5, 3.3, and 10 mM. The speciation diagrams were constructed using the following equilibrium reactions for the binary H^+-$H_2VO_4^{2-}$ system [see equation (4.1)], and two ternary system, H^+-$H_2VO_4^{2-}$ $-C_6H_5O_7^{3-}$ and H^+-$H_2VO_4^{2-}$ $-H_2PO_4^-$ [see equation (4.2) and (4.3)]. The alternate formulas were provided in the format of the equations provided for comparison.[137, 149-150]

$$p\mathrm{H}^+ + q\mathrm{H_2VO_4^-} \rightleftarrows (\mathrm{H}^+)_p(\mathrm{H_2VO_4^{2-}})_q \quad (4.1)^{137}$$

$$p\mathrm{H}^+ + q\mathrm{H_2VO_4^-} + r\mathrm{C_6H_5O_7^{3-}} \rightleftarrows (\mathrm{H}^+)_p(\mathrm{H_2VO_4^{2-}})_q(\mathrm{C_6H_5O_7^{3-}})_r \quad (4.2)^{149}$$

$$pH^+ + qH_2VO_4^- + rH_2PO_4^- \rightleftarrows [(H^+)_p(H_2VO_4^{2-})_q(H_2PO_4^-)_r]^{p-q-r} \text{ (4.3)}^{150}$$

Table 4.1. Formation Constants of Vanadate Species in a 0.6M NaCl system

(p, q)	log β	Formula	Extended formula
BINARY SYSTEM (H^+-$H_2VO_4^-$) REF (2)			
−1, 1	−7.92	HVO_4^{2-}	$(H^+)_{-1}(H_2VO_4^{2-})$
−2, 2	−15.17	$V_2O_7^{4-}$	$(H^+)_{-2}(H_2VO_4^{2-})_2$
−1, 2	−5.25	$HV_2O_7^{3-}$	$(H^+)_{-1}(H_2VO_4^{2-})_2$
0, 2	2.77	$H_2V_2O_7^{2-}$	$(H_2VO_4^{2-})_2$
−2, 4	−8.88	$V_4O_{13}^{6-}$	$(H^+)_{-2}(H_2VO_4^{2-})_4$
−1, 4	0.22	$HV_4O_{13}^{5-}$	$(H^+)_{-1}(H_2VO_4^{2-})_4$
0, 4	10.0	$V_4O_{12}^{4-}$	$(H_2VO_4^{2-})_4$
0, 5	12.4	$V_5O_{15}^{5-}$	$(H_2VO_4^{2-})_5$
4, 10	52.1	$V_{10}O_{28}^{6-}$	$(H^+)_4(H_2VO_4^{2-})_{10}$
5, 10	58.1	$HV_{10}O_{28}^{5-}$	$(H^+)_5(H_2VO_4^{2-})_{10}$
6, 10	61.9	$H_2V_{10}O_{28}^{4-}$	$(H^+)_6(H_2VO_4^{2-})_{10}$
7, 10	63.5	$H_3V_{10}O_{28}^{3-}$	$(H^+)_7(H_2VO_4^{2-})_{10}$
2, 1	6.96	VO_2^+	$(H^+)_2(H_2VO_4^{2-})_{10}$
(p, q, r)	**log β**	**Formula**	**Extended formula**
TERNARY SYSTEM (H^+-$H_2VO_4^{2-}$-$C_6H_5O_7^{3-}$) REF (3)			
1, 0, 1	5.217	Cit^{2-}	$(H^+)(Cit^{3-})$
2, 0, 1	9.298	Cit^-	$(H^+)_2(Cit^{3-})$
3, 0, 1	12.067	Cit	$(H^+)_3(Cit^{3-})$
1, 2, 1	12.84	$(H^+)(H_2VO_4^{2-})_2(Cit^{3-})$	
2, 2, 1	19.68	$(H^+)_2(H_2VO_4^{2-})_2(Cit^{3-})$	
3, 2, 1	24.12	$(H^+)_3(H_2VO_4^{2-})_2(Cit^{3-})$	
3, 1, 1	18.35	$(H^+)_3(H_2VO_4^{2-})(Cit^{3-})$	
2, 1, 1	14.1	$(H^+)_2(H_2VO_4^{2-})(Cit^{3-})$	
4, 2, 2	31.3	$(H^+)_4(H_2VO_4^{2-})_2(Cit^{3-})_2$	
5, 2, 2	35.3	$(H^+)_5(H_2VO_4^{2-})_2(Cit^{3-})_2$	
6, 2, 2	39.2	$(H^+)_6(H_2VO_4^{2-})_2(Cit^{3-})_2$	
(p, q, r)	**log β**	**Formula**	**Extended formula**
TERNARY SYSTEM (H^+-$H_2VO_4^{2-}$-$H_2PO_4^-$) REF (4)			
−2, 0, 1	−17.650	PO_4^{3-}	$[(H^+)_{-2}(H_2PO_4^-)]^{3-}$
−1, 0, 1	−6.418	HPO_4^{2-}	$[(H^+)_{-1}(H_2PO_4^-)]^{2-}$
1, 0, 1	1.772	H_3PO_4	$[(H^+)(H_2PO_4^-)]$
9, 14, 1	90.7	$H_3PV_{14}O_{42}^{6-}$	$[(H^+)_9(H_2VO_4^{2-})_{14}(H_2PO_4^-)]^{6-}$
10, 14, 1	94.84	$H_4PV_{14}O_{42}^{5-}$	$[(H^+)_{10}(H_2VO_4^{2-})_{14}(H_2PO_4^-)]^{5-}$
11, 14, 1	96,41	$H_5PV_{14}O_{42}^{4-}$	$[(H^+)_{11}(H_2VO_4^{2-})_{14}(H_2PO_4^-)]^{4-}$

As described previously, the equations above describe the nature of the complexes that form. For example, HVO_4^{2-} is described as minus HVO_4^{2-} - H^+ and thus the species is described as (−1,1) where the p being −1.[137, 149] To quantify the V-species of decavanadate that are present in the growth assay media, we carried out speciation analyses modeling experimentally the distribution of vanadium species in the media. This model can analyze the experimental conditions found in solution prepared by the addition of metavanadate and exposed to the conditions of the cell growth assay. We used the reactions reported previously with regard to the exchange of labile oxovanadates[92, 97, 125, 137-139, 146, 149, 153-155], the formation of the VCit complex[125, 149], the formation of the PV complex[153, 155], and the thermodynamics relating to the decavanadate deprotonation reactions[97, 146, 154]. The known speciation parameters used for vanadate at various pH values were measured in the presence of 0.6M NaCl to keep the salt concentration constant for all the components in the system. As shown in Figure 4.3, the species composition for the conditions of two different concentrations of vanadium (3.3mM and 10mM) are illustrated.

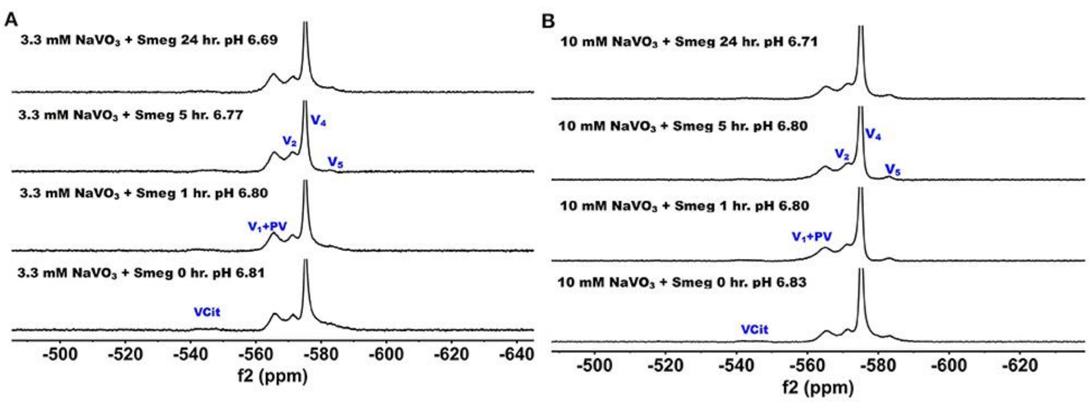

Figure 4.3. The ^{51}V NMR spectra of media in which *M. smeg* had grown at 0, 1, 5, and 24 h time points. Data for two concentrations are shown in (A) 3.3 mM V_1 treatment (3.3 mM V-atoms) and (B) 10 mM V_1 treatment (10 mM V-atoms). See Figure 4.4B caption for key to labeling.

As discussed above, the vanadium samples prepared with decavanadate will not contain this speciation distribution because all V(V) was converted to V_{10}. The addition of this solution to the media will only slowly hydrolyze the V_{10} species to the equilibrium oxovanadate mixture if above or near pH 7. The speciation analysis of the conditions observed in the media with freely exchangeable oxovanadate shown in Figure 4.4 demonstrate that an observable amount of VCit complex forms. Depending on the concentration of the vanadium, the contribution of VCit is larger percentage wise at the lower concentrations of vanadate; for example, at 0.005 and 1.0mM V atoms at neutral pH the amount is 75–80% (in terms of mole fraction) of VCit complex.

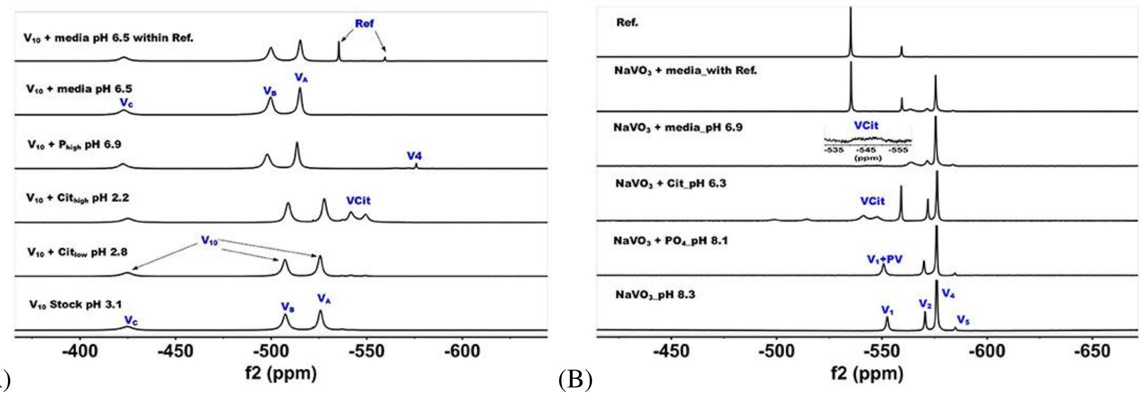

(A) (B)

Figure 4.4. (A) [51]V NMR (78.9 MHz) spectra are shown of solution of decavanadate (10 mM V_{10}, 100 mM V-atoms). The samples are from the bottom up diluted V_{10} stock solution (100 mM V-atom) at pH 3.1; 10 mM V_{10} in the presence of 0.48 mM and 0.97 mM citrate at pH 2.8 and 2.2, respectively; 10 mM V_{10} in the presence of 24 mM P_i at pH 6.9; and finally 10 mM V_{10} in the presence of Middlebrook 7H9 broth medium supplemented with 10% ADC enrichment (5% BSA, 2% dextrose, 5% catalase), glycerol (0.2%, v/v) and Tween 80 (0.05%, v/v) recorded both in the absence and the presence of a capillary reference of 100 mM Na_3VO_4.
(B) [51]V NMR (78.9 MHz) spectra are shown of solution of colorless oxovanadate (40 mM V_1, 40 mM V-atoms). The samples are from the bottom up diluted V_1 stock solution (40 mM V-atom) at pH 8.3; 10 mM V_{10} in the presence of 24 mM P_i at pH 8.1; 10 mM V_{10} in the presence of 0.48 mM citrate at pH 6.3, and finally 10 mM V_{10} in the presence of Middlebrook 7H9 broth medium supplemented with 10% ADC enrichment (5% BSA, 2% dextrose, 5% catalase), glycerol (0.2%, v/v) and Tween 80 (0.05%, v/v) recorded both in the absence and the presence of a capillary reference of 100 mM Na_3VO_4. The spectrum labeled Reference is of the capillary reference alone (top spectrum). The key to the signals: V-oligomers, V_1 monomer; V_2, dimer; V_4, tetramer; V_5, pentamer; VCit, V-citrate complex; PV, vanadate-phosphate complex.

In contrast, at 10mM V-atoms at neutral pH the amount is ~10%. However, if the amounts are calculated, this would correspond to 0.0004, and 1.0mM VCit complex in the media. These observations are consistent with the very strong formation constant for VCit. The PV complex, however, is much less stable, and even though there is much more phosphate in the assay, the PV complex is only observed in a significant concentration at high V and Pi concentrations (5 and 24mM, respective). Although the PV complex is only observed in high concentrations at mM V-treatments the shifting of the V_1 signal attests to the presence of the PV adduct in the assays with M. tb and M. smeg. The results shown in Figure 4.5 are in general agreement with the experimental data obtained in Figures 4.3, 4.4 with regard to formation of the VCit and PV complexes. Figure 4.5 shows that there are four different VCit complexes formed at

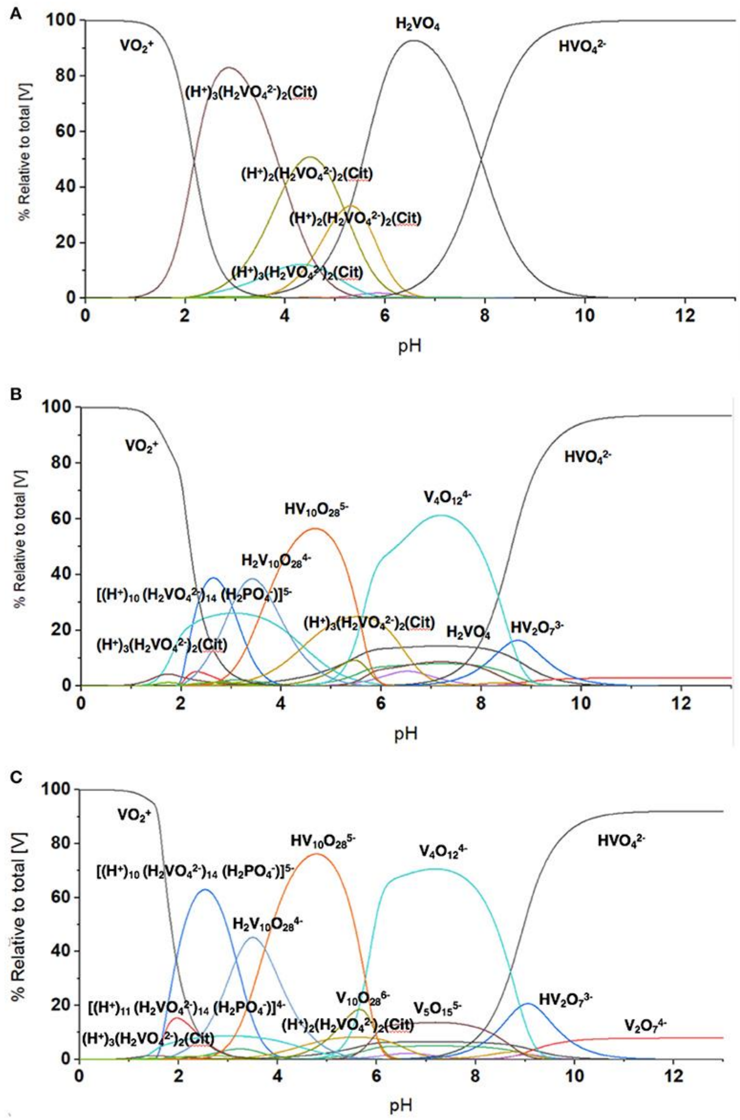

Figure 4.5. The evaluation of the speciation at different vanadium concentration using HySS Program (vs. 2009) (Alderighi et al., 1999). The speciation diagram shown was calculated at several vanadium (V-atom) concentrations in the presence of 0.48 mM citrate and 24 mM phosphate found in the growth media and (A) 5.0 μM vanadate, (B) 3.3 mM vanadate, and (C) 10 mM vanadate. Note, the concentrations of different species regardless of nuclearity are here shown in terms of V-atoms.

low vanadium concentration, but at higher concentration and in the presence of phosphate two major VCit complexes formed.

There are several assumptions on which these estimations are based, including the differences in ionic strengths, the low concentration of the vanadium used, and the fact that some reduction takes place during the growth experiment to be changing the concentrations somewhat of the VCit and PV complexes. Regardless, our general considerations demonstrate that VCit and PV complexes should form as predicted by the speciation analysis and reflect the equilibrium mixture observed by NMR analysis.[137, 149-150]

Vanadium Coordination Complexes

For vanadium coordination complexes, we investigated vanadium dipicolinates to evaluate oncolytic virus infection efficacy based on their chemical and antidiabetic properties and explore their predicted effects in enhancing RNA oncolytic viruses. As the compound would fall apart over time, we wanted to know what species of the compound would exist at various concentrations and pH.

Solution speciation were measured using potentiometry and spectroscopic methods resulting in quantification of species with defined stoichiometry. Details in the speciation of V derivatives have been described. The vanadium complexes are defined by the notation (p, q). Equation (4.4) shows H^+, a metal ion (M) forming a complex with the stoichiometry defined by p and q in an equilibrium reaction, respectively. The resulting formation constant β (p, q) is shown in equation (4.5), where the concentrations of H^+, M are multiplied with each other and divided by the concentration of the complex. Speciation chemistry is defined by a series of constants that represent the system [126, 156]. Using these constants will allow for prediction of species distribution at defined parameters.

$$pH^+ + qM + \rightleftharpoons (H^+)_p(M)_q \qquad (4.4)$$

$$\beta\ (p,q) = \frac{(H^+)_p(M)_q}{(H^+)^p(M)^q} \qquad (4.5)$$

$$pH^+ + qM + rL \rightleftharpoons (H^+)_p(M)_q(L)_r \qquad (4.6)$$

$$\beta\,(p, q, r) = \frac{(H^+)_p(M)_q(L)_r}{(H^+)^p(M)^q(L)^r} \qquad (4.7)$$

Formation constants are reported in the literature values at a 0.40 ionic strength for $[VO_2dipic]^-$ and $[VO_2dipic\text{-}OH]^-$ [93, 157]. However, a comparison of more derivatives was done at a lower ionic strength.[120] The vanadate oligomeric speciation constants are reported at several ionic strengths including 0.15[158], 0.40[92], 0.60[137] and 3.00[138]. We carried out NMR studies quantitating $[VO_2dipic]^-$ both at low ionic strength (no salts added), at 0.15 and at 0.40 to evaluate the effects of ionic strength of intact complex, Figure 4.6. The spectra in Figure 4.6 show that the ratio of complex to free dipic ligand signal varies significantly with changes in ionic strength. Since the concentration of intact complex is dependent on ionic strengths, we modelled the speciation profile to accurately estimate the amounts of intact complexes during the biological treatment (see the Supplemental Material).

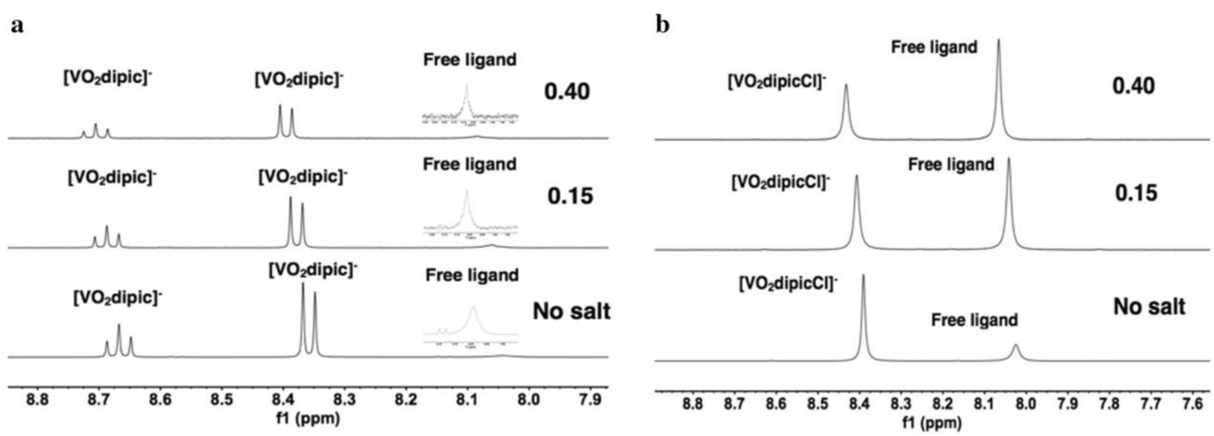

Figure 4.6. The ^{1}H NMR spectra recorded in solutions of $[VO_2dipic]^-$ at pH 6.00 (**a**) and $[VO_2dipicCl]^-$ at pH 6.00 (**b**) at no added salt (bottom), 0.15 M KCl and at 0.40 M KCl

The vanadium complexes are defined by the notation (p, q, r). Equation (4.6) shows H^+, a metal ion (M), and a ligand (L) forming a complex with the stoichiometry defined by p, q, and r in an equilibrium reaction, respectively. The resulting formation constant β (p, q, r) is shown in equation (4/7), where the concentrations of H^+, M, and L are multiplied with each other and divided by the concentration of the complex. Speciation chemistry is defined by a series of constants that represent the system [126, 156]. Using these constants will allow for prediction of species distribution at defined parameters. The formation constants are known for some ionic strengths, and speciation profiles can be calculated for these conditions using the known pH-dependent apparent equilibrium constants, see Eqs. (4.5) and (4.7). NMR measurements were done to determine the amounts of the parent $[VO_2dipic]^-$ complex at 0.40 ionic strength to confirm the reported values.[92] Then, NMR studies were performed at other ionic strengths to verify the known $[VO_2dipic]^-$. These studies confirmed the amounts of both $[VO_2dipic]^-$ and $[VO_2dipic\text{-}Cl]^-$ present to quantify the amounts of $[VO_2dipic]^-$ and $[VO_2dipic\text{-}Cl]^-$ under varying conditions. Using the formation constants, speciation profiles could be calculated using the HySS2009 program) and were used to predict the parent $[VO_2dipic]^-$ complex at the ionic strength 0.40 at which the formation constants have been reported for both vanadate oligomers and the $[VO_2dipic]^-$ complex (Figure 4.7).[18, 92] These calculations allow comparisons between calculated and experimentally measured $[VO_2dipic]^-$ to verify the approach. The speciation profiles should be calculated at the ionic strength of the cell culture media, and this ionic strength is calculated using Eq. (4.5). The details of the calculation are shown in the Supplemental Material, and the result was found to be 0.17. Accordingly, the speciation evaluations in this manuscript were continued using an ionic strength of 0.15. NMR measurements were done at ionic strength I = 0.15. This was followed by calculations carried out using the oxovanadate formation constants determined at ionic strength I = 0.15. We also investigated $Na[VO_2^-$ dipic-OH]. Studies of this system were carried out in detail and are presented in the Supplemental Material. The medium that has an ionic strength of 0.20 or 0.15 was used.[92]

For vanadium dipic, the ionic strength of the media was calculated using equation (4.3) as the system was different. The 40 components in the media were evaluated with regard to the charge

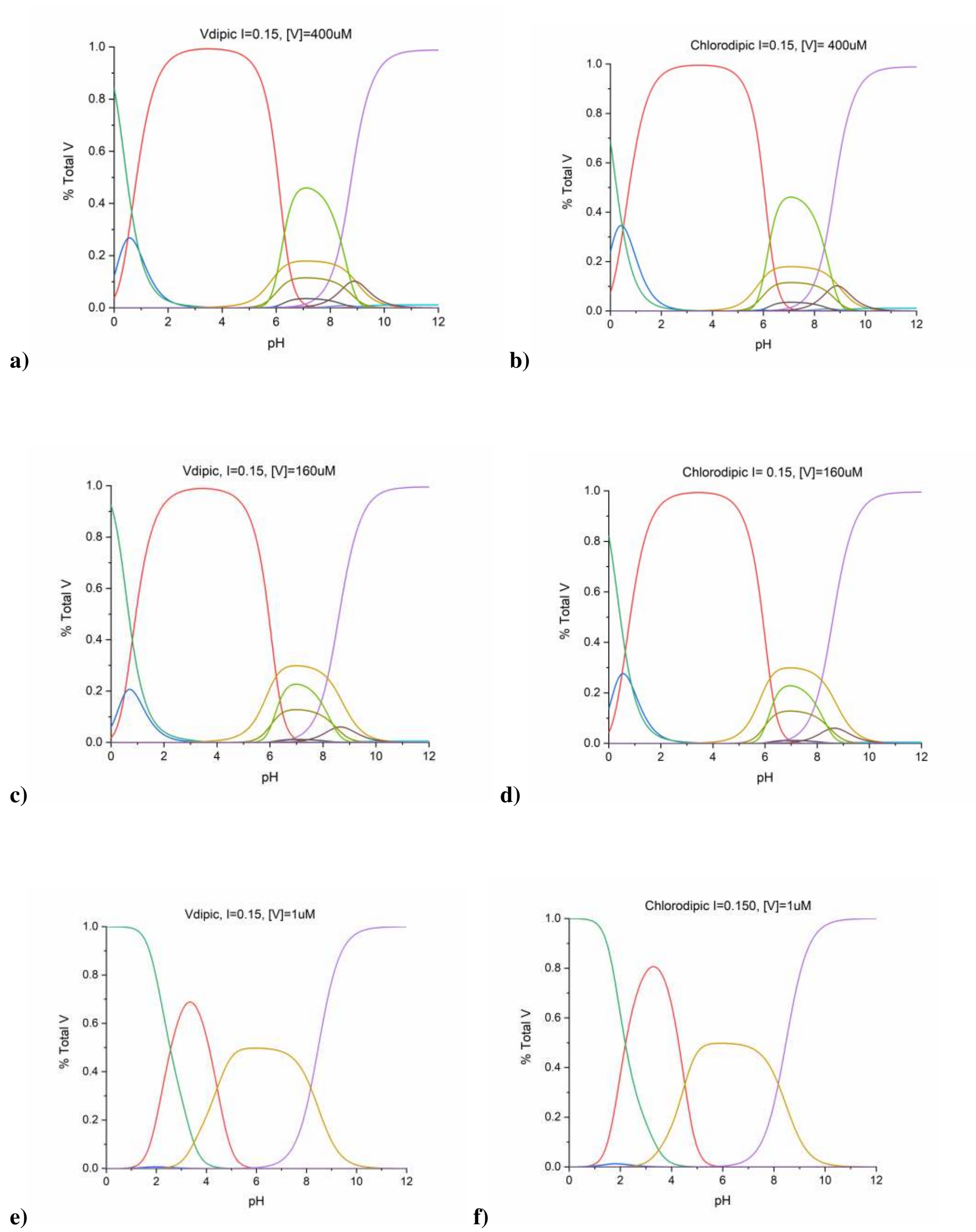

Figure 4.7. The speciation profiles for $[VO_2dipic]^-$ (a, c, e) and $[VO_2dipic\text{-}Cl]^-$ (b, d, f) is shown using total V-concentrations of 400 µM mM (a, b), 160 µM (c, d) and 1.0 **µ**M (e, f). The calculations were done using the vanadate oligomerization constants for 0.15 M NaCl (add ref). Key for curves: red $[VO_2dipic]^-$ or $[VO_2dipic\text{-}Cl]^-$; blue $H[VO_2dipic]$ or $H[VO_2dipic\text{-}Cl]$; purple V_1; green VO^{2+}; light green and beige V_4 species

and their respective contribution to the ionic strength. Assuming that the contributions of serum albumin and other minor component were negligible, the total ionic strength was found to be 0.17. This ionic strength is similar to the speciation studies reported generated in aqueous solutions with

NaCl up to an ionic strength of 0.15. The constants were determined in these studies for vanadate oligomers and were chosen to be used for prediction of speciation in media described in this work. Spectra of the $[VO_2dipic]^-$ complex, the free dipic ligand and the corresponding $[VO_2dipic\text{-}Cl]^-$ complex and its free ligand at 0.15 ionic strength were recorded using ^{51}V and ^{1}H NMR spectroscopy. These NMR spectra are shown in supplemental materials (Figs. S4.1 – S4.4). Using the measured pKa value for H_2dipic and $H_2dipic\text{-}Cl$ and the apparent formation constants for $[VO_2(dipic)]^-$ and $[VO_2dipic\text{-}Cl]^-$ allowed for the calculation of speciation profiles for both complexes. The speciation of these systems is shown in Figure S4.8 from pH 5 through 9 at the concentration that the NMR spectra were recorded. However, for studies described here, the speciation profile was calculated for 0.16 mM which is near or at the concentration where the greatest amount of virus enhancement was observed.

According to the speciation profiles for the low end of the dose response range (0.002 μM) there is little intact $[VO_2dipic]^-$ and $VO_2dipic\text{-}Cl]^-$complex, whereas at the high end of the dose response range (0.4 mM) an observable amount of both complexes is present. Peak GFP count was observed at 160 μM for both $[VO_2dipic]^-$ and $[VO_2dipic\text{-}OH]^-$ complexes and at 400 μM for the $[VO_2dipic\text{-}Cl]^-$ complex. Viability and GFP data for the $[VO_2dipic]^-$, $[VO_2dipic\text{-}OH]^-$ and $[VO_2dipic\text{-}Cl]^-$ complexes are indistinguishable from the effects observed with vanadate at 160 μM. Although the complexes may hydrolyze in aqueous solution some intact complex may facilitate the uptake of the compounds by the oncolytic virus or the cancer cell so the interactions of the $[VO_2dipic\text{-}Cl]^-$ complex was explored by studies in the microemulsion cellular system for comparison with similar studies done with $[VO_2dipic]^-$.

Conclusion

At the conditions of the two different environments, we find that our complexes, both a coordination complexes and a polyoxometalate completely fall apart under biological conditions after 24 hours. We show two representative studies, one in anticancer cells and another in a bacterial system. For one system this is ideal as the complex should fall apart after a given amount of time as the vanadium decomposition products are useful. For the other, ideally, we would like the compound to last longer as the complex itself is the most effective at the treatment.

Chapter 5- Conclusions

Cancer is still one of the leading causes of death in the United States and it is vital to keep cancer research ongoing. Although many potential treatments such as nanomaterials, heat, organic compounds, and polymers are being investigated, research for metal complexes as a cancer treatment tend to be focused towards platinum based drugs which is unsustainable in the long term as platinum is rare, expensive, and used in much more than just medicines.[159] As such, finding alternative complexes would be desirable. Metals such as gallium, rhenium, cobalt, gold and zinc are options, but vanadium has already proven to have medicinal properties that makes it promising for further research not only as the base metal, but also as varying coordination complexes.[159-161] BMOV and BEOV were considered as possible diabetes drug candidates but ran out of money during Phase 2 testing, decavanadate has been reported to inhibit the growth rates of tuberculosis and ortho and metavanadate have been shown to significantly increase the growth rate of oncolytic viruses for immunotherapy options.[8, 15]

As of currently, the [VO(HSHED)(DTB)] complex is still our most potent compound with a cytotoxicity against T98g cells that was 12-fold more toxic than cisplatin.[7] Ideally, we would like to improve on this compound so it will be effective for clinical trials. There are multiple areas that can be modified as reported in the earlier sections. For the vanadium Schiff base, we wanted to improve both the hydrophobicity and the biological activity in T98g cells. In Chapter 2, our structure activity relationship studies for our vanadium Schiff base series have shown that the catecholate ligand has the highest impact on the hydrophobicity. The modification of the salicylaldehyde portion of the compound showed less impact with the halogen modification, but the fact that the activity and hydrophobicity does change with the EWG shows that the salicylaldehyde can modify the properties of the compound as a whole. Rather than halogenation of the salicylaldehyde portion of the Schiff base and increasing electronegativity, adding more sterically hindered substituents would be an alternative approach that led to more efficacious compounds. More electron donating groups on the salicylaldehyde portion of the compound may also be a target. Our attempts at EDG on the catechol caused the compound to hydrolyze and fall apart in minutes, but if we combine an EDG modification on the salicylaldehyde with very bulky hydrophobic groups on the catecholate ligand, the complex may last longer and have desirable redox properties. Another modification site would also be on the hydroxyethyl diamine portion of the Schiff base complex. There have been attempts to modify this area, but the activity and the stability were shown to be significantly lower when the hydroxyl group was removed from that portion of the molecule. Perhaps adding substituents to the side chain rather than replacing the ligand entirely would be more effective. The -OH group may be hydrogen bonding to either the vanadium metal or the catechol ligand. The main focus should be on the catecholato ligand as that has shown to have the largest effect on the hydrophobicity. Vanadium Schiff base complexes with the base catecholato ligand and the methyl catecholato ligand tend to fall apart within 1-10 minutes in cell culture media. The [VO(HSHED)(DTB)] complex can last up to 24 hours which gives the compound time to reach the active site and cause cytotoxic effects to the cancer cells before falling apart.

In Chapter 3, we introduced the development of the adamantanol catecholato ligand as an alternative to the di-*tert*-butyl catecholato with this idea in mind. If the bulky di-tert butyl ligand showed activity through hydrophobicity, then a bulkier ligand would stand to reason to have both a greater hydrophobicity and biological activity. Based on preliminary studies on the vanadium Schiff base complex, it is stable up to 24 hours, but we do observe that the compound then hydrolyzes into the vanadium (IV) tris catecholato species. How this may affect the cytotoxicity is still being researched, although it has been shown that it may cause the compound to have overall less cytotoxicity than the [VO(HSHED)(DTB)] complex. Lastly in Chapter 4, we show that while metal complexes have potential as drug candidates, the hydrolysis products always have to be kept in consideration. As the vanadium Schiff bases have shown, even though the main complex is what provides the most cytotoxicity to the cancer cells, the decomposition products have activity of their own both towards the cancer cells as well as regular cells.

As mentioned previously, we have observed the formation of vanadium (IV) tris adamantyl catecholato, and while it forms during the hydrolysis of the vanadium Schiff bases, it has not been isolated and investigated as another possible cytotoxic drug. This may be another avenue worth investigating as the catecholato ligand has shown to have the largest impact on the hydrophobicity of the complexes. The vanadium tris di-*tert*-butyl catechol has been shown to also have cytotoxic effects, but the complex falls apart rapidly in water or cell culture media. The vanadium tris adamantyl catecholate may be able to stay intact for longer periods of time.

While vanadium coordination chemistry can be one of the more challenging fields of study because of how many different species to consider based on factors like concentrations, ionic strengths, pHs, and other environmental effects, there is so much potential in the field of vanadium chemistry. The research shown here is only scratching the surface of what could be a viable effective treatment to some of the worst forms of cancer out there. From straight intratumoral or intravenous drugs to creating environments for other treatments to work in tandem, there is still so much work to be done. Based on the comprehensive structure relationship activity studies I have done, my coworkers have taken what I have researched and are building compounds that build off the foundation that I have made. From the [VO(HSHED)(DTB)] compound, we now have discovered and synthesized three new compounds that are on the same level of biological activity as our best complex. I wish them the best in their research as the more potent the compounds are, the better our cancer treatments will be in the future. I greatly appreciate the opportunity to develop these projects and I only hope that it was a start into more metal drug synthesis research.

References

1. Pessoa, J. C.; Boas, L. V., Vanadium. *Coord. Chem. Rev.* **1987**.
2. Cornman, C. R.; Zovinka, E. P.; Meixner, M. H., Vanadium(IV) Complexes of an Active-Site Peptide of a Protein Tyrosine Phosphatase *Inorg. Chem.* **1995,** *34*, 5099-5100.
3. Crans, D. C.; Chen, H.; Anderson, O. P.; Miller, S. M., Vanadium(V)-Protein Model Studies: Solid-State and Solution Structure. *J. Am. Chem. Soc.* **1993,** *115*, 6769-6776.
4. Crans, D. C.; Bunch, R. L.; Theisen, L. A., Interaction of Trace Levels of Vanadium(1V) and Vanadium(V) in Biological Systems. *J. Am. Chem. Soc.* **1989,** *111*, 7597-7607.
5. Pessoa, J. C.; Etcheverry, S.; Gambino, D., Vanadium compounds in medicine. *Coord. Chem. Rev.* **2015,** *301*, 24–48.
6. Rehder, D., The (biological) speciation of vanadate(V) as revealed by (51)V NMR: A tribute on Lage Pettersson and his work. *J. Inorg. Biochem.* **2015,** *147*, 25-31.
7. Levina, A.; Pires Vieira, A.; Wijetunga, A.; Kaur, R.; Koehn, J. T.; Crans, D. C.; Lay, P. A., A Short-Lived but Highly Cytotoxic Vanadium(V) Complex as a Potential Drug Lead for Brain Cancer Treatment by Intratumoral Injections. *Angew Chem Int Ed Engl* **2020**.
8. Selman, M.; Rousso, C.; Bergeron, A.; Son, H. H.; Krishnan, R.; El-Sayes, N. A.; Varette, O.; Chen, A.; Le Boeuf, F.; Tzelepis, F.; Bell, J. C.; Crans, D. C.; Diallo, J. S., Multi-modal Potentiation of Oncolytic Virotherapy by Vanadium Compounds. *Mol Ther.* **2018,** *26* (1), 56-69.
9. Griffin, E.; Levina, A.; Lay, P. A., Vanadium(V) tris-3,5-di-tert-butylcatecholato complex: Links between speciation and anti-proliferative activity in human pancreatic cancer cells. *J. Inorg. Biochem.* **2019,** *201*, 110815.
10. Levina, A.; Crans, D. C.; Lay, P. A., Speciation of metal drugs, supplements and toxins in media and bodily fluids controls in vitro activities. *Coord. Chem. Rev.* **2017,** *352*, 473-498.
11. Oun, R.; Moussa, Y. E.; Wheate, N. J., The side effects of platinum-based chemotherapy drugs: a review for chemists. *Dalton Trans.* **2018,** *47* (19), 6645-6653.
12. Miller, R. P.; Tadagavadi, R. K.; Ramesh, G.; Reeves, W. B., Mechanisms of Cisplatin nephrotoxicity. *Toxins (Basel)* **2010,** *2* (11), 2490-2518.
13. Wang, D.; Lippard, S. J., Cellular processing of platinum anticancer drugs. *Nat. Rev. Drug Discov.* **2005,** *4* (4), 307-320.
14. Coluccia, M.; Natile, G., Trans-Platinum Complexes in Cancer Therapy. *Anticancer Agents Med Chem* **2007,** *7*, 111-123.
15. Samart, N.; Arhouma, Z.; Kumar, S.; Murakami, H. A.; Crick, D. C.; Crans, D. C., Decavanadate Inhibits Mycobacterial Growth More Potently Than Other Oxovanadates. *Front. Chem.* **2018,** *6*, 519.
16. Bergeron, A.; Kostenkova, K.; Selman, M.; Murakami, H. A.; Owens, E.; Haribabu, N.; Arulanandam, R.; Diallo, J. S.; Crans, D. C., Enhancement of oncolytic virotherapy by vanadium(V) dipicolinates. *Biometals* **2019,** *32* (3), 545-561.
17. Althumairy, D.; Murakami, H. A.; Zhang, D.; Barisas, B. G.; Roess, D. A.; Crans, D. C., Effects of vanadium(IV) compounds on plasma membrane lipids lead to G protein-coupled receptor signal transduction. *J. Inorg. Biochem.* **2020,** *203*, 110873.

18. Alderighi, L.; Gans, P.; Ienco, A.; Peters, D.; Sabatani, A.; Vacca, A., Hyperquad simulation and speciation (HySS): a utility program for the investigation of equilibria involving soluble and partially soluble species. *Coord. Chem. Rev.* **1999,** *184*, 311-318.
19. Rehder, D., The role of vanadium in biology. *Metallomics* **2015,** *7* (5), 730-742.
20. Thompson, K. H.; Orvig, C., Vanadium in diabetes: 100 years from Phase 0 to Phase I. *J. Inorg. Biochem.* **2006,** *100* (12), 1925-1935.
21. Chatkon, A.; Barres, A.; Samart, N.; Boyle, S. E.; Haller, K. J.; Crans, D. C., Guanylurea metformium double salt of decavanadate, (HGU+)4(HMet+)2(V10O286−)·2H2O. *Inorganica Chim. Acta* **2014,** *420*, 85-91.
22. Cornman, C. R.; Colpas, G. J.; Hoeschele, J. D.; Kampf, J.; Pecoraro, V. L., Implications for the Spectroscopic Assignment of Vanadium Biomolecules: Structural and Spectroscopic Characterization of Monooxovanadium(V) Complexes Containing Catecholate and Hydroximate Based Noninnocent Ligands. *J. Am. Chem. Soc.* **1992,** *114* (25), 9925-9933.
23. Hirooka, Y.; Kasuya, H.; Ishikawa, T.; Kawashima, H.; Ohno, E.; Villalobos, I. B.; Naoe, Y.; Ichinose, T.; Koyama, N.; Tanaka, M.; Kodera, Y.; Goto, H., A Phase I clinical trial of EUS-guided intratumoral injection of the oncolytic virus, HF10 for unresectable locally advanced pancreatic cancer. *BMC Cancer* **2018,** *18* (1), 596.
24. Mohan, A.; Harris, K.; Bowling, M. R.; Brown, C.; Hohenforst-Schmidt, W., Therapeutic bronchoscopy in the era of genotype directed lung cancer management. *J. Thorac. Dis.* **2018,** *10* (11), 6298-6309.
25. Newman, J. H.; Chesson, C. B.; Herzog, N. L.; Bommareddy, P. K.; Aspromonte, S. M.; Pepe, R.; Estupinian, R.; Aboelatta, M. M.; Buddhadev, S.; Tarabichi, S.; Lee, M.; Li, S.; Medina, D. J.; Giurini, E. F.; Gupta, K. H.; Guevara-Aleman, G.; Rossi, M.; Nowicki, C.; Abed, A.; Goldufsky, J. W.; Broucek, J. R.; Redondo, R. E.; Rotter, D.; Jhawar, S. R.; Wang, S. J.; Kohlhapp, F. J.; Kaufman, H. L.; Thomas, P. G.; Gupta, V.; Kuzel, T. M.; Reiser, J.; Paras, J.; Kane, M. P.; Singer, E. A.; Malhotra, J.; Denzin, L. K.; Sant'Angelo, D. B.; Rabson, A. B.; Lee, L. Y.; Lasfar, A.; Langenfeld, J.; Schenkel, J. M.; Fidler, M. J.; Ruiz, E. S.; Marzo, A. L.; Rudra, J. S.; Silk, A. W.; Zloza, A., Intratumoral injection of the seasonal flu shot converts immunologically cold tumors to hot and serves as an immunotherapy for cancer. *Proc Natl Acad Sci U S A* **2020,** *117* (2), 1119-1128.
26. Madani, S.; Naderi, N.; Dissanayake, O.; Tan, A.; Seifalian, A. M., A new era of cancer treatment: carbon nanotubes as drug delivery tools. *Int. J. Nanomedicine* **2011,** *6*, 2963-2979.
27. Levina, A.; Lay, P. A., Stabilities and Biological Activities of Vanadium Drugs: What is the Nature of the Active Species? *Chem Asian J.* **2017,** *12* (14), 1692-1699.
28. Levina, A.; Lay, P. A., Metal-Based Anti-diabetic Drugs: Advances and Challenges. *Dalton Trans.* **2011,** *40* (44), 11675-11686.
29. Safitri, A.; Levina, A.; Lee, J.; Carter, E. A.; Lay, P. A. In *Biospectroscopy for studying the influences of anti-diabetic metals (V, Cr, Mo, and W) to the insulin signaling pathway*, AIP Conf. Proc. , 2017; p 020019.
30. Milsmann, C.; Levina, A.; Harris, H. H.; Foran, G. J.; Turner, P.; Lay, P. A., Charge Distribution in Chromium and Vanadium Catecholato Complexes: X-ray Absorption Spectroscopic and Computational Studies. *Inorg. Chem.* **2006,** *45* (12), 4743-4754.
31. Levina, A.; Foran, G. J.; Pattison, D. I.; Lay, P. A., X-ray Absorption Spectroscopic and Electrochemical Studies of Tris(catecholato(2−))chromate(V/IV/III) Complexes. *Angew Chem Int Ed Engl* **2004,** *43*, 462-465.

32. Crans, D. C.; Koehn, J. T.; Petry, S. M.; Glover, C. M.; Wijetunga, A.; Kaur, R.; Levina, A.; Lay, P. A., Hydrophobicity may enhance membrane affinity and anti-cancer effects of Schiff base vanadium(v) catecholate complexes. *Dalton Trans.* **2019,** *48* (19), 6383-6395.
33. Crans, D. C.; Henry, L.; Cardiff, G.; Posner, B. I., Developing Vanadium as an Antidiabetic or Anticancer Drug: A Clinical and Historical Perspective. *Met. Ions Life Sci.* **2019,** *19* (203-230).
34. Lima, L. M. A.; Murakami, H.; Gaebler, D. J.; Silva, W. E.; Belian, M. F.; Lira, E. C.; Crans, D. C., Acute Toxicity Evaluation of Non-Innocent Oxidovanadium(V) Schiff Base Complex. *Inorganics* **2021,** *9* (42), 1-17.
35. Levina, A.; Crans, D. C.; Lay, P. A., Advantageous Reactivity of Unstable Metal Complexes: Potential Applications of Metal-Based Anticancer Drugs for Intratumoral Injections. *Pharmaceutics* **2022,** *14* (4).
36. Manganaro, J.; Levina, A.; Lay, P. A.; Crans, D. C., Potential Applications of Vanadium-Based Anticancer Drugs for Intratumoral Injections. *Med. Sci. Forum* **2022,** *2* (in press).
37. Hamid, O.; Ismail, R.; Puzanov, I., Intratumoral Immunotherapy-Update 2019. *Oncologist* **2020,** *25* (3), 423-438.
38. Shul'pin, G. B.; Kozlov, Y. N.; Shul'pina, L. S., Metal Complexes Containing Redox-Active Ligands in Oxidation of Hydrocarbons and Alcohols: A Review. *Catalysts* **2019,** *9* (12).
39. Goncharova-Zapata, O.; Chatterjee, P. B.; Hou, G.; Quinn, L. L.; Li, M.; Yehl, J.; Crans, D. C.; Polenova, T., Effect of Ancillary Ligand on Electronic Structure as Probed by (51)V Solid-State NMR Spectroscopy for Vanadium-o-Dioxolene Complexes. *CrystEngComm* **2013,** *15* (43).
40. Jiang, S.; Chen, S.; Guo, H.; Yang, F., "Turn-on" far-red fluorescence sensor for Y3+ based on Schiff-based tetraphenylethylene. *Dyes and Pigments* **2020,** *183*.
41. Li, S.; Pei, M.; Wan, T.; Yang, H.; Gu, S.; Tao, Y.; Liu, X.; Zhou, Y.; Xu, W.; Xiao, P., Self-healing hyaluronic acid hydrogels based on dynamic Schiff base linkages as biomaterials. *Carbohydr. Polym.* **2020,** *250*, 116922.
42. Modak, P.; Hammond, W.; Jaffe, M.; Nadig, M.; Russo, R., Dynamic, 3D Schiff base networks for medical applications. *J. Appl. Polym. Sci.* **2020,** *137* (43).
43. Yan, X. J.; Wang, Z. G.; Wang, Y.; Huang, Y. Y.; Liu, H. B.; Xie, C. Z.; Li, Q. Z.; Xu, J. Y., A dual-functional fluorescent probe for sequential determination of Cu(2+)/S(2-) and its applications in biological systems. *Spectrochim Acta A Mol Biomol Spectrosc* **2020,** *243*, 118797.
44. More, M. S.; Joshi, P. G.; Mishra, Y. K.; Khanna, P. K., Metal complexes driven from Schiff bases and semicarbazones for biomedical and allied applications: a review. *Mater. Today Chem* **2019,** *14*, 100195.
45. Smee, J. J.; Crans, D. C., *Vanadium*. Elsevier Science: Oxford, U.K., 2004; Vol. 4, p 175-239.
46. Xinhau, L.; Soo Lah, M.; Pecoraro, V. L., Vanadium Complexes of the Tridentate Schiff Base Ligand N-Salicylidene-N-(2-hydroxyethyI)ethylenediamine: Acid-Base and Redox Conversion between Vanadium(IV) and Vanadium(V) Imino Phenolates. *Inorg. Chem.* **1988,** *27*, 4657-4664.
47. Thakur, S.; Banerjee, S.; Das, S.; Chattopadhyay, S., DFT study on the redox behavior of two dioxovanadium(v) complexes with N2O donor Schiff base ligands and their use in catalytic oxidation ofortho-aminophenol. *New J. Chem.* **2019,** *43* (47), 18747-18759.
48. Thakur, S.; Drew, M. G. B.; Franconetti, A.; Frontera, A.; Chattopadhyay, S., Stabilization of two conformers via intra- or inter-molecular hydrogen bonds in a dinuclear vanadium(v) complex with a pendant Schiff base: theoretical insight. *RSC Adv* **2019,** *9* (60), 35165-35175.

49. Patel, N.; Prajapati, A. K.; Jadeja, R. N.; Patel, R. N.; Patel, S. K.; Tripathi, I. P.; Dwivedi, N.; Gupta, V. K.; Butcher, R. J., Dioxidovanadium(V) complexes of a tridentate ONO Schiff base ligand: Structural characterization, quantum chemical calculations and in-vitro antidiabetic activity. *Polyhedron* **2020,** *180*.
50. Cooper, S. R.; Koh, Y. B.; Raymond, K. N., Synthetic, structural, and physical studies of bis(triethylammonium) tris(catecholato)vanadate(IV), potassium bis(catecholato)oxovanadate(IV), and potassium tris(catecholato)vanadate (III). *J. Am. Chem. Soc.* **1982,** *104* (19), 5092-5102.
51. Cass, M. E.; Gordon, N. R.; Pierpont, C. G., Catecholate and Semiquinone Complexes of Vanadium. Factors That Direct Charge Distribution in Metal-Quinone Complexes. *Inorg. Chem.* **1986,** *25*, 3962-3967.
52. Chatterjee, P. B.; Goncharov-Zapata, O.; Quinn, L. L.; Hou, G.; Hamaed, H.; Schurko, R. W.; Polenova, T.; Crans, D. C., Characterization of noninnocent metal complexes using solid-state NMR spectroscopy: o-dioxolene vanadium complexes. *Inorg. Chem.* **2011,** *50* (20), 9794-9803.
53. Crans, D. C., Antidiabetic, Chemical, and Physical Properties of Organic Vanadates as Presumed Transition-State Inhibitors for Phosphatases. *J. Org. Chem.* **2015,** *80* (24), 11899-915.
54. Trevino, S.; Diaz, A., Vanadium and insulin: Partners in metabolic regulations. *J. Inorg. Biochem.* **2020,** *208*, 111094.
55. Arhouma, Z.; Murakami, H. A.; Koehn, J. T.; Xiarong Li; Roess, D. A.; Crick, D. C.; Crans, D. C., Exploring Growth of Mycobacterium smegmatis Treated with Anticarcinogenic Vanadium Compounds. *Inorganics* **2022,** *10* (50), 1-22.
56. Sambrock, J.; Fritsch, E. F.; Maniatis, T., *Molecular Cloning, A Laboratory Manual* 2ed.; Cold Spring Harbor: New York, 1989; Vol. 3.
57. Swain, M. Chemicalize. org. www.chemicalize.org.
58. Wittenkeller, L.; Abraha, A.; Ramasamy, R.; Mota de Freitas, D.; Theisen, L. A.; Crans, D. C., Vanadate Interactions with Bovine Cu, Zn-Superoxide Dismutase As Probed by 51V NMR Spectroscopy. *J. Am. Chem. Soc.* **1991,** *113* (21), 7872-7881.
59. Crans, D. C.; Shin, P. K., Characterization of Vanadium(V) Complexes in Aqueous Solutions: Ethanolamine- and Glycine-Derived Complexes. *J. Am. Chem. Soc.* **1994,** *116* (4), 1305-1315.
60. Gritzner, G.; Kuta, J., Recommendations on reporting electrode potentials in nonaqueous solvents (Recommendations 1983). *Pure Appl. Chem.* **1984,** *56* (4), 461-466.
61. Hrbac, J.; Halouzka, V.; Trnkova, L.; Vacek, J., eL-Chem Viewer: a freeware package for the analysis of electroanalytical data and their post-acquisition processing. *Sensors (Basel)* **2014,** *14* (8), 13943-54.
62. Amatore, C.; Azzabi, M.; Calas, P.; Jutand, A.; Lefrou, C.; Rollin, Y., Absolute determination of electron consumption in transient or steady state electrochemical techniques. *J. electroanal. chem. interfacial electrochem.* **1990,** *288* (1-2), 45-63.
63. Izutsu, K., Reference electrodes for use in nonaqueous solutions. In *Handbook of Reference Electrodes*, Springer: 2013; pp 145-187.
64. Mann, C. K.; Barnes, K. K., Electrochemical reactions in nonaqueous systems. **1970**.
65. Kaim, W., The transition metal coordination chemistry of anion radicals. *Coord. Chem. Rev.* **1987,** *76*, 187-235.
66. Kaim, W.; Schwederski, B., Non-innocent ligands in bioinorganic chemistry—An overview. *Coord. Chem. Rev.* **2010,** *254* (13-14), 1580-1588.

67. Ren, S.; Wang, R.; Komatsu, K.; Bonaz-Krause, P.; Zyrianov, Y.; McKenna, C. E.; Csipke, C., Synthesis, biological evaluation, and quantitative structure-activity relationship analysis of new Schiff bases of hydroxysemicarbazide as potential antitumor agents. *J. Med. Chem.* **2002,** *45* (2), 410-419.
68. Weekes, D. M.; Ramogida, C. F.; Jaraquemada-Pelaez, M. G.; Patrick, B. O.; Apte, C.; Kostelnik, T. I.; Cawthray, J. F.; Murphy, L.; Orvig, C., Dipicolinate Complexes of Gallium(III) and Lanthanum(III). *Inorg. Chem.* **2016,** *55* (24), 12544-12558.
69. Viswanadhan, V. N.; Ghose, A. K.; Revankar, G. R.; Robins, R. K., Atomic Physiochemical Parameters for Three Dimensional Structure Directed Quantitative Structure-Activity Relationships. *J. Chem. Inf. Comput. Sci.* **1989,** *29*, 163-172.
70. Marloye, M.; Berger, G.; Gelbcke, M.; Dufrasne, F., A survey of the mechanisms of action of anticancer transition metal complexes. *Future Med. Chem.* **2016,** *8* (18), 2263-2286.
71. Krämer, S. D.; Aschmann, H. E.; Hatibovic, M.; Hermann, K. F.; Neuhaus, C. S.; Brunner, C.; Belli, S., When barriers ignore the "rule-of-five". *Adv. Drug Deliv. Rev.* **2016,** *101*, 62-74.
72. Crans, D. C.; Smee, J. J.; Gaidamauskas, E.; Yang, L., The Chemistry and Biochemistry of Vanadium and the Biological Activities Exerted by Vanadium Compounds. *Chem. Rev.* **2004,** *104*, 849-902.
73. Jones, C. R.; Butts, C. P.; Harvey, J. N., Accuracy in determining interproton distances using Nuclear Overhauser Effect data from a flexible molecule. *Beilstein J. Org. Chem.* **2011,** *7*, 145-150.
74. Noviandri, I.; Brown, K. N.; Fleming, D. S.; Fleming, S.; Gulyas, P. T.; Lay, P. A.; Masters, A. F.; Phillips, L., The Decamethylferrocenium/Decamethylferrocene Redox Couple: A Superior Redox Standard to the Ferrocenium/Ferrocene Redox Couple for Studying Solvent Effects on the Thermodynamics of Electron Transfer. *J. Phys. Chem. B.* **1999,** *103* (32), 6713-6722.
75. Gagne, R. R.; Koval, C. A.; Lisensky, G. C., Ferrocene as an internal standard for electrochemical measurements. *Inorg. Chem.* **1980,** *19* (9), 2854-2855.
76. Koehn, J. T.; Magallanes, E. S.; Peters, B. J.; Beuning, C. N.; Haase, A. A.; Zhu, M. J.; Rithner, C. D.; Crick, D. C.; Crans, D. C., A synthetic isoprenoid lipoquinone, menaquinone-2, adopts a folded conformation in solution and at a model membrane interface. *J. Org. Chem.* **2017,** *83* (1), 275-288.
77. Powell, D. W.; Lay, P. A., The Linkage Isomerisation Reactions of Acetonepentaammineruthenium(III) and -ruthenium(II) Complexes. *Inorg. Chem.* **1992,** *31*, 3542-3550.
78. American Type Culture Collection (ATCC), www.atcc.org. Cell lines: T98g (glioblastoma multiforme, Cat. No. CRL-1690); MDA-MB-231 (metastatic breast adenocarcinoma; Cat. No. HTB-26); PANC-1 (epithelioid carcinoma of the pancreas, Cat. No. CRL-1469); A549 (lung epithelial carcinoma, Cat. No. CCL-185); HFF-1 (normal human foreskin fibroblasts, Cat. No. SCRC-1041).
79. Maia, A.; Wiemann, S., Cancer-Associated Fibroblasts: Implications for Cancer Therapy. *Cancers* **2021,** *13* (14).
80. Molinuevo, M. S.; Barrio, D. A.; Cortizo, A. M.; Etcheverry, S. B., Antitumoral properties of two new vanadyl(IV) complexes in osteoblasts in culture: role of apoptosis and oxidative stress. *Cancer Chemother. Pharmacol.* **2004,** *53* (2), 163-172.
81. Barrio, D. A.; Etcheverry, S. B., Vanadium and bone development: putative signaling pathways. *Can. J. Physiol. Pharmacol.* **2006,** *84* (7), 677-686.

82. He, Z.; Hans, S.; Zhu, H.; Hu, X.; Li, X.; Hou, C.; Wu, C.; Xie, Q.; Li, N.; Du, X.; Ni, J.; Liu, Q., The Protective Effect of Vanadium on Cognitive Impairment and the Neuropathology of Alzheimer's Disease in APPSwe/PS1dE9 Mice. *Front. Mol. Neurosci.* **2020,** *13*.
83. Omidian, S.; Haghbin Nazarak, M.; Bagher, Z.; Moztarzadeh, F., The effect of vanadium ferrite doping on the bioactivity of mesoporous bioactive glass-ceramics. *RSC Adv.* **2022,** *12* (39), 25639-25653.
84. Posner, B. I.; Faure, R.; Burgess, J. W.; Bevan, A. P.; Lachance, D.; Zhang-Sun, G.; Fantus, I. G.; Ng, J. B.; Hall, D. A.; Lum, B. S.; Shaver, A., Peroxovanadium compounds: A new class of potent phosphotyrosine phosphatase inhibitors which are insulin mimetics. *J. Biol. Chem.* **1994,** *269* (6), 4596-4604.
85. Petanidis, S.; Kioseoglou, E.; Hadzopoulou-Cladaras, M.; Salifoglou, A., Novel ternary vanadium-betaine-peroxido species suppresses H-ras and matrix metalloproteinase-2 expression by increasing reactive oxygen species-mediated apoptosis in cancer cells. *Cancer Lett.* **2013,** *335*, 387-396.
86. Yin, C.-X.; Finke, R. G., Vanadium-Based, Extended catalytic lifetime catechol dioxygenases: Evidence for a common catalyst. *J. Am. Chem. Soc.* **2005,** *127*, 9003-9013.
87. Salonen, P.; Savela, R.; Peuronen, A.; Lehtonen, A., Vanadium aminophenolates in catechol oxidation: conformity with Finke's common catalyst hypothesis. *Dalton Trans.* **2021,** *50*, 6088-6099.
88. Hornykiewicz, O., Dopamine (3-Hydroxytyramine) and Brain Function. *Pharmacol. Rev.* **1966,** *18* (2), 925-964.
89. Sokolenko, V. A.; Svirskaya, N. M.; Kogai, T. I.; Karpova, M. S.; Pavlenko, N. I., Diadamantylation of dihydric phenols and their derivatives. *Russ. J. Appl. Chem.* **2008,** *81* (3), 509-510.
90. Korsakova, I. Y.; Safonova, O. A.; Ageeva, O. I.; Shvedov, V. I.; Nikolaeva, I. S.; Pushkina, T. V.; Pershin, G. N.; Golovanova, E. A., Adamantylphenols. II. Synthesis and antiviral activity of brominated hydroquinones and quinones containing an adamantyl substituent. *Pharm. Chem. J.* **1982,** *16*, 127-130.
91. Murakami, H. A.; Uslan, C.; Haase, A. A.; Koehn, J. T.; Vieira, A.; Gaebler, D. J.; Hagan, J.; Beuning, C. N.; Proschogo, N.; Levina, A.; Lay, P. A.; Crans, D. C., Vanadium chloro substituted Schiff base catecholate complexes are reducible, lipophilic, water stable, and have anticancer activities *Inorg. Chem.* **2022,** *61*, 20757-20773.
92. Crans, D. C.; Yang, L.; Jakusch, T.; Kiss, T., Aqueous chemistry of ammonium (dipicolinato)oxovanadate(V): the first organic vanadium(V) insulin-mimetic compound. *Inorg. Chem.* **2000,** *39*, 4409-4416.
93. Crans, D. C.; Mahroof-Tahir, M.; Johnson, M. D.; Wilkins, P. C.; Yang, L.; Robbins, K.; Johnson, A.; Alfano, J. A.; Godzala, M. E., 3rd; Austin, L. T.; Willsky, G. R., Vanadium(IV) and vanadium(V) complexes of dipicolinic acid and derivatives. Synthesis, X-ray structure, solution state properties and effects in rats with STZ-induced diabetes. *Inorg. Chim. Acta* **2003,** *356*, 365-378.
94. Moskovitz, B. L.; Group, A. T. H.-C. S., Clinical trial and tolerance of HPA-23 in patients with acquired immunodeficiency syndrome. *Antimicrob. Agents Chemother.* **1988,** *32*, 1300-1303.
95. Hill, C. L.; Hartnup, M.; Faraj, M.; Weeks, M.; Prosser-Mccartha, C. M.; Brown, R. B. J.; al., e., Polyoxometalates as inorganic anti-HIV-1 compounds. Structure-activity relationships. *Adv. Chemotherapy AIDS* **1990**, 33-41.

96. Rhule, J. T.; Hill, C. L.; Judd, D. A.; Schinazi, R. F., Polyoxometalates in medicine. *Chem. Rev.* **1998,** *98*, 327-358.
97. Aureliano, M.; Crans, D. C., Decavanadate (V10O6−28) and oxovanadates: oxometalates with many biological activities. *J. Inorg. Biochem.* **2009,** *103*, 536-546.
98. Fraqueza, G.; De Carvalho, L.; Marques, M. P. M.; Maia, L.; Ohlin, C. A.; Casey, W. H.; al., e., Decavanadate, decaniobate, tungstate and molybdate interactions with sarcoplasmic reticulum Ca^{2+}-ATPase: quercetin prevents cysteine oxidation by vanadate but does not reverse ATPase inhibition. *Dalton Trans.* **2012,** *41*, 12749-12758.
99. Aureliano, M.; Fraqueza, G.; Ohlin, C. A., Ion pumps as biological targets for decavanadate. *Dalton Trans.* **2013,** *42*, 11770-11777.
100. Aureliano, M.; Ohlin, C. A., Decavanadate in vitro and in vivo effects: facts and opinions. *J. Inorg. Biochem.* **2014,** *137*, 123-130.
101. Leon, I. E.; Porro, V.; Astrada, S.; Egusquiza, M. G.; Cabello, C. I.; Bollati-Fogolin, M.; al., e., Polyoxometalates as antitumor agents: bioactivity of a new polyoxometalate with copper on a human osteosarcoma model. *Chem. Biol. Interact.* **2014,** *222*, 87-96.
102. Kioseoglou, E.; Petanidis, S.; Gabriel, C.; Salifoglou, A., The chemistry and biology of vanadium compounds in cancer therapeutics. *Coord. Chem. Rev.* **2015,** *301*, 87-105.
103. Shah, H. S.; Joshi, P. G.; Haider, A.; Kortz, U.; Ur-Rehman, N.; Iqbal, J., Synthesis of chitosan-coated polyoxometalate nanoparticles against cancer and its metastasis. *RSC Adv* **2015,** *5*, 93234-93242.
104. Sun, T. D.; Cui, W.; Yan, M.; Qin, G.; Guo, W.; Gu, H. X.; al., e., Target delivery of a novel Antitumor Organoplatinum(IV)-substituted Polyoxometalate Complex for Safer and more effective colorectal cancer therapy in vivo. *Adv. Mater.* **2016,** *28*, 7397-7404.
105. Fu, D. Y.; Zhang, S. M.; Qu, Z. Y.; Yu, X. H.; Wu, Y. Q.; Wu, L. X., Hybrid assembly toward enhanced thermal stability of virus-like particles and antibacterial activity of Polyoxometalates. *ACS Appl. Mater. Interf.* **2018,** *10*, 6137-6145.
106. Gumerova, N.; Krivosudsky, L.; Fraqueza, G.; Breibeck, J.; Al-Sayed, E.; Tanuhadi, E.; al., e., The P-type ATPase inhibiting potential of polyoxotungstates. *Metallomics* **2018,** *10*, 287-295.
107. Pluskey, S.; Mahroof-Tahir, M.; Crans, D. C.; Lawrence, D. S., Vanadium oxoanions and cAMP-dependent protein kinase: an anti-substrate inhibitor. *Biochem. J.* **1996,** *321*, 333-339.
108. Zhai, F. Y.; Wang, X. H.; Li, D. L.; Zhang, H.; Li, R.; Song, L. S., Synthesis and biological evaluation of decavanadate Na(4)Co(H(2)O)(6)V(10)O(28)center dot 18H(2)O. *Biomed. Pharmacother.* **2009,** *63*, 51-55.
109. Turner, T. L.; Nguyen, V. H.; McLauchlan, C. C.; Dymon, Z.; Dorsey, B. M.; Hooker, J. D.; al., e., Inhibitory effects of decavanadate on several enzymes and Leishmania tarentolae in vitro. *J. Inorg. Biochem.* **2012,** *108*, 96-104.
110. Kioseoglou, E.; Gabriel, C.; Petanidis, S.; Psycharis, V.; Raptopoulou, C. P.; Terzis, A.; al., e., Binary Decavanadate-Betaine composite materials of potential anticarcinogenic activity. *Z. Anorg. Allg. Chem.* **2013,** *639*, 1407-1416.
111. Aureliano, M., Decavanadate contribution to vanadium biochemistry: in vitro and in vivo studies. *Inorganica Chim. Acta* **2014,** *420*, 4-7.
112. Aureliano, M., Decavanadate toxicology and pharmacological activities: V-10 or V-1, both or none? *Oxid. Med. Cell Longev.* **2016**, 1-9.

113. Weinstein, S.; Jahn, W.; Glotz, C.; Schlunzen, F.; Levin, I.; Janell, D.; Yonath, A.; al., e., Metal compounds as tools for the construction and the interpretation of medium-resolution maps of ribosomal particles. *J. Struct. Biol.* **1999,** *127*, 141-151.
114. Auerbach, N., T.; Zarivach, R.; Peretz, M.; Yonath, A., Reproducible growth of well diffracting ribosomal crystals. *Acta Crystallogr. Sec. D.* **2005,** *61*, 713-719.
115. Bashan, A.; Yonath, A., The linkage between ribosomal crystallography, metal ions, heteropolytungstates and functional flexibility. *J. Mol. Struct.* **2008,** *890*, 289-294.
116. Noeske, J.; Wasserman, M. R.; Terry, D. S.; Altman, R. B.; Blanchard, S. C.; Cate, J. H. D., High-resolution structure of the Escherichia coli ribosome. *Nat. Struct. Mol. Biol.* **2015,** *22*, 336-341.
117. Winkler, P. A.; Huang, Y.; Sun, W.; Du, J.; Lu, W., Electron cryo-microscopy structure of a human TRPM4 channel. *Nature* **2017,** *552*, 200-204.
118. Willsky, G. R.; White, D. A.; Mccabe, B. C., Metabolism of added Ortho-Vanadate to Vanadyl and High-molecular weight Vanadates by Saccharomyces-Cerevisiae. *J. Biol. Chem.* **1984b,** *259*, 3273-3281.
119. Willsky, G. R.; Leung, J. O.; Offermann, P. V. J.; Plotnick, E. K.; Dosch, S. F., Isolation and characterization of vanadateresistant mutants of Saccharomyces cerevisiae. *J. Bacteriol.* **1985,** *164*, 611-617.
120. Willsky, G. R.; Chi, L. H.; Godzala, M., 3rd; Kostyniak, P. J.; Smee, J. J.; Trujillo, A. M.; Alfano, J. A.; Ding, W.; Hu, Z.; Crans, D. C., Anti-diabetic effects of a series of vanadium dipicolinate complexes in rats with streptozotocin-induced diabetes. *Coord. Chem. Rev.* **2011,** *255* (19-20), 2258-2269.
121. Delgado, T. C.; Tomaz, A. I.; Correia, I.; Pessoa, J. C.; Jones, J. G.; Geraldes, C. F.; al., e., Uptake and metabolic effects of insulin mimetic oxovanadium compounds in human erythrocytes. *J. Inorg. Biochem.* **2005,** *99*, 2328-2339.
122. Crans, D. C.; Schoeberl, S.; Gaidamauskas, E.; Baruah, B.; Roess, D. A., Antidiabetic vanadium compound and membrane interfaces: interface-facilitated metal complex hydrolysis. *J. Biol. Inorg. Chem.* **2011,** *16* (6), 961-72.
123. Postal, K.; Maluf, D. F.; Valdameri, G.; Rudiger, A. L.; Hughes, D. L.; de Sa, E. L.; al., e., Chemoprotective activity of mixed valence polyoxovanadates against diethylsulphate in E. coli cultures: insights from solution speciation studies. *RSC Adv* **2016,** *6*, 114955-114866.
124. Jakusch, T.; Kiss, T., In vitro study of the antidiabetic behavior of vanadium compounds. *Coord. Chem. Rev.* **2017,** *351*, 118-126.
125. Crans, D. C., Chemistry and insulin-like properties of vanadium(IV) and vanadium(V) compounds. *J. Inorg. Biochem.* **2000,** *80*, 123-131.
126. Crans, D. C.; Woll, K. A.; Prusinskas, K.; Johnson, M. D.; Norkus, E., Metal speciation in health and medicine represented by iron and vanadium. *Inorg. Chem.* **2013,** *52*, 12264-12275.
127. Correia, I.; Roy, S.; Matos, C. P.; Borovic, S.; Butenko, N.; Cavaco, I.; al, e., Vanadium(IV) and copper(II) complexes of salicylaldimines and aromatic heterocycles: Cytotoxicity: DNA binding and DNA cleavage properties. *J. Inorg. Biochem.* **2015,** *147*, 134-146.
128. Pessoa, J. C.; Tomaz, I., Transport of therapeutic Vanadium and Ruthenium complexes by blood plasma components. *Curr. Med. Chem.* **2010,** *17*, 3701-3738.
129. Crans, D. C.; Trujillo, A. M.; Pharazyn, P. S.; Cohen, M. D., How environment affects drug activity: localization, compartmentalization and reactions of a vanadium insulin-enhancing compound, dipicolinatooxovanadium(V). *Coord. Chem. Rev.* **2011,** *255*, 2178-2192.

130. Le, M.; Rathje, O.; Levina, A.; Lay, P. A., High cytotoxicity of vanadium (IV) complexes with 1, 10-phenanthroline and related ligands is due to decomposition in cell culture medium. *J. Biol. Inorg. Chem.* **2017,** *22* (663-672).
131. Baes, C. F., *The Hydrolysis of Cations*. John Wiley & Sons: New York, NY, 1976.
132. Chasteen, N. D., The biochemistry of vanadium. In *Copper, Molybendum, and Vanadium in Biological Systems*, Clarke, M. J.; Goodenough, J. B.; Ibers, J. A.; Jorgensen, C. K.; Mingos, D. M. P.; Neilands, J. B.; Palmer, G. A.; Reinen, D.; Sadler, P. J.; Weiss, R.; Williams, R. J. P., Eds. Springer-Verlag: New York, NY, 1983; pp 105-138.
133. Vilas Boas, L. V.; Pessoa, J. C., Vanadium. In *The Synthesis, Reactions, Properties & Applications of Coordination Compounds*, Wilkinson, G.; Gillard, R. D. S.; Mccleverty, J. A., Eds. Pergamon Press: New York, NY, 1987; pp 453-583.
134. Pope, M. T.; Muller, A., Polyoxometalate chemistry: an old field with new dimensions in several disciplines. *Angew Chem Int Ed Engl* **1991,** *30*, 34-48.
135. Rehder, D., The bioinorganic chemistry of vanadium. *Angew Chem Int Ed Engl* **1991,** *30*, 148-167.
136. Crans, D. C.; Peters, B. J.; Wu, W.; McLauchlan, C. C., Does Anion-Cation Organization in Na+-containing X-ray crystal structures relate to solution interactions in inhomogeneous nanoscale environments: Sodiumdecavanadate in solid state materials, minerals and microemulsions. *Coord. Chem. Rev.* **2017,** *344*, 115-130.
137. Pettersson, L.; Hedman, B.; Andersson, I.; Ingri, N., Multicomponent polyanions. 34. P potentiometric and 51V NMR study of equilibria in the H+-HVO42- system in the 0.6 M Na(Cl) medium covering the range 1£-1g[H+]£10. *Chem. Scrip.* **1983,** *22*, 254-264.
138. Pettersson, L.; Andersson, I.; Hedman, B., Multicomponent polyanions. 37. A potentiometric and 51V-NMR study of equilibria in the H+-HVO2−4 system in 3.0 M-Na(ClO4) medium covering the range 1£-1g[H+]£10. *Chem. Scrip.* **1985,** *25*, 309-317.
139. Crans, D. C.; Rithner, C. D.; Theisen, L. A., Application of Time-Resolved 51V 2D NMR for Quantitation of Kinetic Exchange Pathways between Vanadate Monomer, Dimer, Tetramer, and Pentamer. *J. Am. Chem. Soc.* **1990,** *112*, 2901-2908.
140. Evans, H. T. J., The molecular structure of the isopoly complex ion, decavanadate ($V_{10}O_6^{-28}$). *Inorg. Chem.* **1966,** *5*, 967-977.
141. Clare, B. W.; Kepert, D. L.; Watts, D. W., Acid decompositon of decavanadate-specific salt effects. *J. Chem. Soc. Dalton Trans.* **1973,** *22*, 2481-2487.
142. Clare, B. W.; Kepert, D. L.; Watts, D. W., Kinetic study of the acid decomposition of decavanadate. *J. Chem. Soc. Dalton Trans.* **1973,** *22* (2479-2487).
143. Druskovich, D. M.; Kepert, D. L., Base decomposition of decavanadate. *J. Chem. Soc. Dalton Trans.* **1975,** *22*, 847-851.
144. Comba, P.; Helm, L., The solution structure and reactivity of decavanadate. *Helv. Chim. Acta* **1988,** *71*, 1406-1420.
145. Kustin, K., Aqueous vanadium ion dynamics relevant to bioinorganic chemistry: a review. *J. Inorg. Biochem.* **2015,** *147*, 32-38.
146. Baruah, B.; Roden, J. M.; Sedgwick, M.; Correa, N. M.; Crans, D. C.; Levinger, N. E., When is water not water? Exploring water confined in large reverse micelles using a highly charged inorganic molecular probe. *J. Am. Chem. Soc.* **2006,** *128*, 12758-12765.

147. Crans, D. C.; Rithner, C. D.; Baruah, B.; Gourley, B. L.; Levinger, N. E., Molecular Probe Location in Reverse Micelles Determined by NMR Dipolar Interactions. *J. Am. Chem. Soc.* **2006,** *128*, 4437-4445.
148. Sanchez, L., I.; Baruah, B.; Alvarez, S.; Werst, K. R.; Segaline, N. A.; Levinger, N. E.; al., e., Size and shape trump charge in interactions of oxovanadates with self-assembled interfaces: application of continuous shape measure analysis to the decavanadate anion. *New J. Chem.* **2016,** *40*, 962-975.
149. Ehde, P. M.; Andersson, I.; Pettersson, L., Multicomponent Polyanion. 43. A Study of Aqueous Equilibria in the Vanadocitrate System. *Acta Chem. Scand.* **1989,** *43*, 136-143.
150. Selling, A.; Andersson, I.; Pettersson, L.; Schramm, C. M.; Downey, S. L.; Grate, J. H., Multicomponent Polyanions. 47. The Aqueous Vanadophosphate System. *Inorg. Chem.* **1994,** *33*, 3141-3150.
151. Carsella, J. S.; Sanchez, L., I.; Bonetti, S. J.; Crans, D. C., Selenium speciation in the Fountain Creek Watershed correlates with water hardness, Ca and Mg levels. *Molecules* **2017,** *22*, 1-16.
152. Bbl(TM), D., Middlebrook 7H9 Broth. In *Middlebrook ADC Enrichment*, 2nd ed ed.; 2018.
153. Gresser, M. J.; Tracy, A. S.; Parkinson, K. M., Vanadium(V) oxyanions: the interaction of vanadate with pyrophosphate, phosphate, and arsenate. *J. Am. Chem. Soc.* **1986,** *108*, 6229-6234.
154. Crans, D. C., Fifteen years of dancing with vanadium. *Pure Appl. Chem.* **2005,** *77*, 1497-1527.
155. Andersson, I.; Gorzsas, A.; Kerezsi, C.; Toth, I.; Pettersson, L., Speciation in the aqueous H+/H2VO4-H+2O2/phosphate system. *Dalton Trans.* **2005,** *22*, 3658-3666.
156. Kiss, T.; Jakusch, T.; Hollender, D.; Dornyei, A.; Enyedy, E. A.; Pessoa, J. C.; Sakurai, H.; Sanz-Medel, A., Biospeciation of antidiabetic VO(IV) complexes. *Coord. Chem. Rev.* **2008,** *252* (10), 1153-1162.
157. Crans, D. C.; Yang, L.; Alfano, J. A.; Chi, L.; W., J.; Mahroof-Tahir, M.; Robbins, K.; Toloue, M. M.; Chan, L. K.; Plante, A. J.; Grayson, R. Z.; Willsky, G. R., (4-Hydroxypyridine-2,6-dicarboxylato)oxovanadate(V)-a new insulin-like compound: chemistry, effects on myoblast and yeast cell growth and effects on hyperglycemia in rats with STZ-induced diabetes. *Coord. Chem. Rev.* **2003,** *237*, 13-22.
158. Elvingson, K.; Gonzalez Baro, A.; Pettersson, L., Speciation in Vanadium Bioinorganic Systems. 2. An NMR, ESR, and Potentiometric Study of the Aqueous H+-Vanadate-Maltol System. *Inorg. Chem.* **1996,** *35*, 3388-3393.
159. Johnstone, T. C.; Suntharalingam, K.; Lippard, S. J., Third row transition metals for the treatment of cancer. *Philos Trans A Math Phys Eng Sci* **2015,** *373* (2037).
160. Desoize, B., Metals and metal compounds in cancer treatment. *Anticancer Res.* **2004,** *3a*, 1529-1544.
161. Collery, P.; Mohsen, A.; Kermagoret, A.; D'Angelo, J.; Morgant, G.; Desmaele, D.; Tomas, A.; Collery, T.; Wei, M.; Badawi, A., Combination of Three Metals for the Treatment of Cancer: Gallium, Rhenium and Platinum. 1. Determination of the Optimal Schedule of Treatment. *Anticancer Res.* **2012,** *32*, 2769-2781.

Appendix A – Supplementary Information Corresponding to Chapter 2

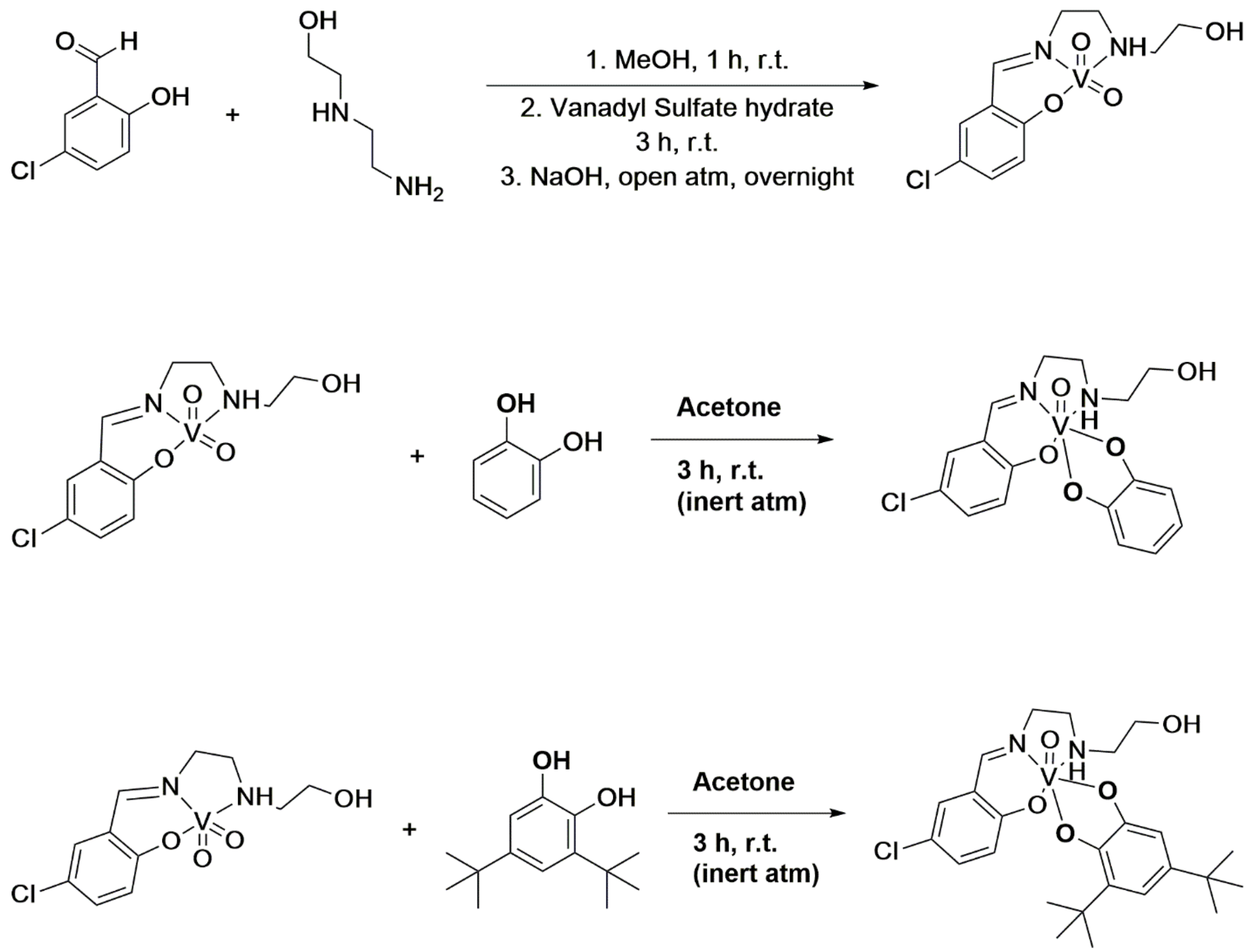

Figure S2.1-S2.3 showing the synthesis of [VO_2(Cl-HSHED)], [VO(Cl-HSHED) (Cat)], [VO(Cl HSHED)(DTB)]

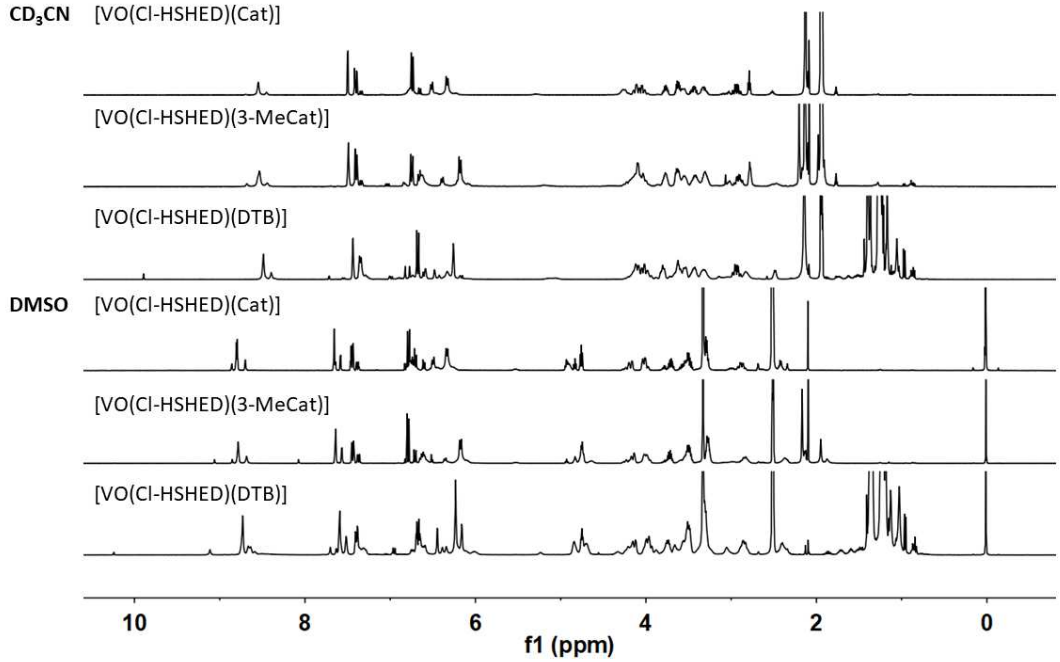

Figure S2.4. 1D ^{1}H NMR (400 MHz) of [VO(Cl-HSHED)(Cat)], [VO(Cl-HSHED)(3-MeCat)], [VO(Cl-HSHED)(DTB)] in CD_3CN and DMSO.

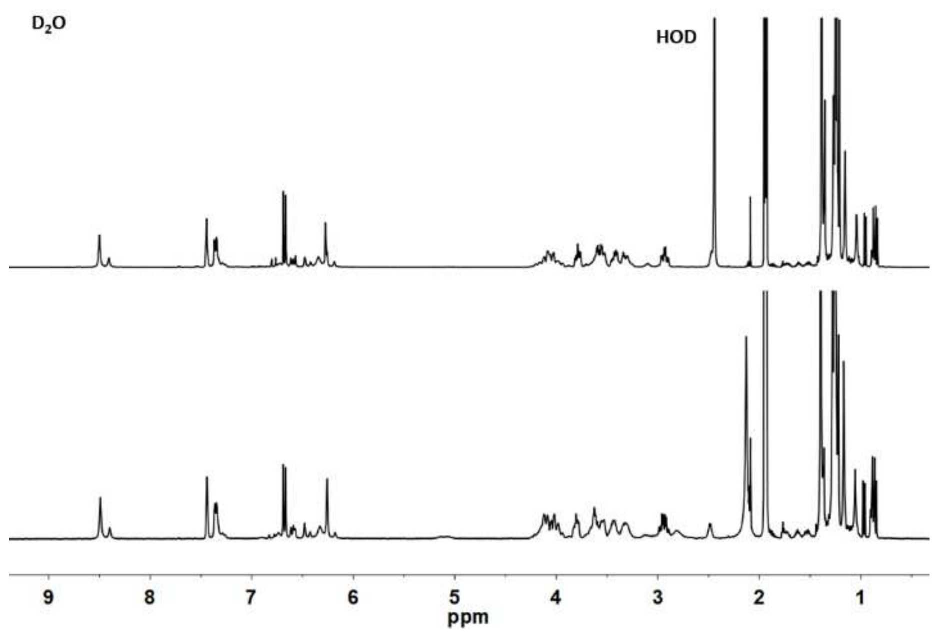

Figure S2.5. ^{1}H NMR (400MHz) of 1mM [VO(Cl-HSHED)(DTB)] in CD_3CN with one drop of D2O (top) and without (bottom).

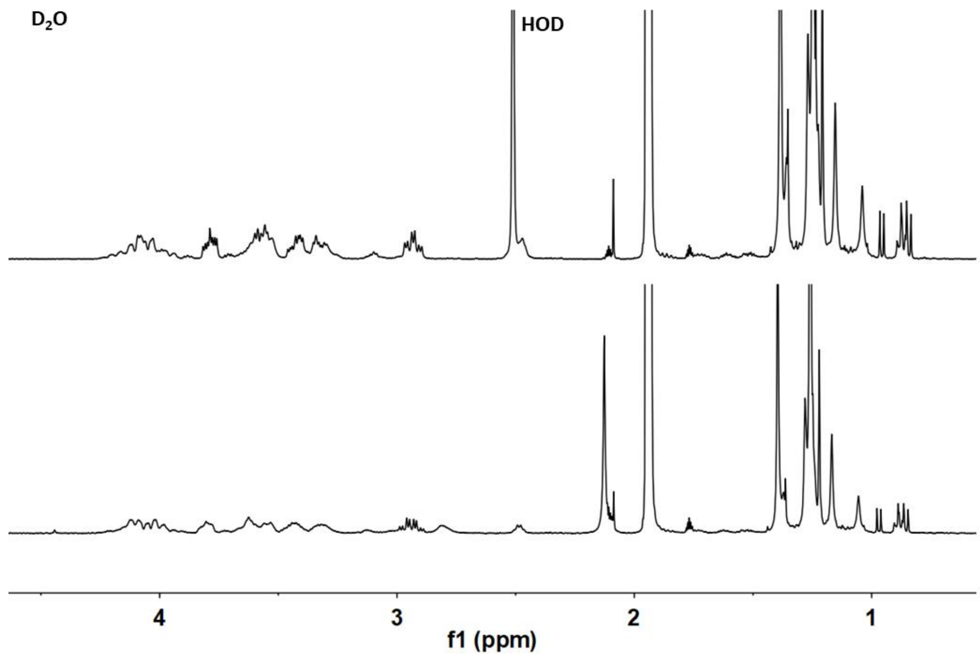

Figure S2.6. ^{1}H NMR (400MHz) aliphatic region of 1mM [VO(Cl-HSHED)(DTB)] in CD_3CN with one drop of D2O (top) and without (bottom).

Spiking the ^{1}H NMR CD_3CN sample with D_2O removed the broad signal at 2.8 ppm (NH proton), as well as an intensity within the 4 ppm multiplet (OH proton). The interpretation of the coupling based on the spiking experiment was as follows: The D_2O spike changed the coupling pattern of a peak at 2.92 ppm from a dq to a dt, signifying the loss of the coupling to the NH proton. In the COSY, a correlation between $H_{s/t}$ and a peak at 2.92 assigned to H_u or H_v. The peak at 2.92 ppm also correlated to a peak at 3.54 ppm being the corresponding proton to $H_{u/v}$. A peak at 3.79 ppm is a ddd, a peak at 3.57 ppm is a multiplet, a peak at 3.43 ppm is a ddd, and a peak at 3.32 ppm is a td. The coupling patterns of peaks 3.43 and 3.32 were indicative of an AB pattern and were assigned to H_w and H_x. The remaining peaks at 3.79 ppm and 3.57 ppm were assigned to H_y and H_z. Not only did the D_2O remove the exchangeable OH and NH protons, but the integrations and the resolution of the remaining coupling patterns were simplified assisting the interpretation of the solution structure. This simplification may not only be due to removal of the N-H coupling, since each of the geometric isomers has two potential diastereomers due to the chirality around the coordinated secondary amine that would give distinct NMR signals if both existed in solution. The rapid exchange of the N-D group on the NMR timescale in the presence of D_2O would lead to rapid equilibration of such diastereomers and, hence, a single set of signals for each set of diastereomers.

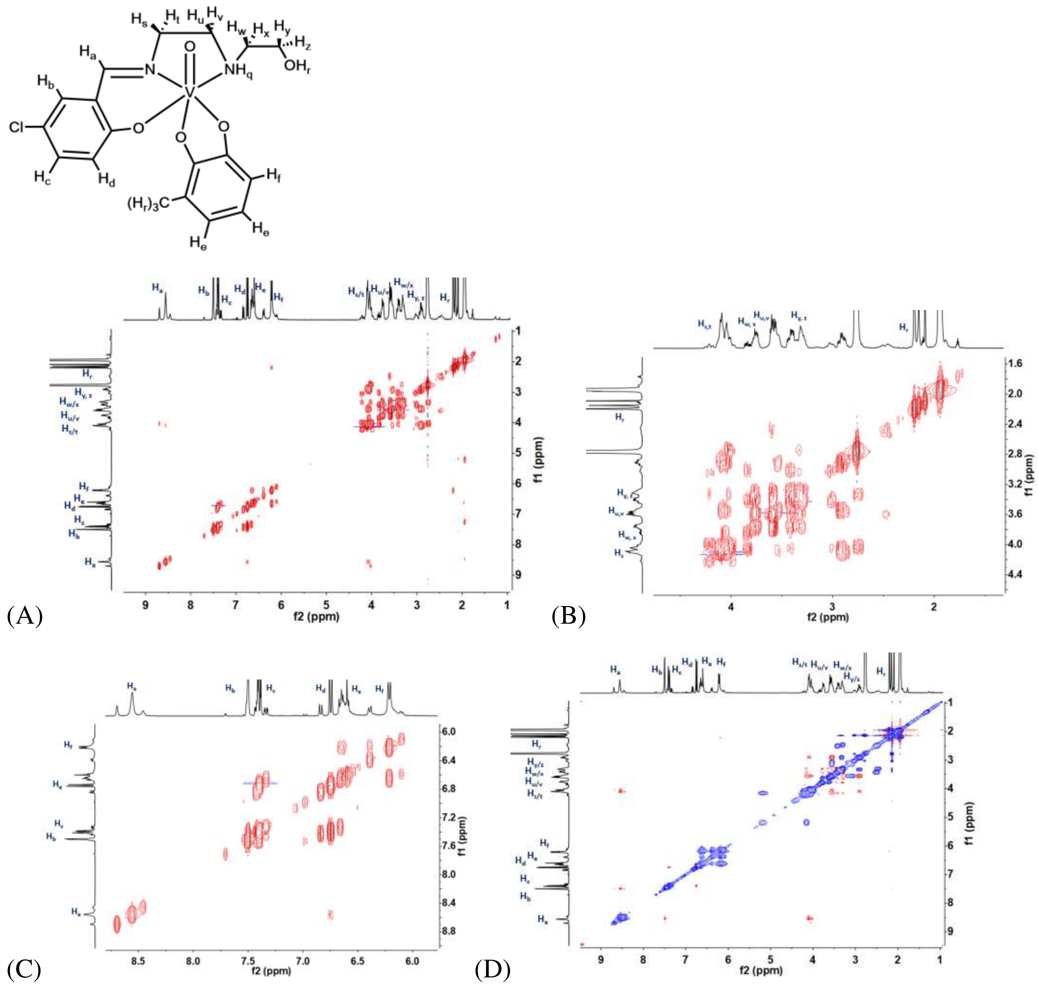

(A) (B) (C) (D)

Figure S2.7. ^{1}H-^{1}H COSY and ^{1}H-^{1}H NOESY NMR (400MHz) spectra of 10mM [VO(Cl-HSHED)(3-MeCat)] in CD_3CN and a D_2O spike at 26°C. (A) Full ^{1}H-^{1}H COSY NMR spectrum of [VO(Cl-HSHED)(3-MeCat)] in CD_3CN. (B) Zoom in of aromatic region ^{1}H-^{1}H COSY NMR spectrum of [VO(Cl-HSHED)(3-MeCat)]. (C) Zoom in of aliphatic region ^{1}H-^{1}H COSY NMR spectrum of [VO(Cl-HSHED)(3-MeCat)]. (D) Full ^{1}H-^{1}H NOESY NMR spectrum of [VO(Cl-HSHED)(3-MeCat)]. Blue intensity contours represent negative NOE's and red intensity contours represent positive NOE's. A standard NOESY sequence was used consisting of 200-256 transients with 16 scans in the f1 domain using a 500 ms mixing time and a 1.5 s relaxation delay. The structures of and [VO(Cl-HSHED)(3-MeCat)] are shown with a proton labelling scheme key.

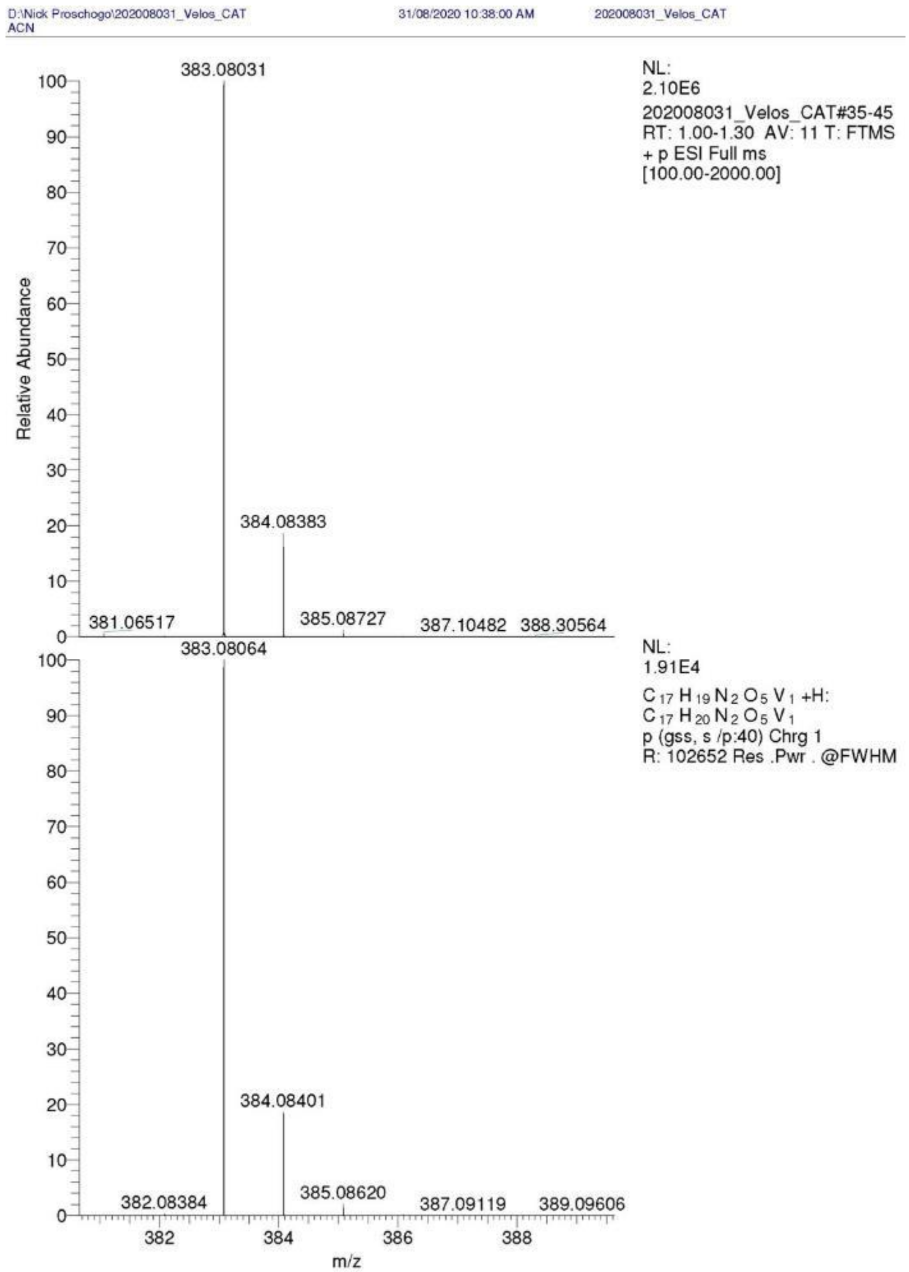

Figure S2.8. Experimental (top) and simulated (bottom) spectra of [VO(HSHED)(Cat)]

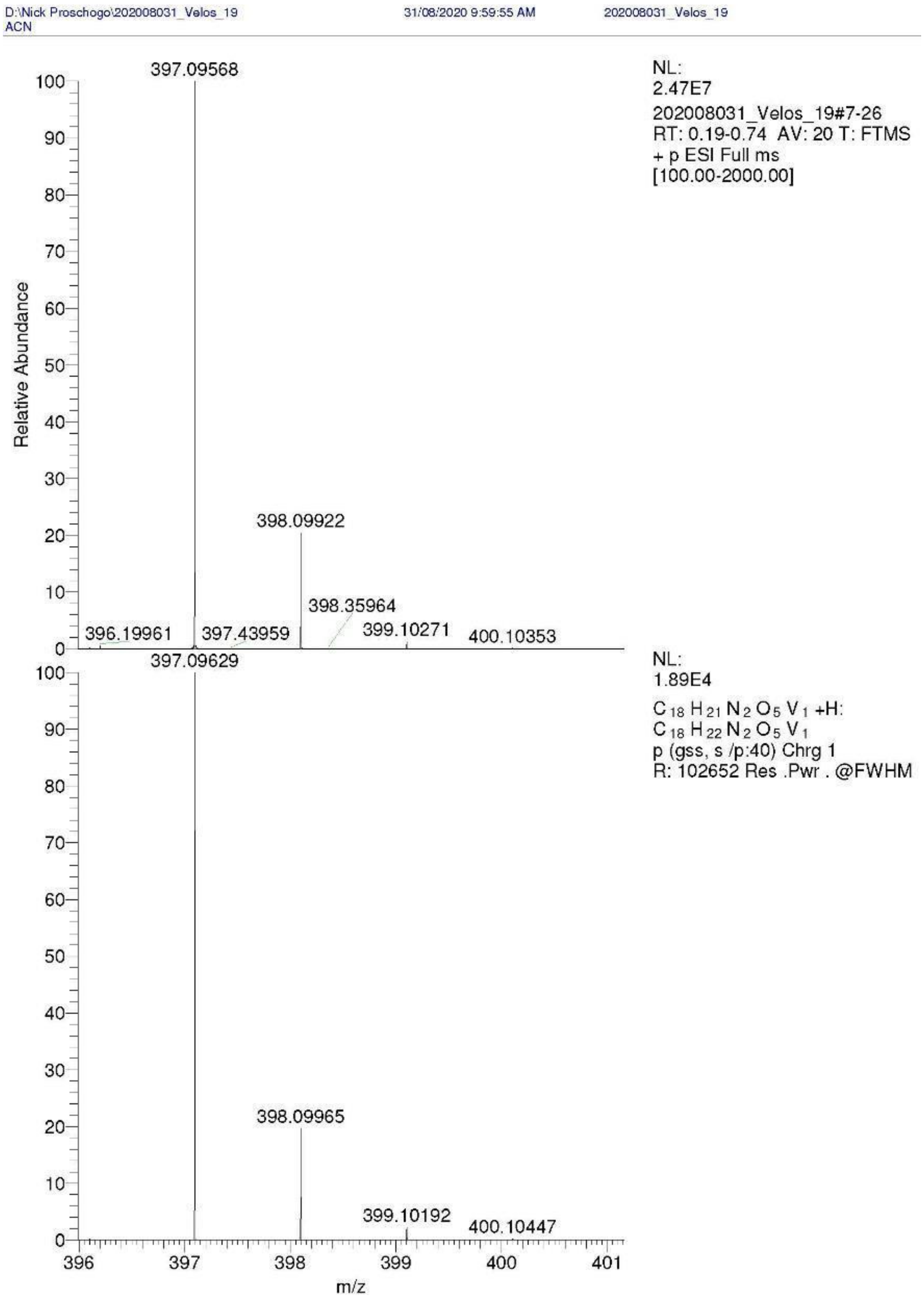

Figure S2.9. Experimental (top) and simulated (bottom) spectra of [VO(HSHED)(3-MeCat)]

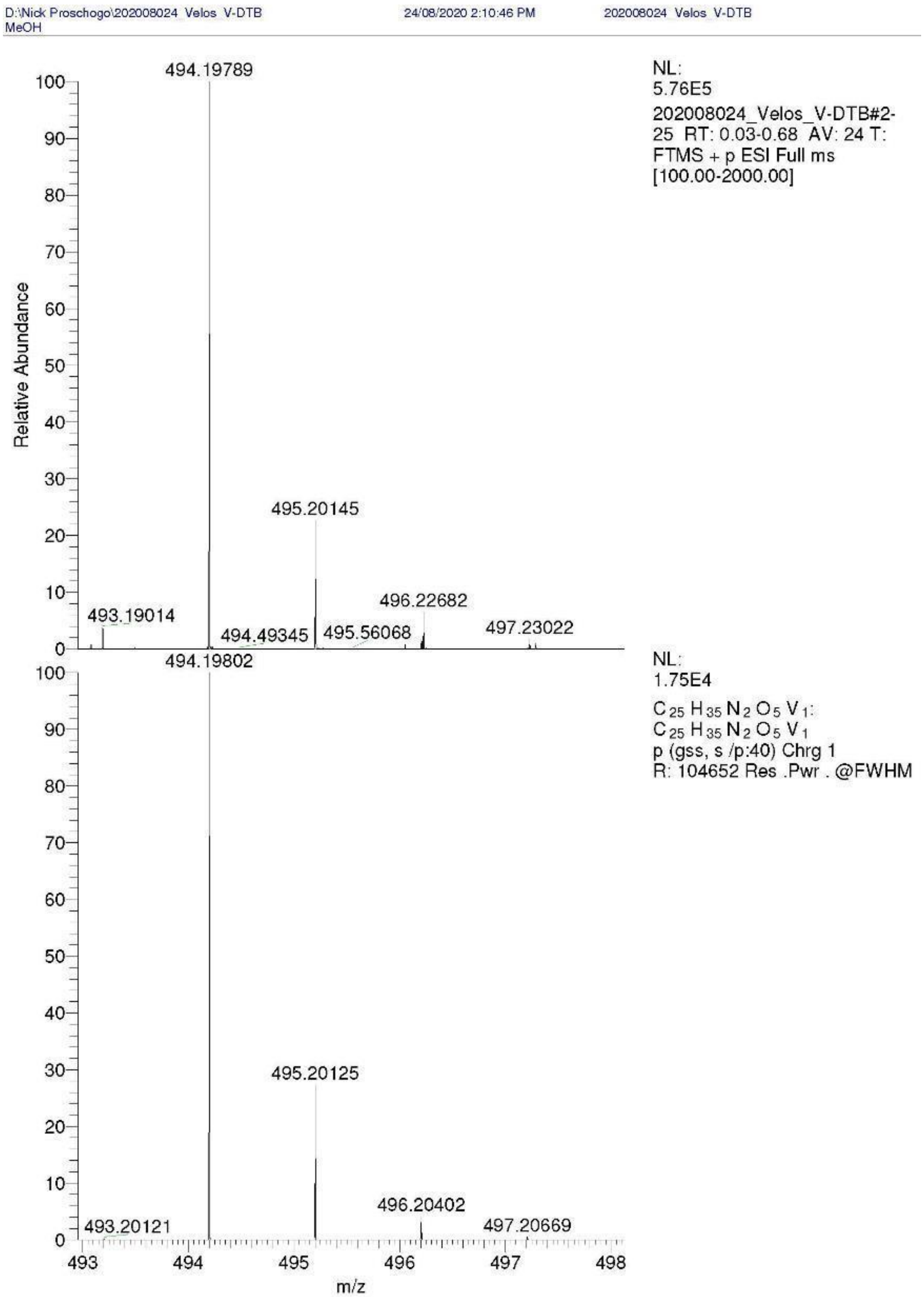

Figure S2.10. Experimental (top) and simulated (bottom) spectra of [VO(HSHED)(DTB)]

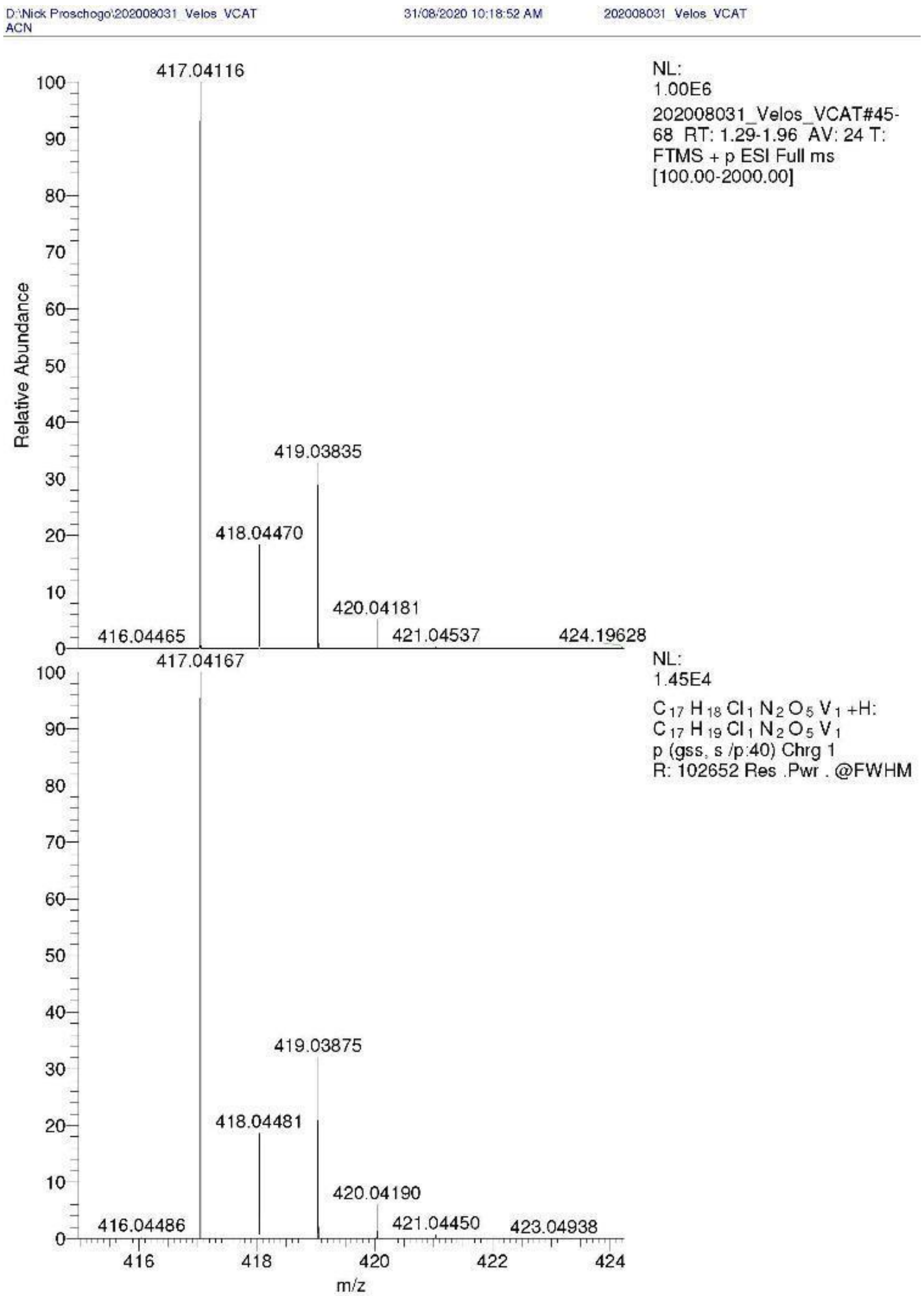

Figure S2.11. Experimental (top) and simulated (bottom) spectra of [VO(Cl-HSHED)(Cat)]

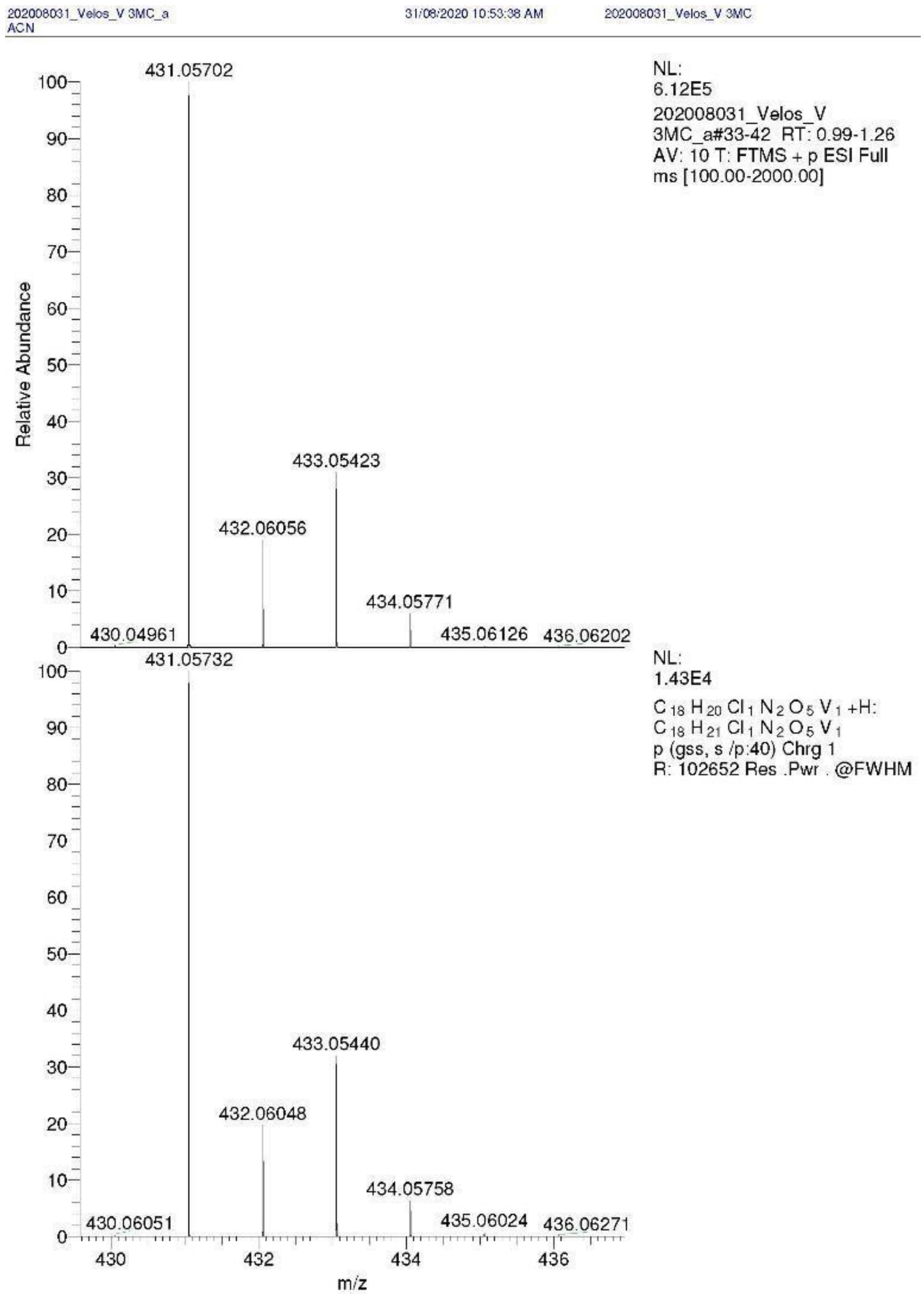

Figure S2.12. Experimental (top) and simulated (bottom) spectra of [VO(Cl-HSHED)(3-MeCat)]

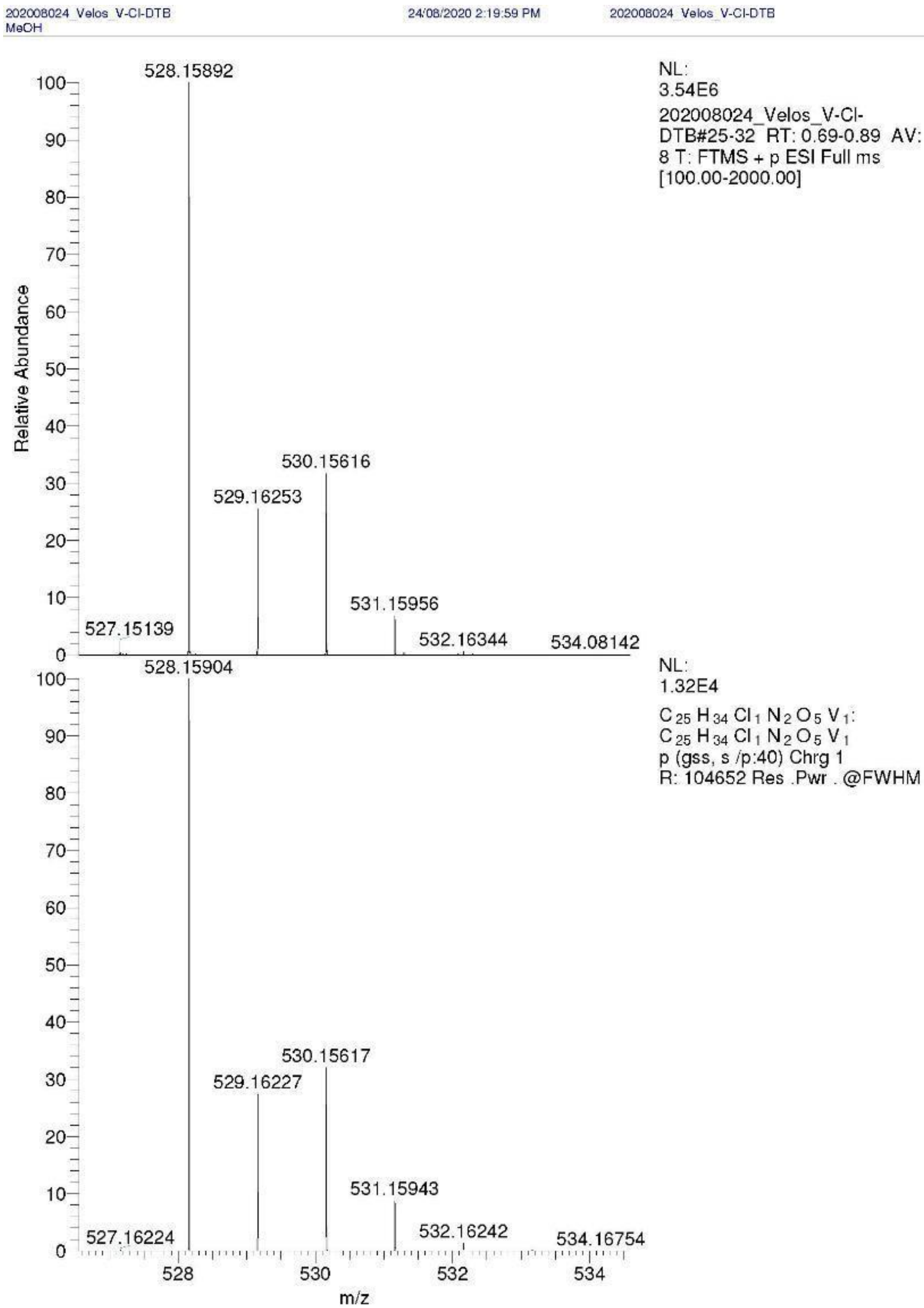

Figure S2.13. Experimental (top) and simulated (bottom) spectra of [VO(Cl-HSHED)(DTB)]

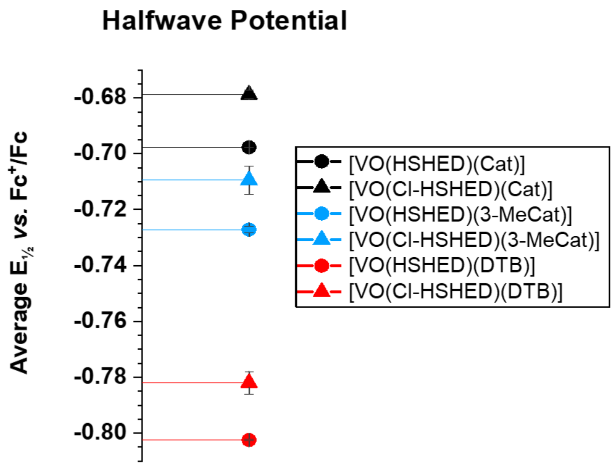

Figure S2.14. Halfwave potentials of VO(Cl-HSHED) and VO(HSHED) complexes in acetonitrile, run at 100mV/sec in triplicate. An internal standard of ferrocene at 2mM was used.

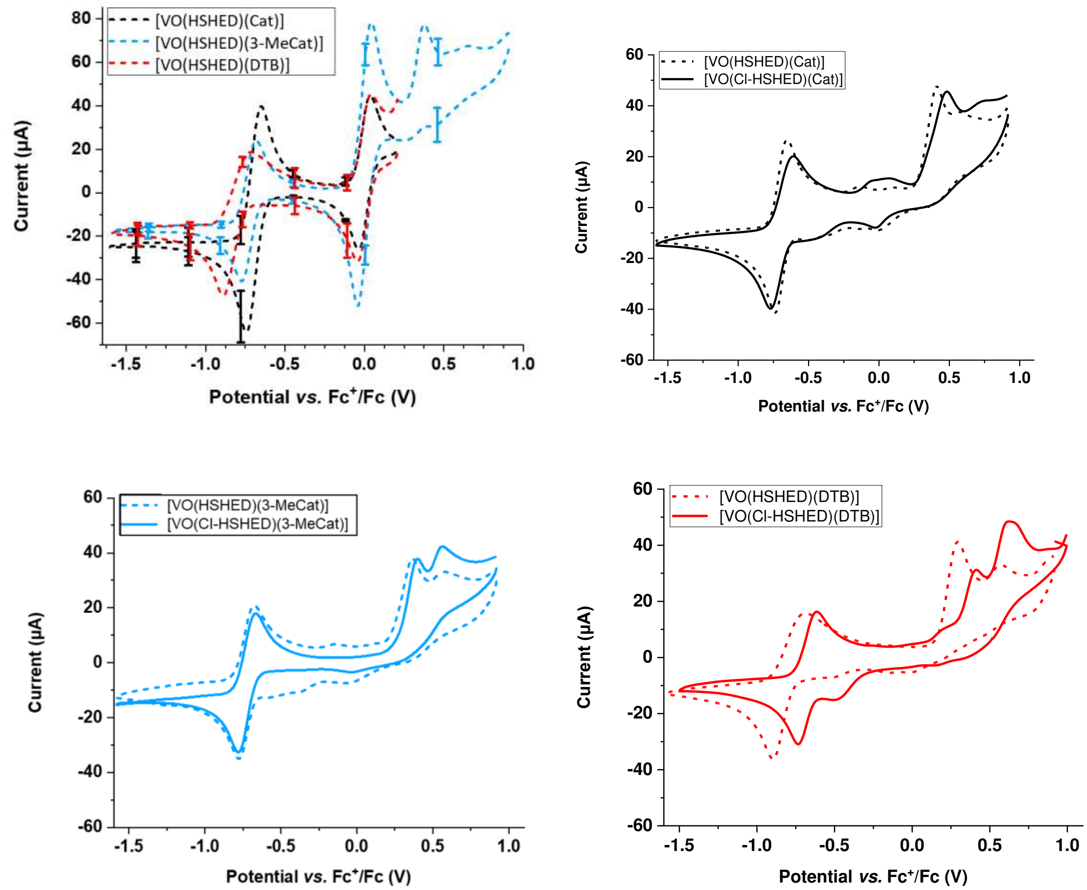

Figure S2.15. Comparison of Cyclic Voltammograms of 2.0 mM [VO(Cl-HSHED)(Cat)], [VO(Cl-HSHED)(3-MeCat)], [VO(Cl-HSHED)(DTB)] and corresponding [VO(HSHED)(Cat)], [VO(HSHED)(3-MeCat)], [VO(HSHED)(DTB)] of the complexes, 100 mM of TBAP in CH_3CN, run at 100 mV s^{-1}.

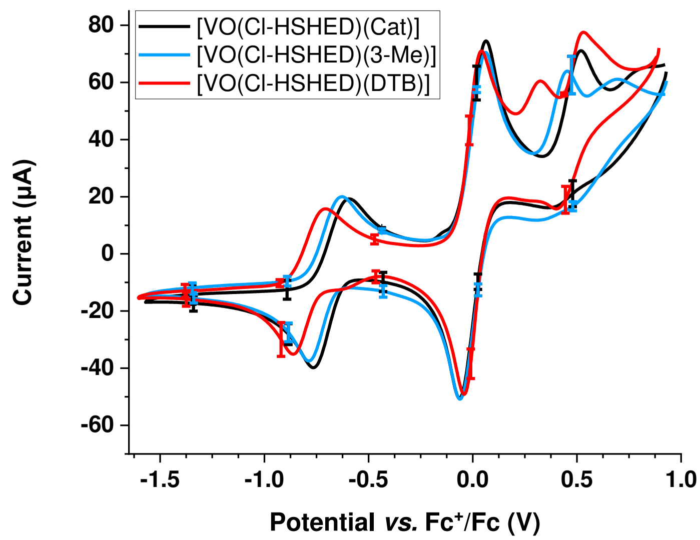

Figure S2.16. Superimposed Cyclic Voltammograms of 2.0 mM of [VO(Cl-HSHED)(Cat)], [VO(Cl-HSHED)(3-Me)], [VO(Cl-HSHED)(DTB)], and [VO(HSHED)(Cat)], [VO(HSHED)(3-Me)], [VO(HSHED)(DTB)], 2mM Ferrocene, 100 mM of TBAP in CH_3CN. Error bars show standard deviation of the CV ran in triplicate samples.

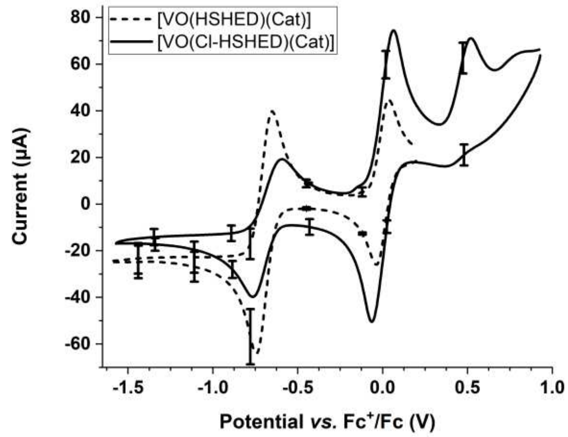

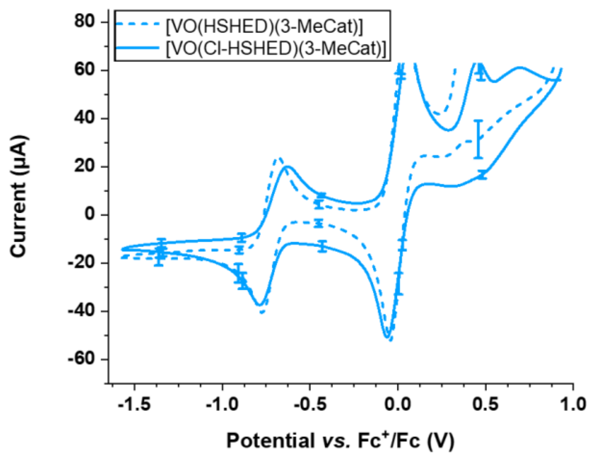

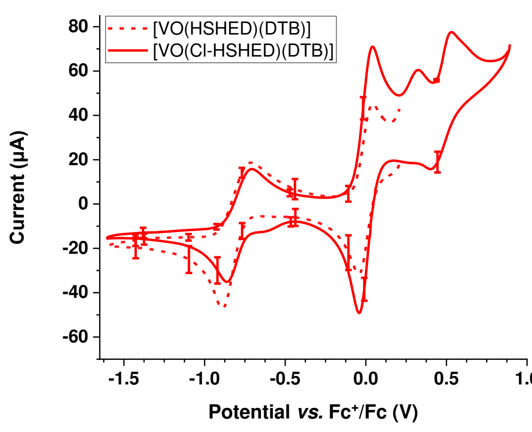

Figure S2.17. Comparison of Cyclic Voltammograms of 2.0 mM [VO(Cl-HSHED)(Cat)], [VO(Cl-HSHED)(3-MeCat)], [VO(Cl-HSHED)(DTB)] and corresponding [VO(HSHED)(Cat)], [VO(HSHED)(3-MeCat)], [VO(HSHED)(DTB)] of the complexes, 2 mM Ferrocene, 100 mM of TBAP in CH_3CN. Error bars show standard deviation of the CV ran in triplicate samples.

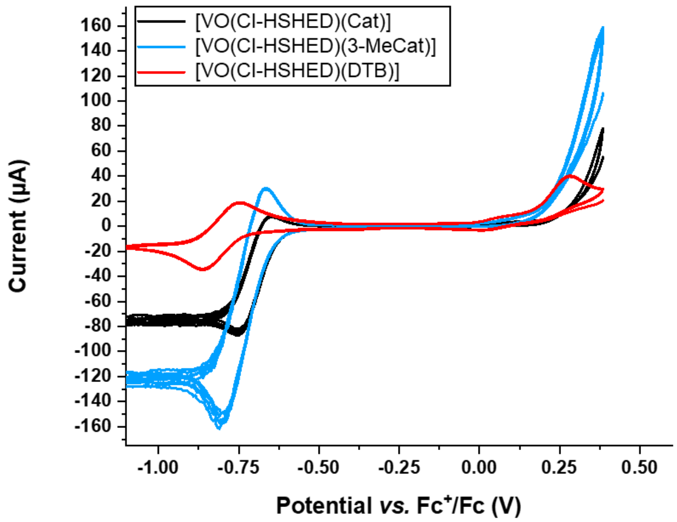

Figure S2.18. Comparison of a hysteresis set of cyclic voltammograms of approx 2.0 mM [VO(Cl-HSHED)(Cat)], [VO(Cl-HSHED)(3-MeCat)], [VO(Cl-HSHED)(DTB)], 100 mM of TBAP in CH_3CN. The CV consisted of 10 sements, with a CV from 0.5V to -1V and back to 0.5V being repeated 5 times.

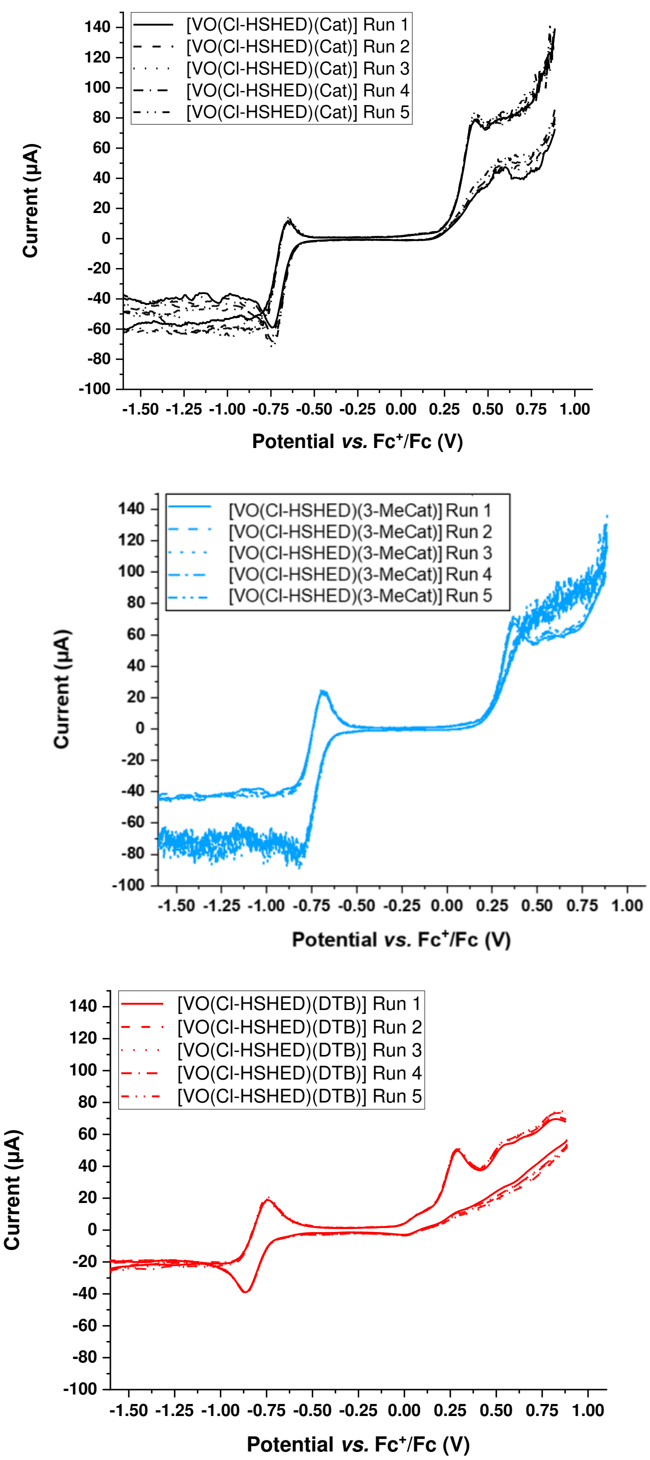

Figure S2.19. Comparison of Cyclic Voltammograms of 2.0 mM [VO(Cl-HSHED)(Cat)], [VO(Cl-HSHED)(3-MeCat)], [VO(Cl-HSHED)(DTB)], 100 mM of TBAP in CH_3CN. Successive CV's from 1V to -1.5V and from -1.5V to 1V were run on one sample five times within a short period of time.

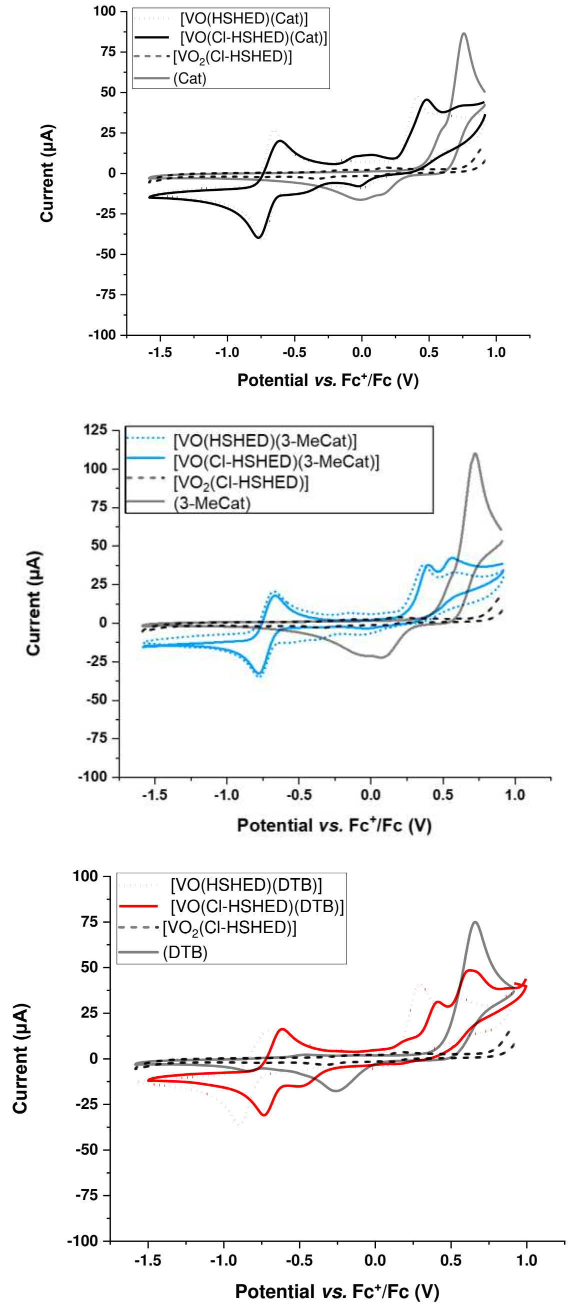

Figure S2.20. Comparison of Cyclic Voltammograms of 2.0 mM [VO(Cl-HSHED)(Cat)], [VO(Cl-HSHED)(3-MeCat)], [VO(Cl-HSHED)(DTB)], to the precursor [VO_2(Cl-HSHED)] and the ligands (Cat), (3-MeCat) and (DTB) with 100 mM of TBAP in CH_3CN.

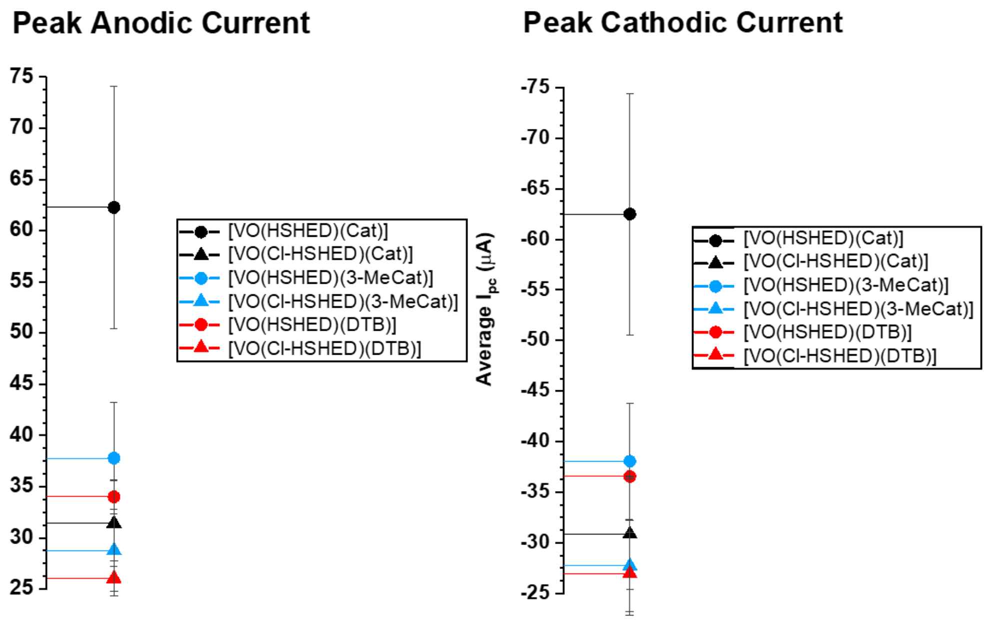

Figure S2.21. Comparison of peak anodic and cathodic currents of the vanndium redox peak around -0.8V of 2.0 mM [VO(Cl-HSHED)(Cat)], [VO(Cl-HSHED)(3-MeCat)], [VO(Cl-HSHED)(DTB)] and corresponding [VO(HSHED)(Cat)], [VO(HSHED)(3-MeCat)], [VO(HSHED)(DTB)] of the complexes, 2 mM Ferrocene, 100 mM of TBAP in CH_3CN. CV's were run on triplicate samples.

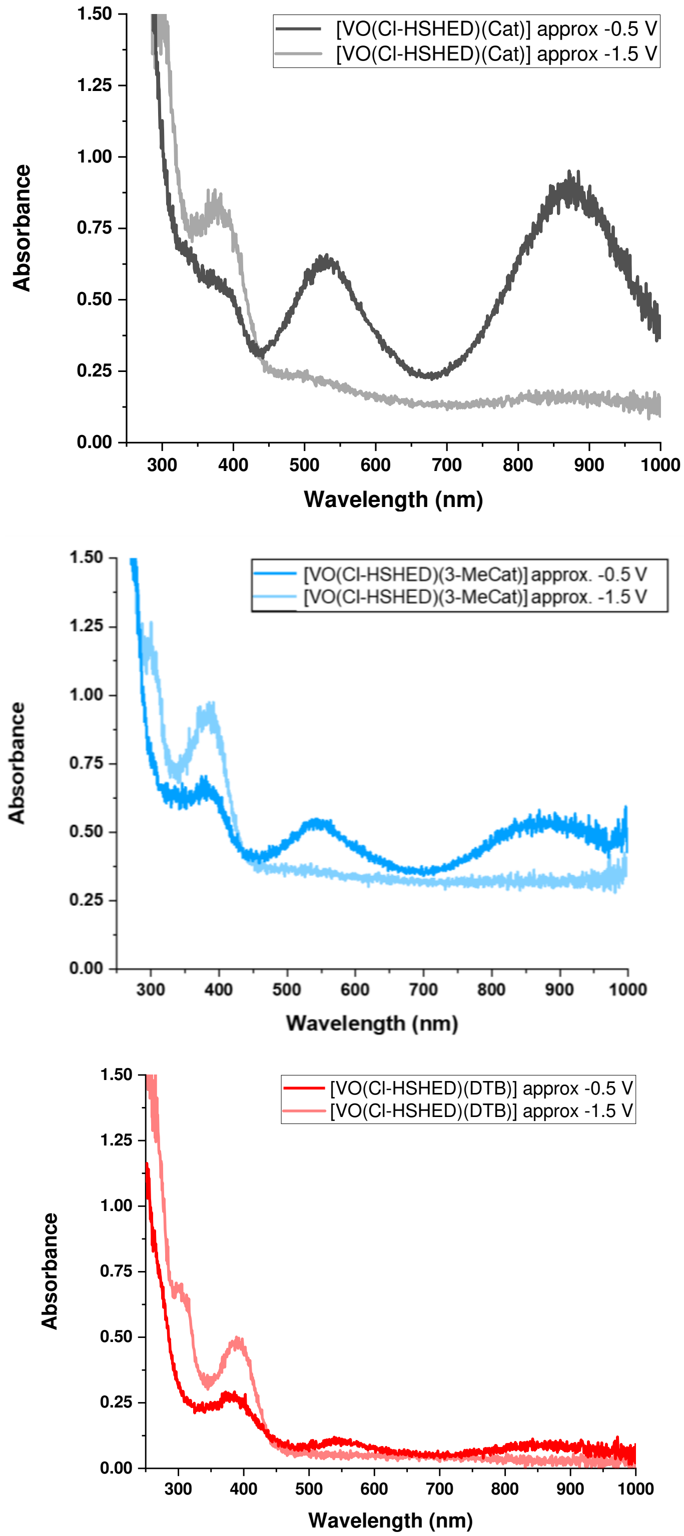

Figure S2.22. Comparison of Spectroelectrochemistry of 2.0 mM [VO(Cl-HSHED)(Cat)], [VO(Cl-HSHED)(3-MeCat)], [VO(Cl-HSHED)(DTB)], with 100 mM of TBAP in CH_3CN. Spectra were run before the vanadium redox peak (approx -0.5V) and after (approx -1.5V).

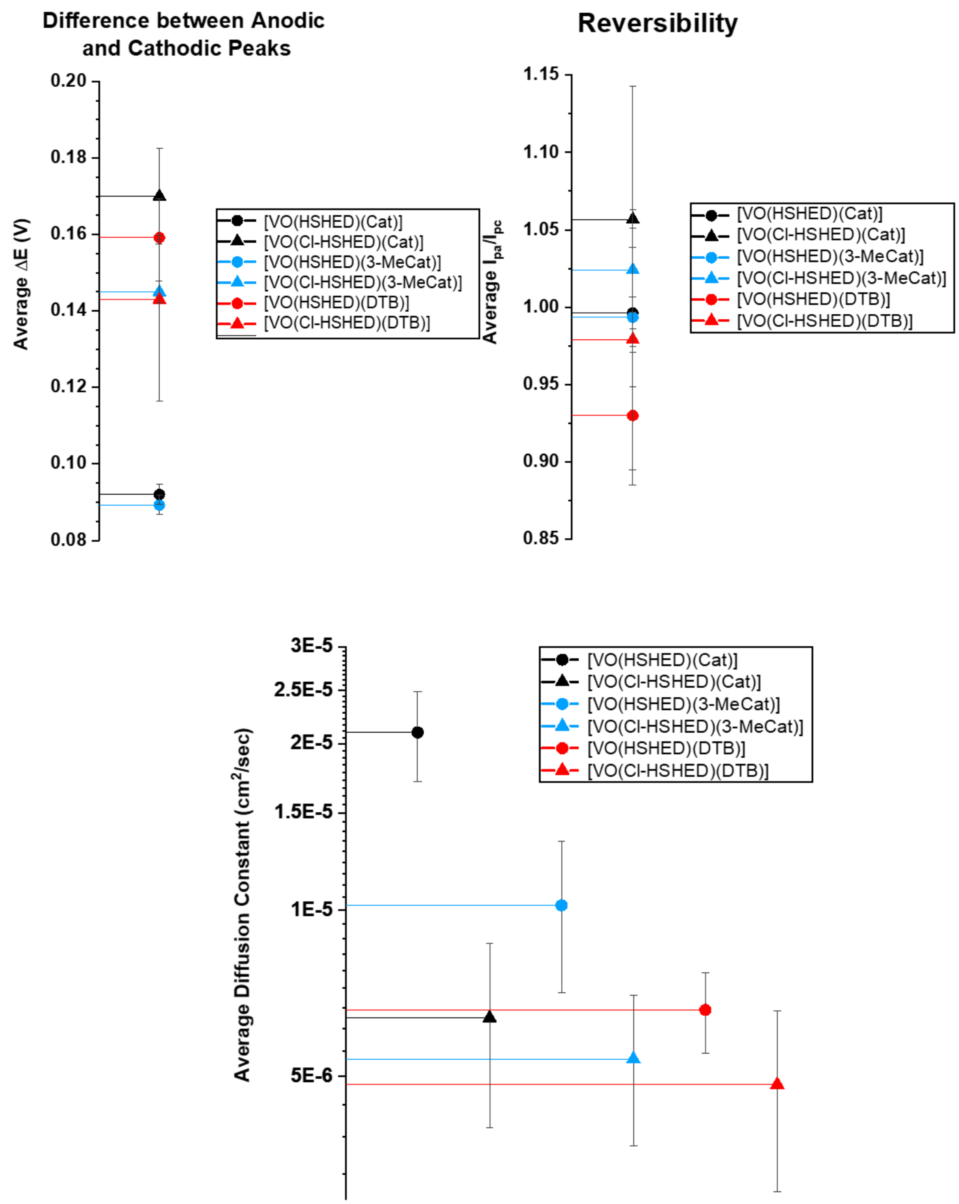

Figure S2.23. Comparison of the difference between peak anodic and cathodic currents of the vanadium redox peak around -0.8V, the I_{pa}/I_{pc} value of those current as a measure of reversibility, and the calculated average diffusion constants of 2.0 mM [VO(Cl-HSHED)(Cat)], [VO(Cl-HSHED)(3-MeCat)], [VO(Cl-HSHED)(DTB)] and corresponding [VO(HSHED)(Cat)], [VO(HSHED)(3-MeCat)], [VO(HSHED)(DTB)], 2 mM Ferrocene, 100 mM of TBAP in CH_3CN. CV's were run on triplicate samples.

Table S2.1 $E_{1/2}$ potentials and other electrochemical data for the V(V/IV) couples of the Cl-HSHED and HSHED catecholate complexes with standard deviations from three samples.					
Complex	Average $E_{1/2}$ vs $Me_{10}Fc^+/Me_{10}Fc$ (V)	ΔE of V couples (V)	ΔE of Fc (V)	I_{pa} (µA)	I_{pc} (µA)
[VO(Cl-HSHED)(Cat)]	-0.173±0.002	0.17 ± 0.01	0.13± 0.01	31± 4	-31± 5
[VO(Cl-HSHED)(DTB)]	-0.203±0.002	0.14 ± 0.03	0.087 ± 0.003	26 ± 2	-27 ± 4
[VO(Cl-HSHED)(3-MeCat)]	-0.276±0.005	0.145 ± 0.003	0.12 ± 0.02	29 ± 4	-28 ± 5
[VO(HSHED)(Cat)]	-0.192±0.002	0.092 ± 0.003	0.074 ± 0.005	62 ± 12	-63 ± 12
[VO(HSHED)(DTB)]	-0.221±0.02	0.159 ± 0.001	0.085 ± 0.002	34 ± 2	-36.55 ± 0.04
[VO(HSHED)(3-MeCat)	-0.296±0.002	0.089 ± 0.003	0.0835 ± 0.0006	38 ± 5	-38 ± 6

Information of calculation of the diffusion constant (D_{co})

To calculate the diffusion coefficient (D_{co}) the Randles-Sevcik equation was used, with the solution assumed to be at 25 ºC and standard temperature and pressure (STP) conditions.

$$\text{Equation 1: } D_{co} = \left(\frac{I_p}{2.69*10^5*n^{\frac{3}{2}}*A_E*C*v^{\frac{1}{2}}}\right)^2$$

I_p is the peak current from a voltammogram in amps. The number of electrons transferred is n, which is equal to 1 for these compounds. A_E is the area of the working electrode, 0.07069 cm^2. C is the concentration of the analyte in the solution in mol/cm^3. The scan rate is v, in volts per second.

Table S2.2. Electrochemical data for the V(V/IV) couples of the Cl-HSHED and HSHED catecholate complexes ran at 50mV/sec

Complex	$E_{1/2}$ vs. Fc^+/Fc (V)	ΔE of V couples (V)	ΔE of Fc (V)	D_{co} * 10^{-6} (cm^2/sec)	I_{pa} (μA)	I_{pc} (μA)	I_{pa}/I_{pc} (μA)
[VO(Cl-HSHED)(Cat)]	-0.680± 0.003	0.14 ± 0.01	0.104 ± 0.009	10 ± 3	25± 4	-27± 4	0.917± 0.004
[VO(Cl-HSHED)(DTB)]	-0.783	0.143	0.078	4	22	-17	1.26
[VO(Cl-HSHED)(3-MeCat)]	-0.709 ± 0.004	0.1211 ± 0.0001	0.10 ± 0.01	8 ± 2	22 ± 3	-23 ± 3	0.93± 0.02

Electrochemical data for the V(V/IV) couples of the Cl-HSHED and HSHED catecholate complexes ran at 25mV/sec

Complex	$E_{1/2}$ vs. Fc^+/Fc (V)	ΔE of V couples (V)	ΔE of Fc (V)	D_{co} * 10^{-6} (cm^2/sec)	I_{pa} (μA)	I_{pc} (μA)	I_{pa}/I_{pc} (μA)
[VO(Cl-HSHED)(Cat)]	-0.682± 0.003	0.121 ± 0.009	0.093 ± 0.005	11 ± 3	19± 3	-21± 2	0.88± 0.03
[VO(Cl-HSHED)(DTB)]	-0.790±0.004	0.106 ± 0.004	0.086 ± 0.004	4.3 ± 0.3	14.7± 0.7	-13.0 ± 0.6	1.1± 0.1
[VO(Cl-HSHED)(3-MeCat)]	-0.712 ± 0.001	0.107 ± 0.003	0.090 ± 0.008	8 ± 2	16 ± 3	-17 ± 2	0.93± 0.03

To aid our design of hydrophobic compounds, we estimated logP values (Partition coefficients). Estimated logP values were calculated from Chemicalize which is a program that can calculate logP values for organic molecules based on structure. Since the program is designed more for organic molecules rather than our coordination complexes which contain some coordinate bonds, we explored multiple different options in our structures for the calculation of logP. Shown in Table S2.3, the headings indicate how the compound was presented in Chemicalize for calculations as the values changed based on categorization of the bonds: Coordinate bonding, covalently bonding through 4-coordinate neutral nitrogens, covalently bonding through 4-coordinate positive charged nitrogen. Although the bond between the metal center to the amine should be a coordinate bond, because Chemicalize is mostly used for organic compounds, we used covalent bonds for calculation purposes. Coordinate refers to the structure being drawn with coordinate bonding from the metal center to the amine, while covalent refers to the structure being drawn with covalent bonding from the metal center to the amine. The experimentally observed properties followed the logP values of a neutral covalent bonding and these values were used for our studies.

Table S2.3. Calculated LogP Values

[VO(X-HSHED)(Cat)] X = H, Cl	Cat	Coordinate	Covalent- Neutral N	Covalent - Positive N
Cl	Cat	-2.482	2.126	-0.546
Cl	3-MeCat	-2.015	2.593	-0.078
Cl	DTB	0.772	5.38	2.709
H	Cat	-3	1.608	-1.064
H	3-MeCat	-2.533	2.075	-0.596
H	DTB	0.254	4.862	2.191

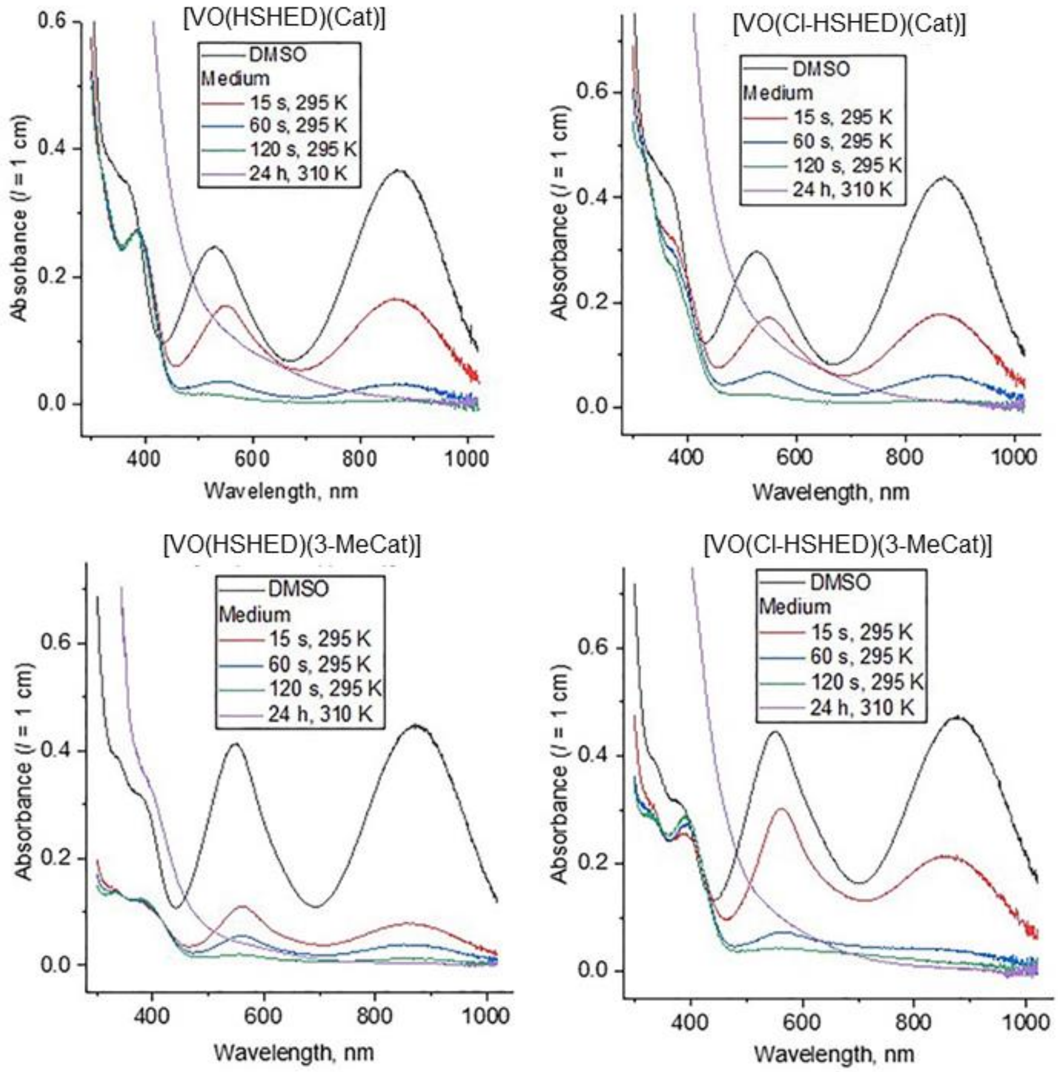

Figure S2.24a. Typical time-dependent UV-Vis spectra of V(V) complexes in fully supplemented cell culture medium ([V] = 100 µM, 295 K or 310 K).

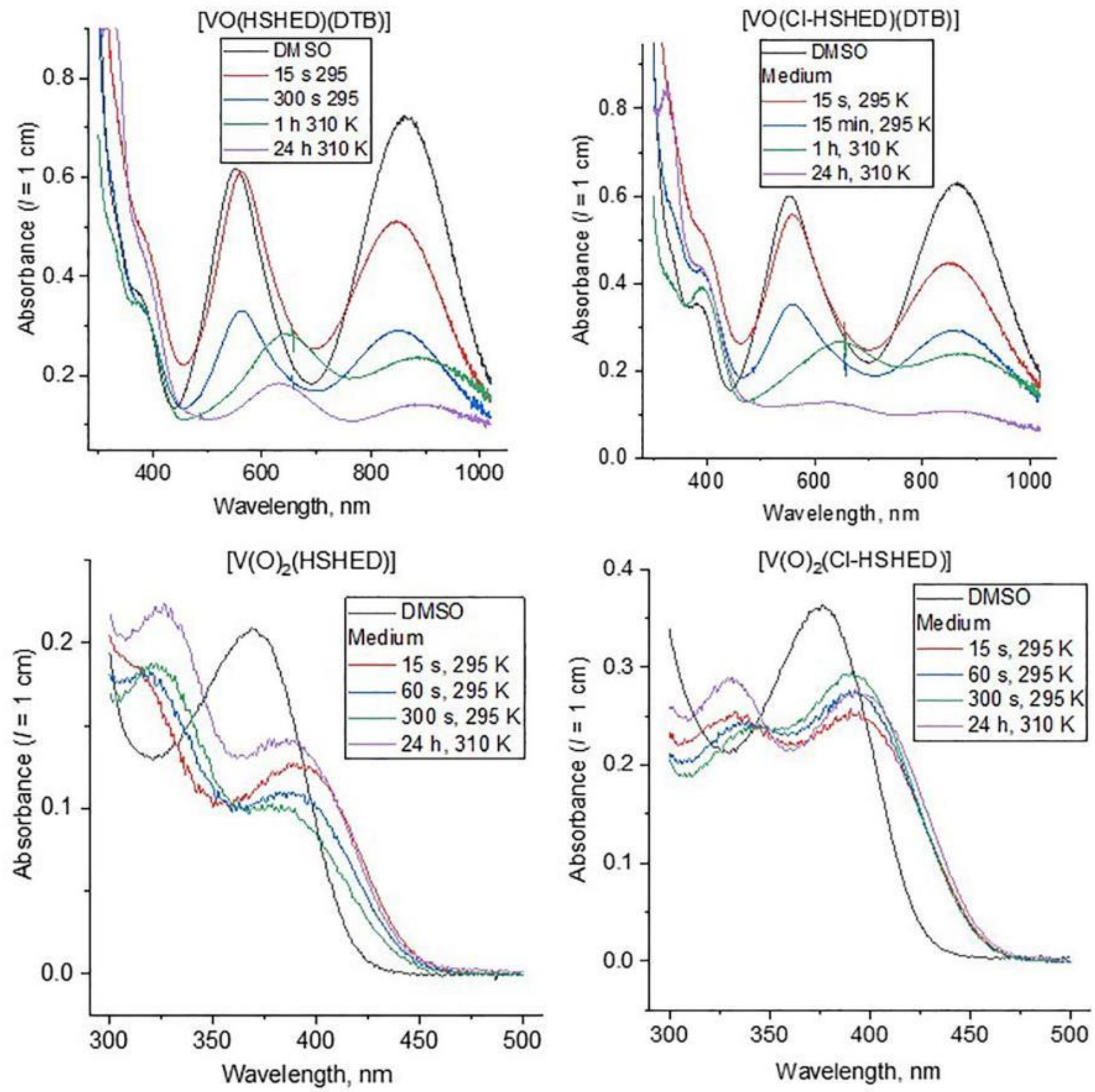

Figure S2.24b. Typical time-dependent UV-Vis spectra of V(V) complexes in fully supplemented cell culture medium ([V] = 100 μM, 295 K or 310 K).

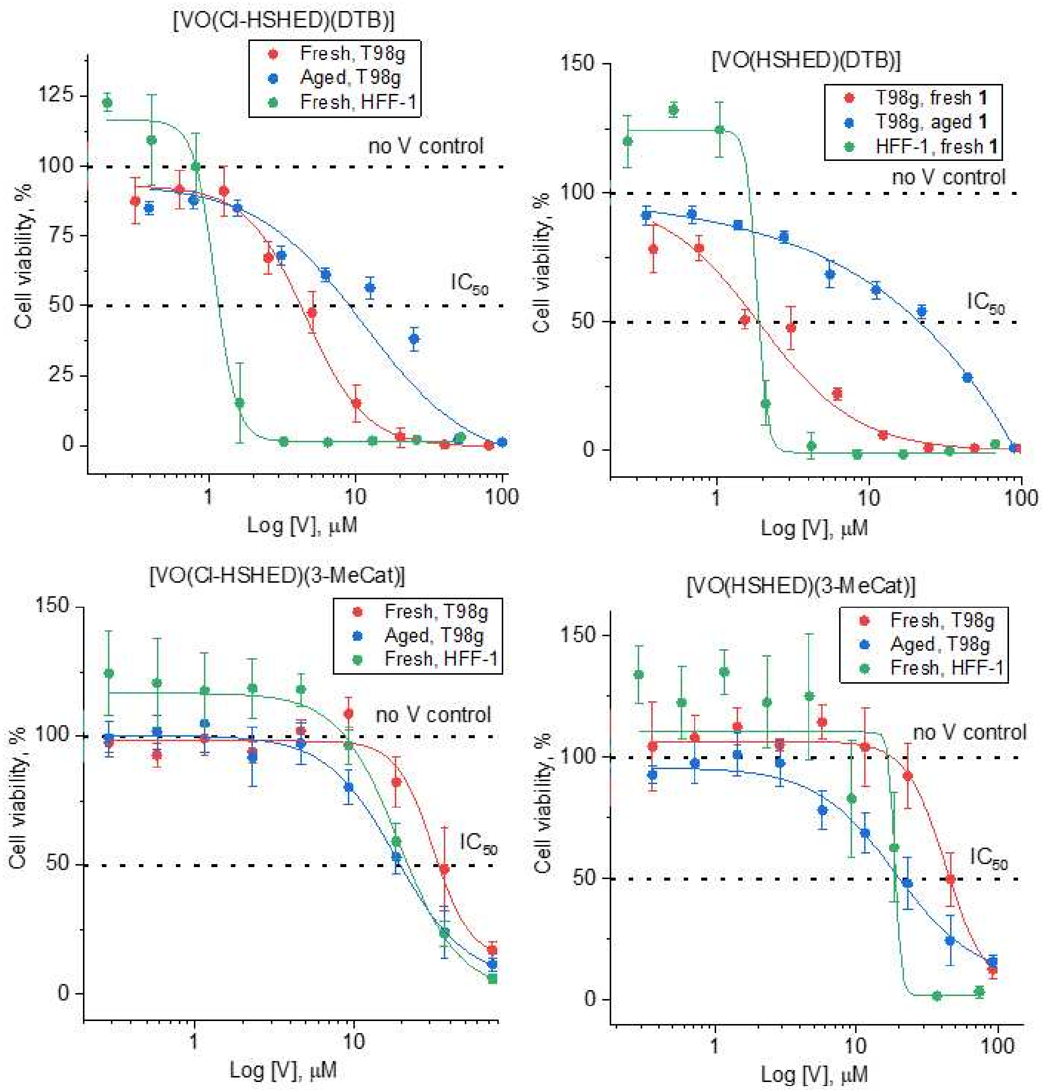

Figure S2.25a. Typical concentration dependencies of cell viabilities (72 h assays). Points are the experimental values, and curves are sigmoidal fits of the experimental data. Error bars represent errors and standard deviations of six replicate wells.

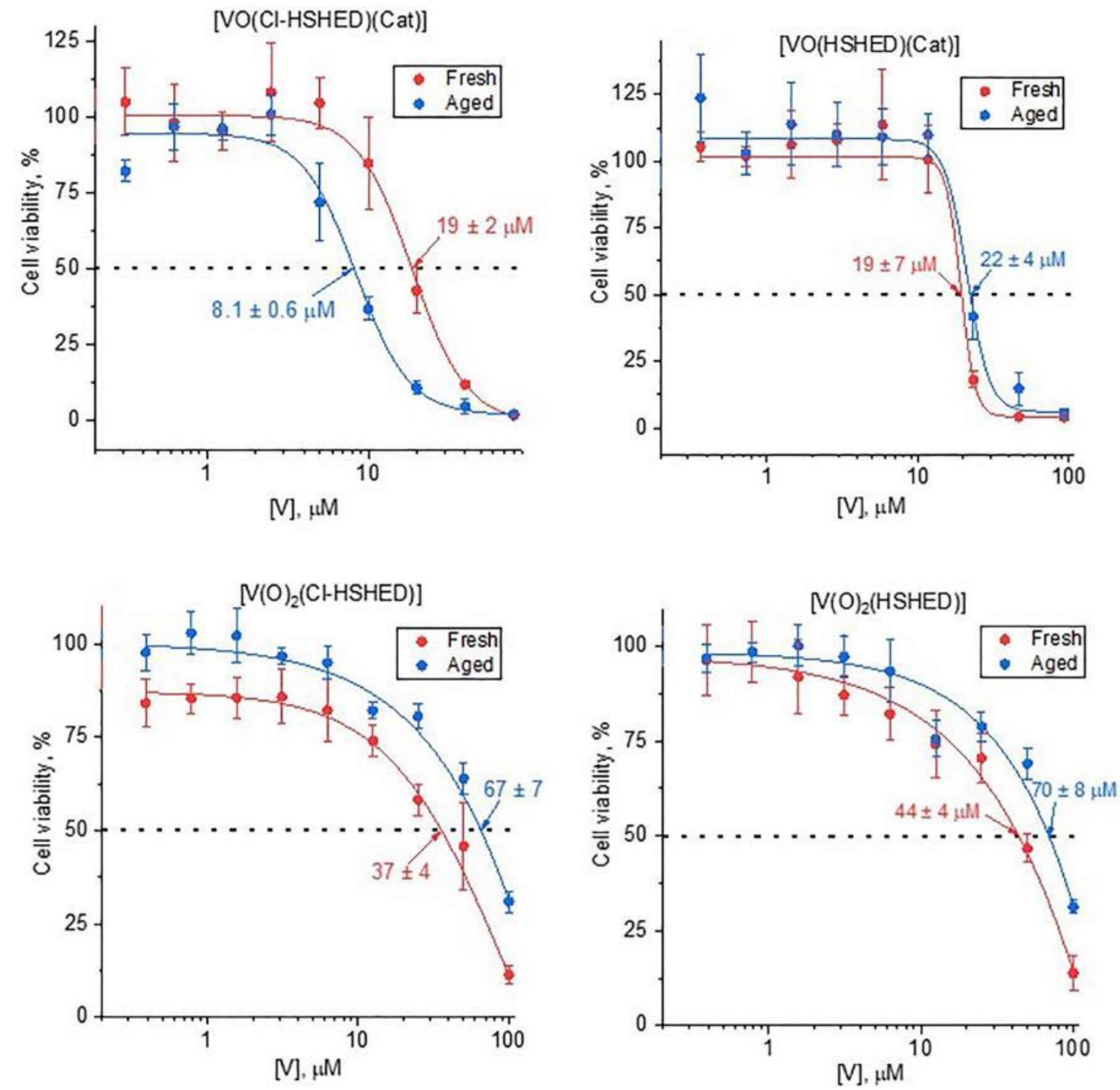

Figure S2.25b. Typical concentration dependencies of cell viabilities (72 h assays). Points are the experimental values, and curves are sigmoidal fits of the experimental data. Error bars represent errors and standard deviations of six replicate wells.

Appendix B- Supplementary Information Corresponding to Chapter 3

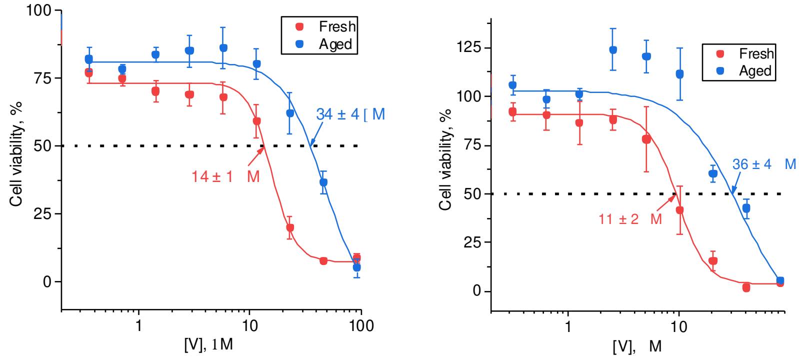

Figure S3.1. Two series of studies of the effects of [VO(HSHED)(Ad)] on T98g cells show that the effects of these compounds reproduce nicely not only showing similar patterns, but the IC_{50} values being within 25% reproducible.

Appendix C – Supplementary Information Corresponding to Chapter 4

NMR spectra were recorded under conditions that speciation constants were determined previously (Crans et al 2000), and the experimental data was compared with these data. Once the previous work was verified, we used this data and recorded spectra at lower ionic strength for the fit in the cell culture media. This section thus describe how constants were obtained at the ionic strength consistent with that of the cell culture assays.

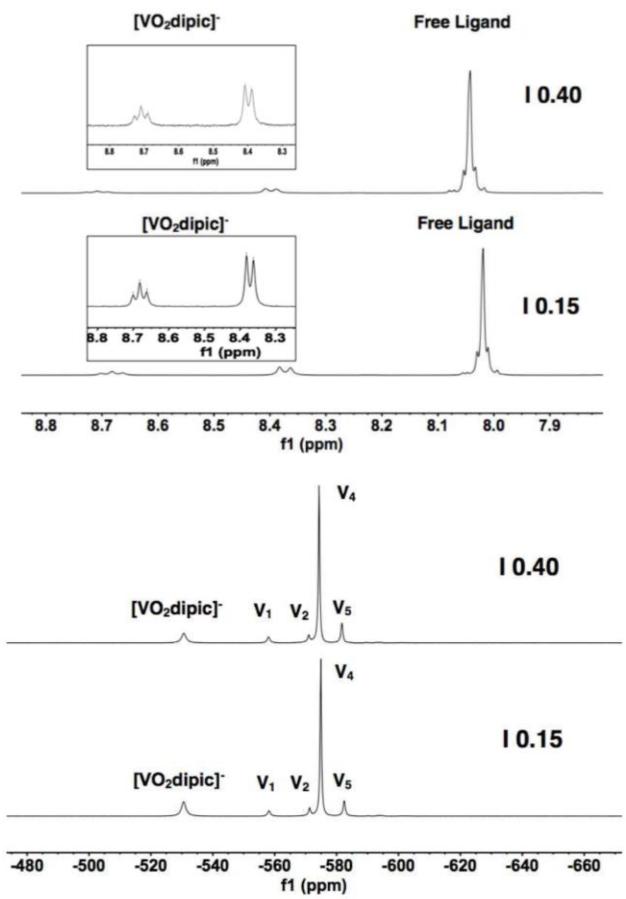

Figure S4.1. $[VO_2dipic]^-$ at pH = 6.60. The ^1H NMR spectra (a) and the ^{51}V NMR spectra (b) of aqueous solutions containing $[VO_2dipic]^-$ are shown

Using the data shown in for $[VO_2dipic]^-$ in Figure S4.1, the concentrations of the species present at a given pH were calculated. The following concentrations were obtained by ^{51}V NMR spectroscopy: $[VO_2dipic^-]$. $[V_1]$ (=$[H_2VO4]^-$), $[V_2]$, $[V_4]$ and $[V_5]$. The concentrations of

$[VO_2dipic]^-$ and $[dipic_2]$ were obtained by ^1H NMR spectroscopy. Those values were combined in the Supplemental Table S4.1 below and compared to the apparent formation constant calculated in the previous study which was 3.9 x 10^{-2} M^{-1} (Crans et al 2000). The measurements were done in triplicates, and the uncertainties for each concentration were calculated. The objective of the aforementioned calculations was to determine the apparent formation constant for the $[VO_2dipic]^-$ complex by using Equations (S4.1) and (S4.2). The calculation of the formation constants can be done by exclusively using the data obtained by ^{51}V NMR where the $dipic^{2-}$ concentration is calculated by subtracting the concentration of the $[VO_2dipic^-]$ complex from the total concentration (in mM)**,** or by ^1H NMR where the V_1 concentration from the ^{51}V studies is used in the calculation.

$$dipic^{2-} + H_2V — [VO_2dipic]^- \qquad \text{(S4.1)}$$

$$K_{eq} = \frac{[VO_2dipic]^-}{[dipic^{2-}][H_2VO_4^-]} \qquad \text{(S4.2)}$$

Table S4.1. The concentrations, experimentally determined by ^{51}V and ^1H NMR, that were used to calculate the values for the apparent formation constant according to Eq 4.5.

			^{51}V NMR	^{51}V NMR	^{51}V NMR	^1H NMR	^1H NMR	^{51}V NMR	^1H NMR
[V-atom] mM	Ionic Strength	pH	$[VO_2dipic]^-$	dipic	V_1	$[VO_2dipic]^-$	dipic	Formation Constant	Formation Constant
5.00	0.40	6.69	0.85 (± 0.07)	4.15 (± 0.07)	0.60 (± 0.04)	0.85 (± 0.07)	4.15 (± 0.07)	**340**	**340**
5.00	0.40	6.60	0.75 (± 0.07)	4.25 (± 0.07)	0.60 (± 0.04)	0.75 (± 0.07)	4.25 (± 0.07)	**290**	**290**
5.00	0.40	6.55	0.80 (± 0.07)	4.20 (± 0.07)	0.65 (± 0.04)	0.90 (± 0.07)	4.20 (± 0.07)	**370**	**370**
5.00	0.40	6.60	0.90 (± 0.07)	4.10 (± 0.07)	0.65 (± 0.04)	0.90 (± 0.07)	4.20 (± 0.07)	**290**	**290**

5.00	0.40	6.66	0.75 (± 0.07)	4.25 (± 0.07)	0.55 (± 0.04)	0.75 (± 0.07)	4.25 (± 0.07)	**320**	**320**
							Average	**320 (± 30)**	**320 (± 30)**

Once the data at the 0.40 ionic strength was verified, similar measurements were done at the 0.15

ionic strength. Those measurements allowed the remaining data in Table S4.2 to be constructed. The difference in those two values was used to determine the b needed for the HySS calculations of the speciation. Once this difference was determined, the corresponding apparent constants for the $[VO_2dipic\text{-}Cl]^-$ and $[VO_2dipic\text{-}OH]^-$ were obtained.

Table S4.2. The concentrations, experimentally determined by ^{51}V and ^{1}H NMR, that were used to calculate the values for the apparent formation constant according to Eq S4.2.

			^{51}V NMR	^{51}V NMR	^{51}V NMR	^{1}H NMR	^{1}H NMR	^{51}V NMR	^{1}H NMR
[V-atom] mM	Ionic Strength	pH	$[VO_2dipic]^-$	dipic	V_1	$[VO_2dipic]^-$	dipic	Formation Constant	Formation Constant
5.00	0.15	6.60	0.65 (± 0.10)	4.35 (± 0.10)	1.05 (± 0.18)	0.65 (± 0.10)	4.35 (± 0.10)	**124**	**149**
5.00	0.15	6.60	0.75 (± 0.10)	4.25 (± 0.10)	0.75 (± 0.18)	0.75 (± 0.10)	4.25 (± 0.10)	**240**	**240**
5.00	0.15	6.60	0.85 (± 0.10)	4.15 (± 0.10)	0.60 (± 0.18)	0.65 (± 0.10)	4.35 (± 0.10)	**230**	**130**
							Average	**156 (± 80)**	**207 (± 50)**
25.00	0.15	6.60	5.00 (± 0.50)	4.70 (± 0.50)	1.00 (± 0.00)	4.75 (± 0.50)	20.25 (± 0.50)	**200**	**240**

25.00	0.15	6.60	4.50 (± 0.50)	21.25 (± 0.50)	1.00 (± 0.00)	4.25 (± 0.50)	20.75 (± 0.50)	**180**	**210**
25.00	0.15	6.60	4.00 (± 0.50)	22.00 (± 0.50)	1.00 (± 0.00)	5.25 (± 0.50)	19.75 (± 0.50)	**160**	**270**
							Average	**128 (± 20)**	**237 (± 32)**

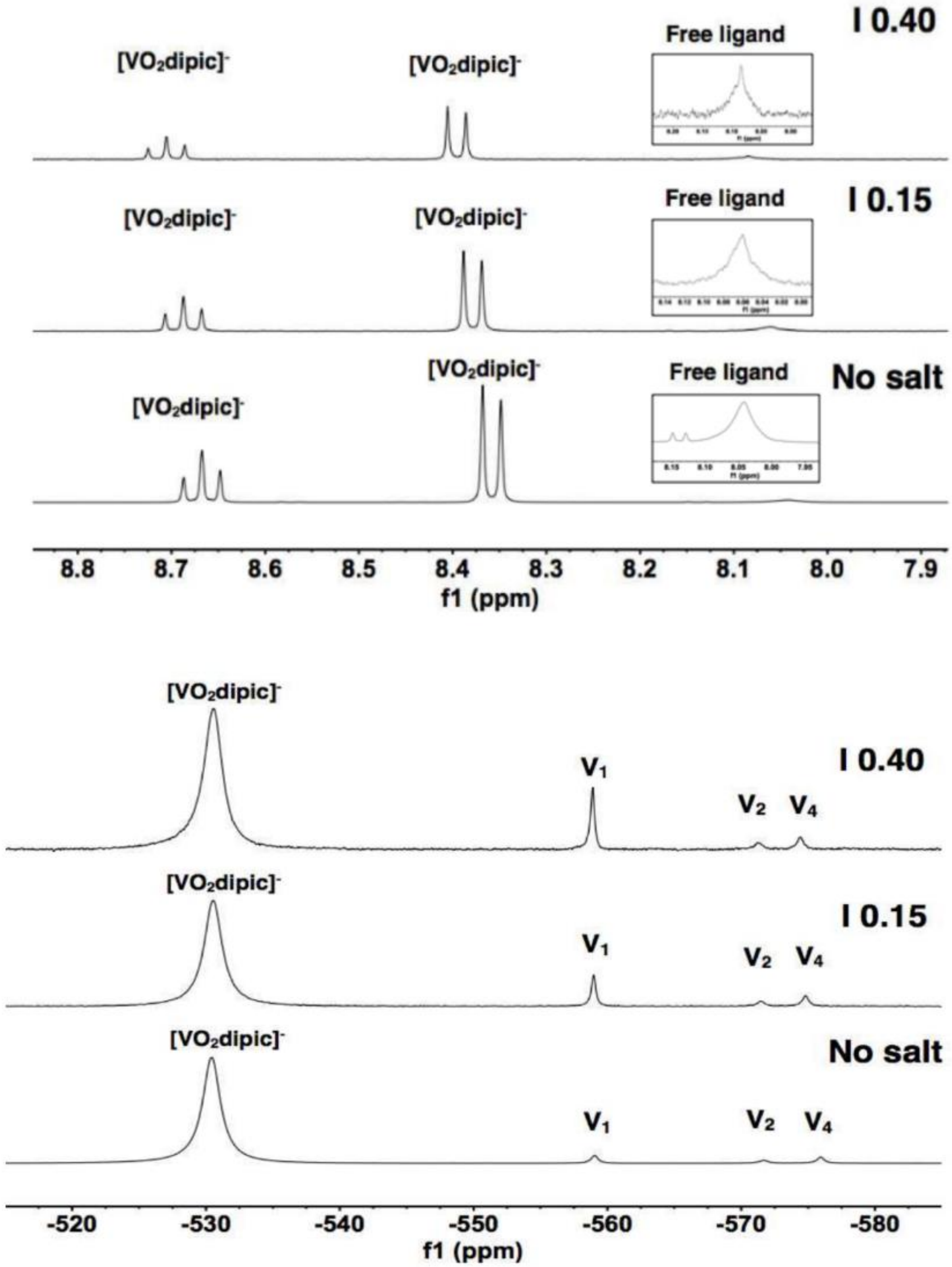

Figure S4.2 $[VO_2dipic]^-$ at pH = 6.00. The ^1H NMR spectra (a) and the ^{51}V NMR spectra (b) of aqueous solutions containing $[VO_2dipic]^-$ are shown.

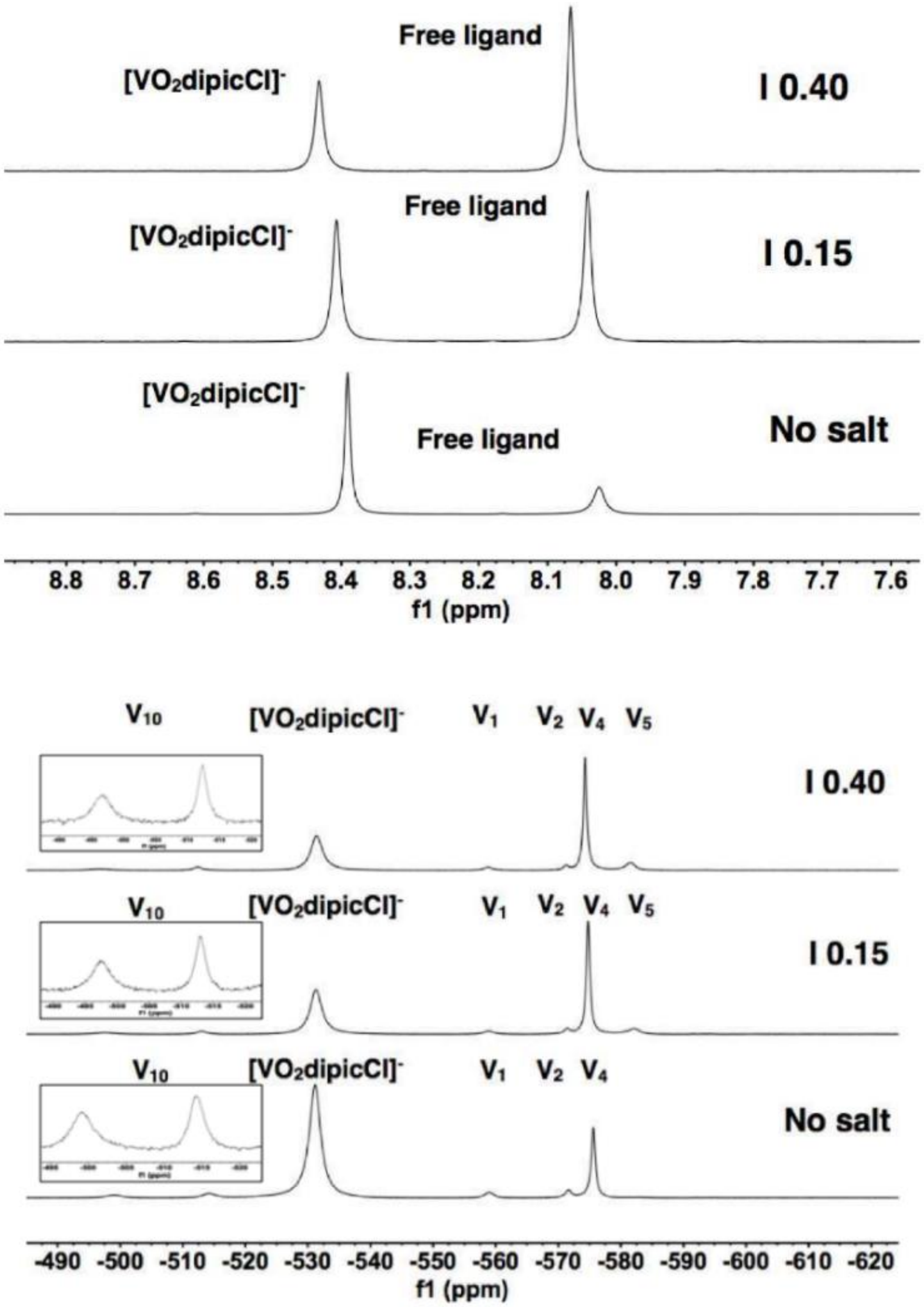

Figure S4.3. $[VO_2dipic\text{-}Cl]^-$ at pH = 6.00. The ^1H NMR spectra (a) and the ^{51}V NMR spectra (b) of aqueous solutions containing $[VO_2dipic\text{-}Cl]^-$ are shown

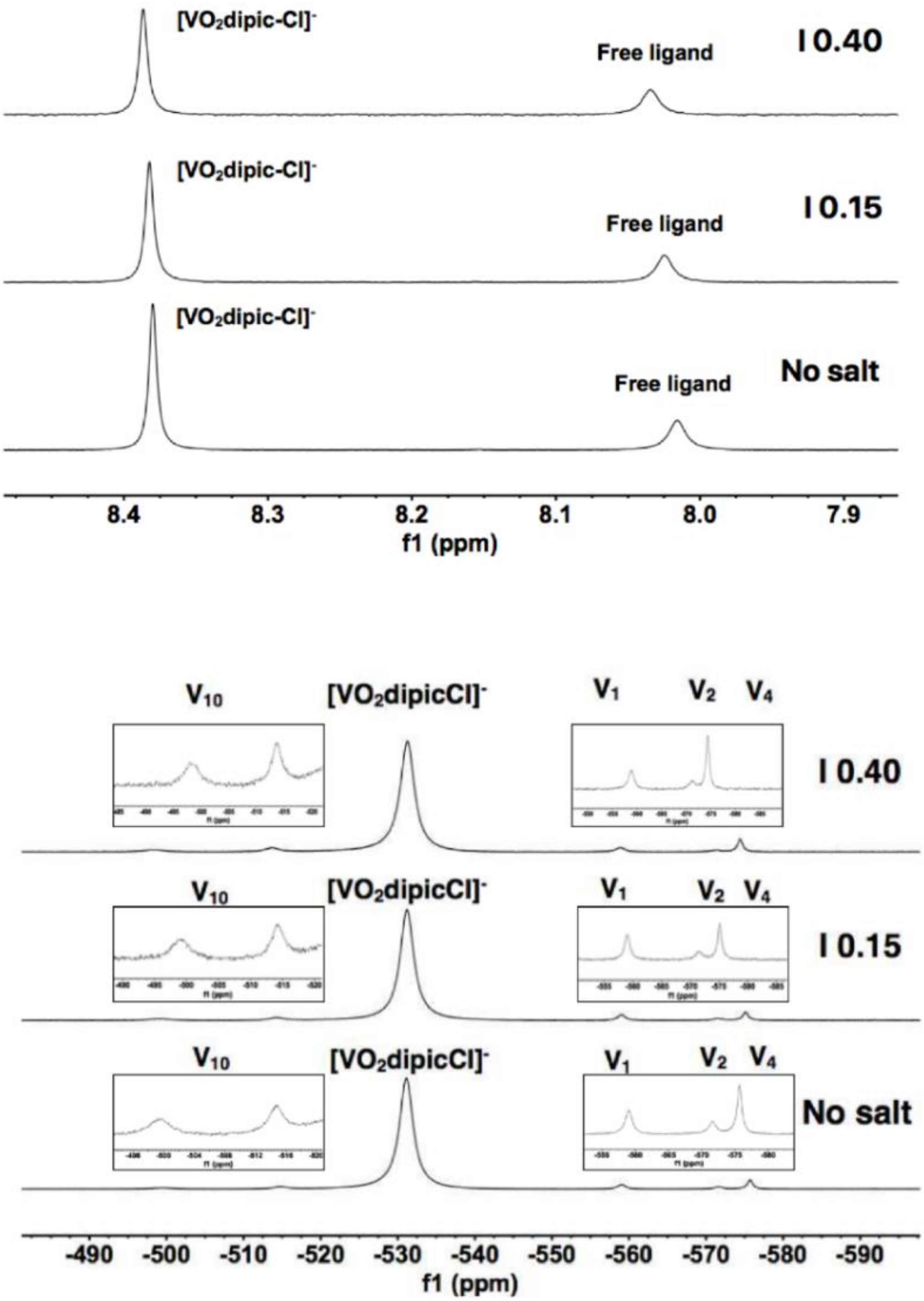

Figure S4.4. $[VO_2dipic\text{-}Cl]^-$ at pH = 5.50. The ^1H NMR spectra (a) and the ^{51}V NMR spectra (b) of aqueous solutions containing $[VO_2dipic\text{-}Cl]^-$ are shown

Speciation Calculations

Additional information is provided regarding the assumptions made for speciation calculations. Species distribution diagrams were calculated by using HySS 2009 software [1]. The citrate and the phosphate concentrations were set as constants to 0.48 mM and 24 mM respectively. The vanadium concentrations that were investigated were concentrations of 5 uM, 1 mM, and 10 mM.

Table S4.3. Formation constants of Vanadate species in a 0.6M NaCl system Table 1. Notations, Compositions, Formation Constants (log ß), and Acidity Constants (pKa) for the H^+-$H_2VO_4^-$, System [**I = 0.6**) NaCl, 25 °C]

(p,q)	Formula	log β	Ref
-1, 1	HVO_4^{2-}	-7.92	Pettersson 1983
-2, 2	$V_2O_7^{4-}$	-15.17	
-1, 2	$HV_2O_7^{3-}$	-5.25	
0, 2	$H_2V_2O_7^{4-}$	2.77	
-2, 4	$V_4O_{13}^{6-}$	-8.88	
-1, 4	$HV_4O_{13}^{6-}$	0.22	
0, 4	$V_4O_{12}^{4-}$	10.0	
0, 5	$V_5O_{15}^{5-}$	12.4	
4, 10	$V_{10}O_{28}^{6-}$	52.1	
5, 10	$HV_{10}O_{28}^{5-}$	58.1	
6, 10	$H_2V_{10}O_{28}^{4-}$	61.9	
7,10	$H_3V_{10}O_{28}^{3-}$	63.5	
2, 1	VO_2^+	6.96	

Table S4.4. Formation constants of Vanadate Citrate species in a 0.6M NaCl system Table 1. Notations, Compositions, Formation Constants (log ß), and Acidity Constants (pKa) for the H^+-$H_2VO_4^-$-, System [**I = 0.6)** NaCl, 25 °C]

(p,q,r)	Formula	log β
1, 0, 1	$C_6H_6O_7^{2-}$	5.217
2, 0, 1	$C_6H_7O_7^-$	9.298
3, 0, 1	$C_6H_8O_7$	12.067
1, 2, 1	$(H^+)(H_2VO_4^{2-})_2(C_6H_5O_7^{3-})$	12.84
2, 2, 1	$(H^+)_2(H_2VO_4^{2-})_2(C_6H_5O_7^{3-})$	19.68
3, 2, 1	$(H^+)_3(H_2VO_4^{2-})_2(C_6H_5O_7^{3-})$	24.12
3, 1, 1	$(H^+)_3(H_2VO_4^{2-})(C_6H_5O_7^{3-})$	18.35
2, 1, 1	$(H^+)_2(H_2VO_4^{2-})(C_6H_5O_7^{3-})$	14.1
4, 2, 2	$(H^+)_4(H_2VO_4^{2-})_2(C_6H_5O_7^{3-})_2$	31.3
5, 2, 2	$(H^+)_5(H_2VO_4^{2-})_2(C_6H_5O_7^{3-})_2$	25.3
6, 2, 2	$(H^+)_6(H_2VO_4^{2-})_2(C_6H_5O_7^{3-})_2$	39.2

Table S4.5. Formation constants of Vanadate Phosphate species in a 0.6M NaCl system Table 1. Notations, Compositions, Formation Constants (log ß), and Acidity Constants (pKa) for the H^+-$H_2VO_4^-$-, System [**I = 0.6)** NaCl, 25 °C]

(p,q,r)	Formula	log β
1, 0, 1	$C_6H_6O_7^{2-}$	5.217
2, 0, 1	$C_6H_7O_7^-$	9.298
3, 0, 1	$C_6H_8O_7$	12.067
1, 2, 1	$(H^+)(H_2VO_4^{2-})_2(C_6H_5O_7^{3-})$	12.84
2, 2, 1	$(H^+)_2(H_2VO_4^{2-})_2(C_6H_5O_7^{3-})$	19.68
3, 2, 1	$(H^+)_3(H_2VO_4^{2-})_2(C_6H_5O_7^{3-})$	24.12
3, 1, 1	$(H^+)_3(H_2VO_4^{2-})(C_6H_5O_7^{3-})$	18.35

Determination of cell culture media ionic strength

The ionic strength, μ, of the media for cell assays was calculated using the equation for ionic strength (S4.3) assuming that the pH of the medium is 7.4.

$$\mu = 1/2 \sum_{1}^{n} c_i z_i^2 \text{ (S4.3)}$$

The composition of the Dulbecco's Modified Eagle's Medium was found from Levina et al. 2017 and the components are listed in Supplemental Table S4.6. The composition of the AlbuMAX was from the product page found on ThermoFisher (https://www.thermofisher.com/order/catalog/product/11020021?CID=AFLBC-11020021) is listed in Supplemental Table S4.7. The composition of the fetal bovine serum used in the calculations was obtained from the average values given in Lindl et al. The charges of each medium component at pH 7.4 were determined and squared. These calculated charges were then multiplied by the corresponding concentration of each ion in the solution. All the ions were summed and then multiplied by one-half to get the ionic strength of 0.17 M. This result allows us to use the experimental values at I = 0.15 M to do the speciation calculations on the vanadium compounds added to the cells. NMR analysis of the compounds in the media showed a significant difference in the concentration of $[VO_2dipic]^-$ at different ionic strengths. This shows the importance of calculating the ionic strength of the media so we know how compounds will speciate once they've been added to the cells and what major compounds will remain to influence the results of the experiment.

Table S4.6. Listing the components in the Dulbecco's Modified Eagle's Medium (Levina et al. 2017) and the components in the AlbuMAX (product page found on ThermoFisher https://www.thermofisher.com/order/catalog/product/11020021?CID=AFLBC-11020021)

Ion	**From Compound**	**Molar Concentration**	**Contribution to Ionic Strength**
Dulbecco's Modified Eagle's Medium (Levina et al. 2017)			
Na (+)	NaCl	1.1E-1	1.1E-1
	$NaHCO_3$	4.4E-2	4.4E-2
	Na_2HPO_4	7.8E-4	1.6E-3
	Sodium Pyruvate	1.0E-3	1.4E-3
	Fetal Bovine Serum	1.4E-3	1.4E-3
	Na_2SeO_3	2.9E-8	5.8E-8
K (+)	KCl	5.4E-3	5.4E-3
	Fetal Bovine Serum	1.1E-4	1.1E-4
Ca (2+)	$CaCl_2$	1.8E-3	7.2E-3
	Fetal Bovine Serum	3.4E-5	1.3E-4
	Calcium d-panthothenate	8.4E-6	3.4E-5
Mg (2+)	$MgSO_4$	8.1E-4	3.2E-3
	Ascorbic Acid Phosphate	7.8E-6	9.4E-5
Se (2+)	Fetal Bovine Serum	3.3E-9	1.3E-8
Urate (+)	Fetal Bovine Serum	1.7E-6	1.7E-6
Creatinine (+)		2.7E-6	2.7E-6
Choline (+)	Choline Chloride	2.9E-5	2.9E-5
$C_{12}H_{18}N_4OS$ (2+)	Thiamine Hydrochloride	1.2E-5	1.2E-5
Cu (2+)	$CuSO_4$	5.0E-9	2.0E-8
Fe (3+)	$Fe(NO_3)_3$	2.5E-7	2.3E-6
Mn (2+)	$MnSO_4$	2.0E-10	8.0E-10
NH_4 (+)	NH_4VO_3	2.5E-9	2.5E-9
Lysine (+)	Amino Acids	2.7E-9	2.7E-9
Histidine (+)	Amino Acids	6.7E-5	6.7E-5
Arginine (+)	Amino Acids	2.0E-5	2.0E-5

Cl (-)	NaCl	1.1E-1	1.1E-1
	KCl	5.4E-3	5.4E-3
	$CaCl_2$	1.8E-3	3.6E-3
	Fetal Bovine Serum	1.0E-3	1.0E-3
	Chloine Chloride	2.9E-5	2.9E-5
	Thiamine Hydrochloride	1.2E-5	1.2E-5
HCO_3 (-)	$NaHCO_3$	4.4E-2	4.4E-2
SO_4 (2-)	$MgSO_4$	8.1E-4	3.2E-3
	$CuSO_4$	5.0E-9	2.2E-8
	$MnSO_4$	2.0E-10	8.0E-10
HPO_4 (2-)	Na_2HPO_4	7.8E-4	3.1E-3
$C_{12}H_{12}O_{18}P_2$ (3-)	Ascorbic Acid Phosphate	7.8E-6	1.4E-4
$C_3H_3O_3$ (-)	Sodium Pyruvate	1.0E-3	1.0E-3
PO_4 (3-)	Fetal Bovine Serum	1.0E-5	9.3E-5
$C_9H_{16}NO$ (-)	Calcium d-panthothenate	8.4E-6	1.7E-5
NO_3 (-)	$Fe(NO_3)_3$	2.5E-7	7.5E-7
SeO_3 (2-)	Na_2SeO_3	2.9E-8	1.2E-7
VO_3 (-)	NH_4VO_3	2.5E-9	2.5E-9
Aspartic Acid (-)	Amino Acids	2.0E-5	2.0E-5
Glutamic Acid (-)	Amino Acids	2.0E-5	2.0E-5
		Sum of Contributions	**0.35 (3.5E-1)**
		Total Ionic Strength	**0.17 (1.7E-1)**

In addition, a number of components, including Albu, were added to the minimal media.

Table S4.7. Listing the components in the Dulbecco's Modified Eagle's Medium (Levina et al. 2017) and the components in the AlbuMAX (product page found on ThermoFisher https://www.thermofisher.com/order/catalog/product/11020021?CID=AFLBC-11020021) that were deemed neutral and not contributing

Compound	**Molar Concentration**
Glucose	2.5E-2
Uncharged Amino Acids (Gln, Ile, Leu, Gly, Ser, Phe, Tyr, Cyt, Met, Ala, Asn, Trp)	3.7E-3

AlbuMax	4.0E-4
Folic Acid	4.1E-6
Glutathione	3.3E-6
Inositol	4.0E-5
Niacinamide	3.3E-5
Pyroxidine hydrochloride	2.0E-5
Riboflavin	1.1E-6
Holo-transferrin	9.4E-8
Insulin	1.7E-6
Penicillin G	1.8E-4
Streptomycin	1.7E-4
Fungizone	1.9E-7
Ethanolamine	3.1E-5
Phenol red	4.2E-5

As summarized in the Supplemental Table S4.8 the total contributions are not small but when all are summed up, it comes out to 0.17. This result show that we should use the parameters reported for 0.15 ionic strength with estimating the content of intact V-complexes.

Parameters for Speciation Calculations at 0.15 ionic strength for [VO2dipic]-, [VO2dipic-Cl]-, and [VO2dipic-OH]-

The speciation profiles are generated using reported values, and those derived in this system. The specific parameters are listed below for an environment near an ionic strength of 0.15.

Table S4.8. Formation constants of Vanadate species in a 0.15M NaCl system Table 1. Notations, Compositions, Formation Constants (log ß), and Acidity Constants (pKa) for the H^+-$H_2VO_4^-$, System [**I = 0.15**) NaCl, 25 °C]

Binary System ($H_2VO_4^-$–H^+)				
(p,q)	Formula	log β	pKa	Ref
1,2	VO_2^+	7.00		Elvingson, K., et al. *Inorg. Chem.* **1996.** *35*, 3388-3393.
1, -1	HVO_4^{2-}	-8.17		
1, 0	$H_2VO_4^-$	0.00	8.17	
2, -2	$H_2V_2O_7^{4-}$	-16.18		

2, -1	$HV_2O_7^{3-}$	-5.85	10.34	
2, 0	$H_2V_2O_7^{2-}$	2.65	8.50	
4, -2	$V_4O_{13}^{6-}$	-9.98		
4, -1	$HV_4O_{12}^{5-}$	-0.63	9.35	
4, 0	$V_4O_{12}^{4-}$	9.24		
5, 0	$V_5O_{15}^{5-}$	11.17		
10, 4	$V_{10}O_{28}^{6-}$	50.28		
10, 5	$HV_{10}O_{28}^{5-}$	56.90	6.62	
10, 6	$H_2V_{10}O_{28}^{4-}$	61.07	4.17	
10, 7	$H_3V_{10}O_{28}^{3-}$	62.93	1.86	

Table S4.9. Formation constants of $[VO_2dipic]^-$ complex in a 0.15M NaCl system. Notations, Compositions, Formation Constants (log ß), and Acidity Constants (pKa) for the $H_2VO_4^-$-H^+-dipic System [I = 0.15 NaCl M, 25 °C]

Binary (H^+-dipic) and Ternary System ($H_2VO_4^-$-H^+-dipic)				
(p,q,r)	Formula	log β	pKa	Ref
0, 1, 1	Hdipic	4.56	4.56	Crans, D. C.; *Inorg. Chem.* **2000,** *39,* 4409-4416.
0, 2, 1	H_2dipic	6.60	2.04	
0, 3, 1	H_3dipic	7.19	0.59	
1, 2, 1	H_2Vdipic	15.41*		
1, 3, 1	H_3Vdipic	15.92*	0.51	

Table S4.10. Formation constants of $[VO_2dipic\text{-}Cl]^-$ complex in a 0.15M NaCl system. Notations, Compositions, Formation Constants (log ß), and Acidity Constants (pKa) for the $H_2VO_4^-$-H^+-dipic-Cl [I = 0.15 NaCl M, 25 °C]

Ternary System ($H_2VO_4^-$-H^+-dipic-Cl)				
(p,q,r)	Formula	log β	pKa	Ref
0, 1, 1	Hdipic-Cl	3.83		Smee, J. J., et al. *J. Inorg. Biochem.* **2009**, *103,* 575-584.
0, 2, 1	H_2dipic-Cl	6.10	2.21	
0, 3, 1	H_3dipic-Cl	6.60	0.50	
1, 2, 1	H_2Vdipic-Cl	15.31*		
1, 3, 1	H_3Vdipic-Cl	15.82*	0.51	

Table S4.11. Formation constants of $[VO_2dipic\text{-}OH]^-$ complex in a 0.15 M NaCl system. Notations, Compositions, Formation Constants (log ß), and Acidity Constants (pKa) for the $H_2VO_4^-$-H^+-dipic-OH [I = 0.15) NaCl M, 25 °C]

Ternary System ($H_2VO_4^-$-H^+-dipic-OH)				
(p,q,r)	Formula	log β	pKa	Ref
0, 0, 1	$DipicO^{3-}$	0.00		Jakusch, T., et al.; *J. Inorg. Biochem.* **2003**, *95*, 1-13.
0, 1, 1	$Dipic\text{-}OH^{2-}$	10.75	10.75	
0, 1, 2	$Hdipic\text{-}OH^-$	13.93	3.08	
0, 1, 3	$H_2Vdipic\text{-}OH$	15.20	1.40	
1, 1, 1	$[VO_2(dipicO)(OH)]^{3-}$	12.70		
1, 1, 2	$[VO_2(dipicO)]^{2-}$	20.56	7.90	
1, 1, 3	$[VO_2(dipic\text{-}OH)]^-$	24.26	3.70	

In addition to the $[VO_2dipic]^-$ and $[VO_2dipic\text{-}Cl]^-$ profiles that are shown in the manuscript, we also show the corresponding profiles for the $[VO_2dipic\text{-}OH]^-$ here, since this compound was also tested. This complex because of the OH group has one more proton and thus one more protonation state. However, the speciation is similar to the other systems if the two speciation steps are combined.

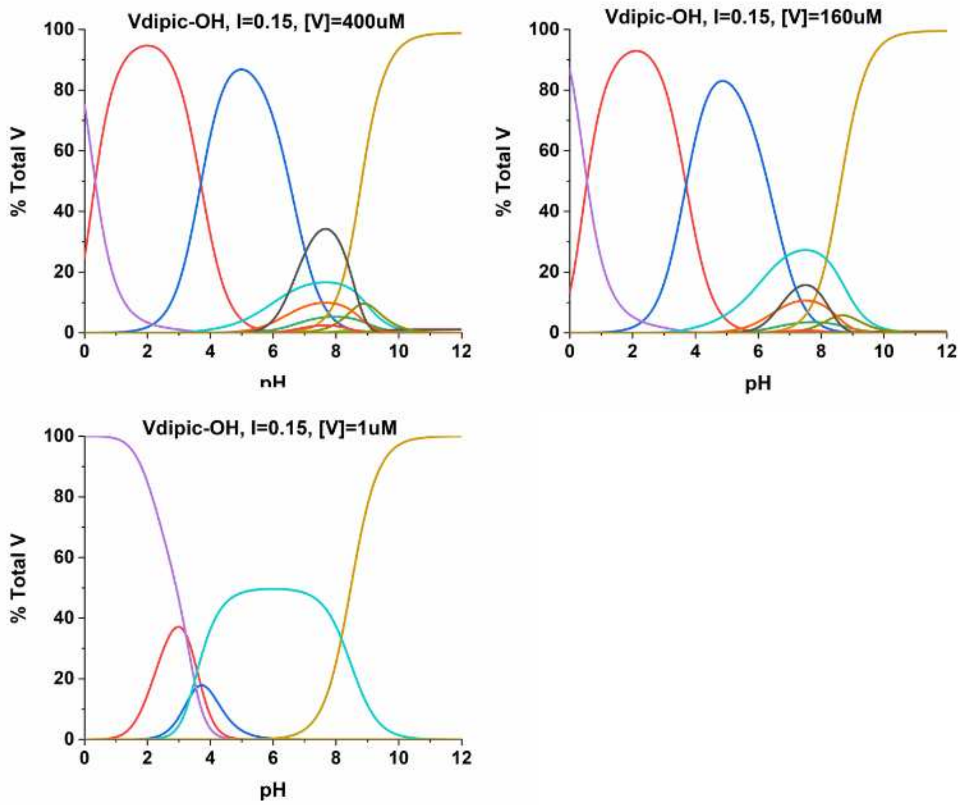

Figure. S4.5. The speciation profile for $[VO_2dipic\text{-}OH]^-$ is shown using total V-concentrations of 0.400 μM, 0.160 μM and 1.0 μM. The calculations were done using the vanadate oligomerization constants for 0.15 M NaCl.

Projects Sorted by Subject

Synthesis

1. Murakami, H. A.; Uslan, C.; Haase, A. A.; Koehn, J. T.; Vieira, A. P.; Gaebler, D. J.; Hagan, J.; Beuning, C. N.; Proschogo, N.; Levina, A.; Lay, P. A.; Crans, D. C. Vanadium chloro substituted Schiff base catecholate complexes are reducible, lipophilic, water stable, and have anticancer activities. *Inorg Chem*. **2022**, *61*, 20757-20773.
2. Bates, A.; Murakami, H. A.; Levina, A.; Lay, P. A.; Crans, D. C. The vanadium Schiff base di-adamantyl catecholate complex with potent anticancer activities. (Manuscript under preparation)
3. "Exploring properties of new non-innocent vanadium(V) compounds and their anti-cancer activities" Canan Uslan Yigit, Heide A. Murakami, Allison A. Haase, Jordan T. Koehn, Adriana Pires Vieira, D. Jackson Gaebler, John Hagan, Cheryle N. Beuning, Victoria R. Bachtell, Nicholas Proschogo, Aviva Levina, Peter A. Lay, Debbie C. Crans, Under Preparation
4. "Exploring properties of new non-innocent vanadium(V) compounds" Allison A. Haase, Heide A. Murakami, Allison A. Haase, Jordan T. Koehn, John Hagan, Cheryle N. Beuning, Aviva Levina, Peter A. Lay, Debbie C. Crans, Under Preparation
5. "Exploring growth of *Mycobacterium Smegmatis* treated with anticarcinogenic vanadium-compounds", Zeyad Arhouma, Heide A. Murakami, Jordan T. Kohen, Xiaorong Li, Deborah A. Roess, Dean C. Crick and Debbie C. Crans, *Inorganics,* **2022** 10, 50 (1-22p). https://doi.org/10.3390/inorganics10040050

6. “Acute toxicity evaluation of non-innocent oxidovanadium(V) Schiff base complex” Lidiane M. A. de Lima, Heide Murakami, D. Jackson Gaebler, Wagner E. Silva, Mônica F. Belian, Eduardo C. Lira and Debbie C. Crans, *Inorganics* **2021**, 9, 42. https://doi.org/10.3390/inorganics9060042

7. “Solution- and gas-phase behavior of decavanadate: implications for mass spectrometric analysis of redox-active polyoxidometalates” Daniel Favre, Cedric E. Bobst, Stephen J. Eyles, Heide Murakami, Debbie C. Crans and Igor A. Kaltashov *Inorg. Chem. Frontiers* 2022 early access DOI: 10.1039/d1qi01618k.

Speciation

8. “Decavanadate inhibits microbacterial growth more potently than other oxovanadates” Nuttaporn Samart, Zeyad Arhouma, Santosh Kumar, Heide A. Murakami, Dean C. Crick and Debbie C. Crans, *Frontiers in Chemistry*, **2018,** 6, article #519 (16p). doi: 10.3389/fchem.2018.00519. PMCID: PMC6255961; PMID: 30515375

9. “Enhancement of oncolytic virotherapy by vanadium(V) dipicolinates” Anabel Bergeron, Kateryna Kostenkova, Mohammed Selman, Heide A. Murakami, Elizabeth Owens, Naveen Haribabu, Rozanne Arulanandam, Jean-Simon Diallo and Debbie C. Crans *Biometals*, **2019**, 32, 545-561. doi: 10.1007/s10534-019-00200-9. PMID: 31209680

Biological Chemistry

10. “Effects of vanadium(IV) compounds on plasma membrane lipids leads to G protein-coupled receptor signal transduction” Duaa Althumairy, Heide A. Murakami, Dongmei

Zhang, B. George Barisas, Deborah A. Roess and Debbie C. Crans *J. Inorg. Biochem.* **2020**, *203*, 110873. doi: 10.1021/acs.inorgchem.9b02848. PMID: 31808684.

11. "Location of menaquinone and menaquinol head groups in model membranes" Cameron Van Cleave, Heide A. Murakami, Nuttaporn Samart, Jordan T. Koehn, Pablo Maldonado, Jr., Heidi D. Kreckel, Elana J. Cope, Andrea Basile, Dean C. Crick and Debbie C. Crans *Can. J. Chemistry*, **2020**, *98,* 307-317

12. "Electron transport lipids fold within membrane-like interfaces" Margaret M Braasch-Turi, Jordan T Koehn, Kateryna Kostenkova, Cameron Van Cleave, Jacob W Ives, Heide A Murakami, Dean C Crick and Debbie C Crans *Frontiers in Chemistry (Chemical Biology)*, 2022, 10, p Article 827530 (1-17) doi: 10.3389/fchem.2022.827530.

13. "Coordination environment changes of the vanadium in vanadium-depending haloperoxidase enzymes" Craig C. McLauchlan, Heide A. Murakami, Craig A. Wallace, and Debbie C. Crans *J. Inorg. Biochem.* **2018,** *186*, 267-279. doi: 10.1016/j.jinorgbio.2018.06.011. PMID: 29990751